UNIVERSIDADE DE LISBOA
FACULDADE DE CIÊNCIAS
DEPARTAMENTO DE QUÍMICA E BIOQUÍMICA

Fluorescence Studies of Protein Aggregation Leading to Amyloid Formation: The Role of Anionic Lipid Membranes

Joana Catarina Ribeiro Ricardo

Dissertação de Tese de Mestrado

Mestrado em Bioquímica

Especialização em Bioquímica

2012

UNIVERSIDADE DE LISBOA
FACULDADE DE CIÊNCIAS
DEPARTAMENTO DE QUÍMICA E BIOQUÍMICA

Fluorescence Studies of Protein Aggregation Leading to Amyloid Formation: The Role of Anionic Lipid Membranes

Joana Catarina Ribeiro Ricardo

Mestrado em Bioquímica

Especialização em Bioquímica

Dissertação de Tese de Mestrado orientada por

Professora Doutora Ana Coutinho

Lisboa

2012

O difícil não é chegar aos grandes,

mas a si próprio.

Almada Negreiros

Foreword

This dissertation describes the work performed under the supervision of Dr. Ana Coutinho in the Biological Fluorescence group from Centro de Química-Física Molecular/ IN - Instituto de Nanociência e Nanotecnologia, at Instituto Superior Técnico, from September 2011 to September 2012.

Joana Catarina Ribeiro Ricardo was the recipient of a research fellowship in the framework of the project "Amyloidogenic Proteins: Role of Lipid-Protein Interaction in Amyloid-like Fibril Formation" (project PTDC/QUI-BIQ/099947/2008), financed by *Fundação para a Ciência e Tecnologia* from *Ministério da Educação e Ciência*.

Acknowledgments

I wish to thank Prof. Manuel Prieto for letting me be a part of the Biological Fluorescence group and for all the knowledge he always has to offer, accompanied by his great humor, kindness and coffees. I also want to show my gratitude to Ana Melo, for her help with daily tasks and with the microscopy experiments, to Dr. Aleksander Fedorov for his help with the time-resolved fluorescence measurements, to Prof. Mário Nuno Berberan Santos for providing the program to analyze fluorescence anisotropy decays with the associative model and to Nuno Bernardes for providing the conditions necessary to concentrate my samples.

Finally, I wish to thank all my colleagues of IN – Institute of Nanoscience and Nanotechnology of Technical University of Lisbon and I want specially and mostly to thank Prof. Ana Coutinho, my supervisor and an excellent professional, who was a real inspiration and gave excellent tutorial and shared her knowledge with me.

I must thank my big family; my parents, Lurdes e Álvaro, who supported me and gave me conditions to carry out my studies, to my sisters, Carla e Marta, for being there since I was a child, that put up with me all along the way and to my bright brother's in law, Flávio e Fernando. Also, to my 6 noisy and lovely nices and nephews, João, Natacha, Rafael, Rodrigo, Carolina and Isaac that always put a smile in my face, whether is with their lovely faces and expressions or with their funny questions. Love you all.

Next to my oldest and newest friends. I owe a word to the oldest for never letting that friendship feeling pass, even if we only get together twice a year. Especially, I thank Pedro, Rita and Luís, for letting me know I can always, since I can remember, count on them. For the funniest and greatest moments of the last almost 10 years. In addition, I've gained a number of friends during my studies, with whom I spent good and bad moments and for whom I must show my appreciation here. Especially, my "godmother" Maria João, and my "godchildren" Mário e Inês, I thank you for making college an experience worth living.

And finally, a very special acknowledgment goes to André, who was the reason I got the strength necessary to finish my course and who always encourages me to pursuit my dreams. To his love, patience, care, companionship and everything else. I love you, this thesis is dedicated to you.

Resumo

Existem diversas doenças humanas, tais como a doença de Alzheimer, doença de Parkinson ou a diabetes *mellitus* tipo II, em que ocorre a formação de depósitos proteicos intra- ou extracelulares designados por fibras amilóide. Os processos que levam as proteínas a sofrer alterações conformacionais que transformam o seu estado nativo num estado parcialmente desnaturado que, posteriormente, conduz a processos irreversíveis de agregação são ainda pouco conhecidos mas de elevado interesse para a comunidade científica. Alguns destes processos podem ser semelhantes ao que ocorre com formulações proteicas desenvolvidas pela indústria farmacêutica durante o seu armazenamento. Deste modo, é urgente esclarecer os mecanismos moleculares que conduzem à agregação e formação de fibras pelas proteínas, assim como determinar a estrutura das fibras amilóides e dos intermediários seus precursores, de modo a ser possível desenvolver compostos eficazes para o tratamento destas doenças e para a preservação dos fármacos.

Actualmente pensa-se que a toxicidade associada a estas doenças provém não das fibras amilóides maduras propriamente ditas mas sim dos seus precursores. Vários estudos recentes apontam para o facto de estes intermediários serem capazes de interagir com as membranas biológicas, o que pode levar à disrupção das mesmas. Com efeito, a capacidade que as membranas lipídicas aniónicas têm em recrutar e induzir alterações conformacionais em diversos péptidos/proteínas amiloidogénicas, que podem levar à formação de agregados com características amilóides, tem sido um tópico de investigação importante nos últimos anos. Em 2004, Kinnunen e colaboradores alargaram este conceito ao propor que as membranas contendo fosfolípidos acídicos podem também desencadear a fibrilhação de várias proteínas não amiloidogénicas, tais como o lisozima e a mioglobina. O lisozima da clara do ovo de galinha (HEWL) é um modelo ideal de uma proteína não amiloidogénica para investigar esta hipótese já que tem sido largamente usado no estudo dos mecanismos moleculares de agregação de proteínas/ formação de fibras *in vitro*.

O presente trabalho visou prosseguir o estudo iniciado no laboratório de acolhimento relativamente ao mecanismo de fibrilhação do HEWL induzido pela sua interação com membranas lipídicas aniónicas. De modo a ser possível aplicar uma grande variedade de técnicas centradas na espectroscopia de fluorescência (medidas em estado estacionário e resolvidas no tempo, assim como a espectroscopia de correlação de fluorescência), a proteína foi derivatizada com uma sonda fluorescente, o éster de succinamida do Alexa 488 (A488). Os estudos foram realizados com sistemas modelo de membranas, vesículas unilamelares grandes (LUVs), preparadas com uma

composição lipídica variável, nomeadamente incluindo diferentes percentagens de um fosfolípido *zwitteriónico* e aniónico (1-palmitoil-2-oleoil-*sn*-glicero-3-fosfocolina (POPC) e 1-palmitoil-2-oleoil-*sn*-glicero-3-fosfoserina (POPS)), respectivamente). Os estudos iniciais realizados evidenciaram que as propriedades de emissão de fluorescência do HEWL derivatizado com A488 (Lz-A488) eram fortemente afectadas quando esta interactuava com lipossomas aniónicos. Tendo por base as variações registadas nos valores dos comprimentos de onda máximos de emissão, intensidade e tempos de vida de fluorescência, foi possível identificar três populações distintas de Lz-A488 em interacção com as membranas, dependentes da razão lípido:proteína usada nos ensaios. Atendendo aos resultados obtidos, sugeriu-se que as populações detectadas poderiam corresponder a intermediários da via de fibrilhação do lisozima induzida pela sua interação com membranas lipídicas aniónicas.

Tendo em conta que as conclusões anteriores são baseadas nas propriedades de emissão de fluorescência do A488, tornou-se imperativo avaliar a capacidade deste fluoróforo em reportar alterações conformacionais sofridas pelo lisozima quando sujeito a condições destabilizadoras. Deste modo, o presente trabalho foi iniciado com a realização de estudos de desnaturação térmica do Lz-A488 através da monitorização da variação das suas propriedades de emissão de fuorescência com a temperatura. Os estudos foram realizados a pH 7.4 e 2.2 já que enquanto as interacções lípido-proteína são habitualmente investigadas a pH neutro, os estudos de fibrlhação *in vitro* desta proteína são frequentemente conduzidos a valores de pH acídicos. Após marcação covalente do lisozima com o A488 e sua posterior purificação por cromatografia de exclusão molecular, confirmou-se que a proteína modificada mantém a sua estrutura nativa à temperatura ambiente através da comparação dos tempos de correlação rotacional obtidos a ambos os valores de pH. Os ensaios de desnaturação térmica efectuados revelaram que o fluoróforo é um bom grupo repórter das alterações conformacionais sofridas pelo lisozima devido à sua susceptibilidade em sofrer extinção de fluorescência via um mecanismo de transferência de electrões foto-induzida. Os resíduos W62 e W63 do lisozima são candidatos potenciais a actuarem como agentes de extinção de fluorescência do fluróforo ligado covalentemente ao resíduo K97 já que se encontram localizados numa região da proteína que tem sido descrita como sendo a primeira a sofrer alterações conformacionais por aumento da temperatura. Os resultados obtidos mostraram ainda que a derivatização da proteína não perturba o seu nível terciário de estrutura de um modo pronunciado pois os valores obtidos para a temperatura de desnaturação térmica do Lz-A488 são concordantes com dados da literatura obtidos por outras técnicas biofísicas.

O passo seguinte deste trabalho consistiu em estudar de que modo a fibrilhação *in vitro* do lisozima afectava as propriedades emissivas do Lz-A488. Os ensaios foram efectuados a pH 2.2 e

57 ºC, sob condições quiescentes. Foram preparadas misturas de lisozima com proporções variáveis de proteína marcada (razões molares de 1/2, 1/8, 1/40, 1/100 e 1/200 Lz-A488/lisozima, concentração de proteína total 0.2 ou 1.0 mM). Em paralelo, foram realizados ensaios controlo da cinética de fibrilhação do lisozima não derivatizado empregando-se as sondas tioflavina T (ThT) e vermelho do Nilo (NR). De acordo com o esperado, as cinéticas apresentaram um comportamento sigmóide característico de um mecanismo do tipo nucleação-polimerização, tendo-se determinado um tempo de latência cerca de 2 dias mais longo para as amostras contendo menor concentração de proteína total. A obtenção de fibras amilóide maduras que ligavam ThT e NR foi confirmada por microscopia confocal de fluorescência (CFM) no final de ambas as cinéticas. Foi ainda determinado que o NR apresenta uma afinidade moderada na sua ligação às fibras amilóide maduras de lisozima (K_d~ 2.0 μM) através da análise das medidas de anisotropia de fluorescência do NR resolvidas no tempo de acordo com um modelo associativo.

Em todas as misturas Lz-A488/lisozima ensaiadas confirmou-se que o lisozima marcado era incorporado nas fibras amilóides maduras através da realização de medidas de CFM. As medidas de anisotropia em estado estacionário e resolvidas no tempo do Lz-A488 revelaram-se extremamente informativas já que permitiram identificar as três fases das cinéticas de fibrilhação de todas as misturas Lz-A488/lisozima, expecto a 1/2. Os tempos de duração das diferentes fases correlacionaram-se bem com os indicados pelas sondas ThT e NR nos ensaios controlo. No caso da mistura 1/2, a anisotropia em estado estacionário do Lz-A488 manteve-se praticamente constante ao longo dos 14 dias de incubação da amostra, resultado este que foi atribuído à ocorrência de migração de energia (homotransferência) entre as proteínas marcadas. Finalmente, os tempos de vida de fluorescência menores medidos para o Lz-A488 incorporado nas fibras amilóides preparadas a partir de amostras contendo proporções mais elevadas de Lz-A488/lisozima (1/2 e 1/8) indicam que a presença de uma grande quantidade de proteína derivatizada na amostra inicial perturba o empacotamento final do Lz-A488 nas fibras.

Por último, estudou-se a capacidade da sonda ThT em reportar a fibrilhação do lisozima na presença de vesículas lipídicas aniónicas. Devido ao seu carácter catiónico, era expectável que esta sonda se ligasse a membranas lipídicas carregadas negativamente, o que foi confirmado através da realização de um estudo da sua partição para lipossomas de POPC contendo proporções variáveis de POPS (10, 20 e 30 mol%) por medidas de fluorescência. Foram também realizados estudos de ligação da sonda ao lisozima monomérico e a fibras amilóide pré-formadas pelo lisozima, na presença e na ausência de vesículas lipídicas aniónicas, de modo a avaliar a competição daqueles dois tipos de estruturas para a ligação da sonda. Os resultados obtidos mostraram que as vesículas lipídicas aniónicas não eram capazes de induzir a formação extensiva de fibras amilóides por parte

do lisozima monomérico. A hipótese de se estabelecer uma interacção forte entre a sonda ThT e as membranas aniónicas que impedisse a sua ligação a estruturas ricas em folhas β foi eliminada através da repetição dos ensaios anteriores com fibras de lisozima pré-formadas. Estes resultados mostram que as variações detectadas, em estudos anteriores, nas propriedades de emissão de fluorescência do Lz-A488 por incubação desta proteína derivatizada com vesículas lipídicas aniónicas serão devidas a alterações na conformação/estado de oligomerização sofridas pelo Lz-A488 sem que ocorra a formação extensiva de agregados com caracteríticas do tipo amilóide.

Palavras-chave

Lisozima; Alexa 488; microscopia e espectroscopia de fluorescência; formação de fibras amilóide; interacção lípido-proteína; sistemas modelo de membranas

Abstract

The ability of anionic lipid membranes to recruit and nucleate amyloid-like assemblies of amyloidogenic proteins/peptides has been a major topic of research. In 2004, Kinnunen and collaborators further extended this concept by proposing that acidic phospholipid-rich membranes could trigger the fibrillation of non-amyloidogenic proteins. Hen egg-white lysozyme is an ideal model non-amyloidogenic protein to investigate this hypothesis as it has been largely used to study the molecular features of protein aggregation in solution.

Previous studies have shown that the fluorescence properties of Alexa488 fluorescently-labeled lysozyme (Lz-A488) in interaction with anionic liposomes critically depended on the protein surface coverage of the liposomes. To clarify the photophysical mechanism underlying these results, thermal denaturation profiles of Lz-A488 were monitored at different pHs using fluorescence spectroscopy. The Alexa488 fluorophore was found to be a sensitive reporter for unfolding transitions of lysozyme due to its sensitivity to a photon-induced electron transfer-based quenching mechanism.

The impact of lysozyme fibrillation on the fluorescence properties of Lz-A488 was also studied using several Lz-A488/lysozyme mixing ratios (1/2, 1/8, 1/40, 1/100 and 1/200). Lz-A488 always formed mixed fibrils with the corresponding unlabeled protein after prolonged incubation at pH 2.2 and 57 ºC. The characteristic stages of nucleation-polymerization kinetics could be clearly identified by tracking the changes in Lz-A488 fluorescence anisotropy during its fibrillation kinetics (mixtures 1/8 to 1/200). Time-resolved fluorescence anisotropy data showed the occurrence of homotransfer between Lz-A488 molecules incorporated in the mixed mature fibrils produced from the mixture 1/2. However, the mixing ratio used affected the final structure of the mixed fibrils produced, as revealed by their mean fluorescence lifetimes.

Finally, competition binding assays of Thioflavin T and lysozyme/ mature lysozyme amyloid fibrils and negatively-charged liposomes were used to show that anionic lipid membranes do not trigger extensive amyloid-like fibril formation of lysozyme at variance with the literature.

Keywords

Hen egg while lysozyme, Alexa 488, fluorescence spectroscopy and microscopy, amyloid fibril formation; lipid-protein interaction; model systems of membranes

Table of Contents

Abbreviations

The acronyms used are expanded on first usage and whenever seemed necessary to improve clarity. For reasons of text economy very common acronyms, scientific or not (such as "RNA" or "USA"), are not expanded nor described. Amino acid residues and sequences are indicated using the one-letter code.

1,8-ANS - 1-anilinonaphthalene-8-sulfonic acid

4LZT – PDB ID of the hen egg white lysozyme protein structure file

A488 – Alexa Fluor 488

A488 SE – Alexa Fluor 488 carboxylic acid, succinimidyl ester (mixed isomers, dilithium salt)

au – arbitrary units

AFM – Atomic Force Microscopy

Aβ - amyloid-β peptide

CD – Circular Dichroism spectroscopy

CF – correction factor

CFM – Confocal Fluorescence Microscopy

Chol - cholesterol

CR – congo red

D/P – dye-to-protein molar ratio

DMSO – dimethylsulphoxide

EC – Enzyme Comission number

EDTA – ethylenediamine-*N,N,N',N'*-tetraacetic acid

FCS – Fluorescence Correlation Spectroscopy

FLIM - Fluorescence Lifetime Imaging Microscopy

HEPES - 4-(2-hydroxyethyl)-1-piperazineethanesulfonic acid

HEWL – hen egg white lysozyme

IAPP - islet amyloid polypeptide

IRF - instrument response function

LUV – large unilamellar vesicle

Lz – lysozyme

Lz-A488 - Alexa 488-fluorescently-labeled lysozyme

NA – numerical aperture

NMR – Nuclear Magnetic Resonance

NR – nile red

PA - phosphatidic acid

PC - phosphatidylcholine

PDB (ID) – Protein Data Bank (identification)

PE - phosphatidylethanolamine

PET - photoinduced electron transfer

PG - phosphatidylglycerol

POPC – 1-palmitoyl-2-oleoyl-*sn*-glycero-3-phosphocholine

POPS – 1-palmitoyl-2-oleoyl-*sn*-glycero-3-phosphoserine

PS - phosphatidylserine

SCOP – structural classification of proteins

SD – standard deviation

SDS - sodium dodecyl sulfate

SM - sphingomyelin

SO – sypro orange

TCSPT - Time-Correlated Single-Photon Timing technique

ThT – thioflavin T

TICT - twisted internal charge transfer

TPE - 2-photon excitation

TTR – transthyretin

UCSF – University of California, San Francisco (San Francisco, California, USA)

UV - ultraviolet

1. Introduction

1.1. Folding and misfolding of proteins

All proteins begin their existence on a ribossome as a linear sequence of amino acid residues. Each polypeptide must fold during and following its synthesis to take up its native conformation and acquire its function. It is believed that the information for proteins' tertiary structure is contained in its amino acid sequence, since each amino acid has a certain propensity to take up a specific secondary structure, like α-helices and β-sheets (Nelson and Cox, 2008). Haber and Anfinsen established in 1962 that the native state of a protein represents its minimum free energy conformation (Haber and Anfinsen, 1962). This concept was revised in the 90's when the folding process of α-lytic protease was proposed to have evolved in a way that is not constrained by the free-energy difference between the native and unfolded states but instead by the size of its unfolding barrier (kinetic rather than thermodynamic control of the folding process) (Sohl *et al*., 1998). Furthermore, it appears that many proteins are natively unfolded in their apo form, and such intrinsically disordered proteins demonstrate that obtaining a functional, defined structure may be dependent upon information outside the amino acid sequence (Hebda and Miranker, 2009).

Protein folding involves multiple pathways in cells and many proteins can only fold correctly with the aid of other proteins (namely chaperones and some enzymes) (Nelson and Cox, 2008). This process cannot be completely random, since the conformational space accessible to a polypeptide chain is astronomically large and proteins fold on a biologically relevant timescale (Bartlett and Radford, 2009). Alternative explanations must be invoked to justify the speed of the folding process, like viewing the folding process as hierarchical, with local secondary structures formed first, guided by molecular interactions established between neighboring amino acid residues, followed by the assemble of these secondary structures until the entire sequence is folded (Bartlett and Radford, 2009). Other possibility is based on the assumption that folding is initiated by a spontaneous collapse of the polypeptide into a 'semi-compact' state, mediated by hydrophobic interactions among nonpolar residues. This state is referred to as a molten globule and is characterized by having a high content of secondary structure but in which many amino acid side chains are still not properly packed (Nelson and Cox, 2008). Nowadays, the folding process is most commonly viewed as a free-energy funnel (Figure 1.1), whereupon semi-stable folding intermediates mark the way to the thermodynamically-stable native structure, guided by the requirement of lowering the global free energy of the protein. As folding progresses, the entropy associated to the different protein conformers decreases, as well as their free energy, and the amount of protein in the native conformation increases in parallel (Bartlett and Radford, 2009).

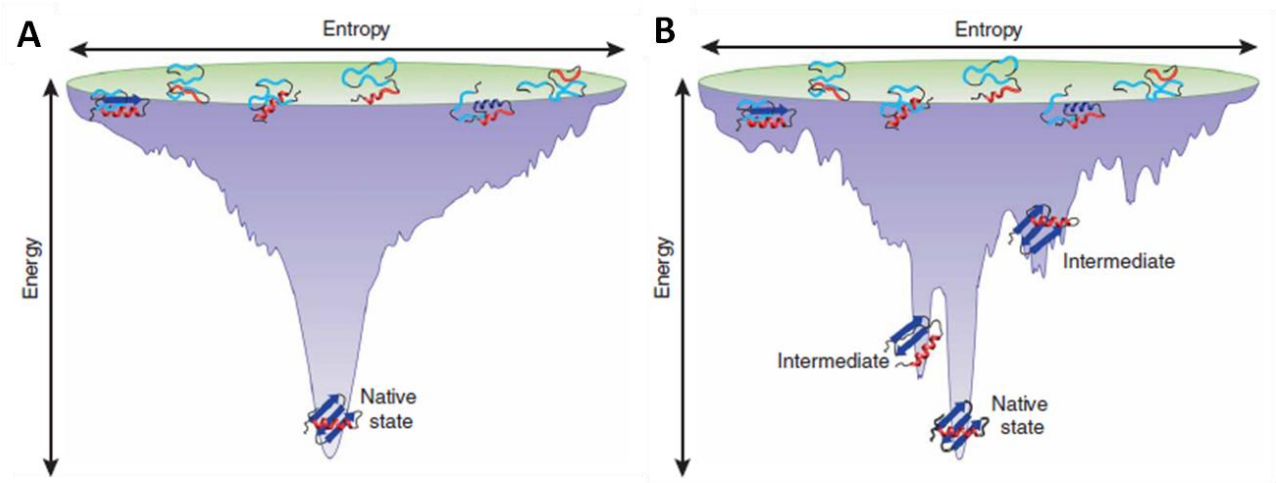

Figure 1.1 – Thermodynamics of protein folding depicted as a free-energy funnel.

(**A**) Ideal folding scenario, in which a protein folds via a two-state transition, only with denatured and native states. (**B**) Rugged landscape in which the polypeptide chain has to navigate, via one or more intermediates, to the native state. Adapted from Bartlett and Radford (2009).

A loss of the three-dimensional protein structure sufficient to cause a loss of its function is called denaturation, which may not be coupled to a complete unfolding of the polypeptide chain. Most proteins can be denatured by heat, extremes of pH, organic solvents (*e.g.* alcohol), detergents or solutes like urea (Dobson, 1999). Heat has a complex effect on the weak hydrogen bonds of a protein; when temperature is increased slowly, the structure remains intact until an abrupt loss of structure usually occurs. This reveals a cooperative transition, where the loss of structure in one part of the protein strongly destabilizes other distant segments. Extremes of pH alter the net charge on the protein, causing electrostatic repulsion and disruption of some hydrogen bonds (Babu and Bhakuni, 1997), whereas the other denaturing agents act primarily by disrupting the hydrophobic interactions that make up the stable core of globular proteins (Nelson and Cox, 2008).

All states available to a peptide or protein must be carefully controlled by the machinery of the cell and its quality control systems. Otherwise, conformational diseases can occur as the disordered states of a protein can easily turn into toxic species. In fact, despite the many cellular processes that assist in protein folding, misfolding may still occur intra- or extracellularly if by some reason a specific peptide or protein fails to adopt or maintain its native functional conformational state (Dobson, 1999). A variety of pathological conditions in humans are associated with a diminishing availability of the protein to play its normal role, or with the conversion of specific peptides or proteins to highly organized fibrillar aggregates, normally referred to as amyloid fibrils (Chiti and Dobson, 2006). In this last case, the misfolding events can often result in a toxic gain-of-function.

1.2. Amyloidogenesis

1.2.1. Amyloid diseases

The term “amyloid” was first used by a german botanist in 1838, to describe a normal amylaceous constituent of plants. In 1854, Virchow used it to describe corpora amylacea in the brain, which he considered identical to starch (Kyle, 2001). Virchow developed the first methods for the detection of amyloid in *ex vivo* material, by staining diseased organ samples with iodine-sulphuric acid treatment (Biancalana and Koide, 2010). This and sodium-sulphuric acid treatment were the first methods to identify extracellular amyloid deposits, followed by the use of metachromatic stains, like methyl violet, which revealed much better than the previous tests. They were eventually replaced by Congo Red (CR) as of 1922 (Kyle, 2001).

Afterwards, the concept of amyloid was expanded to designate diverse localized tissue deposits with the same tinctorial and morphological properties and a similar homogeneous appearance in light microscopy (Rochet and Lansbury Jr, 2000; Sipe *et al*., 2010). The term “intracellular inclusions” has been suggested to describe the fibrils morphologically and structurally related to the extracellular amyloid that are formed inside the cell, sometimes associated with Parkinson’s and Alzheimer’s diseases, for example, like the Lewy bodies or the neurofibrillary tangles, respectively (Chiti and Dobson, 2006; Sipe *et al*., 2010). So the term ‘amyloid’ is nowadays expanded to include these intracellular fibrillar protein deposits. The definition has been further extended to describe synthetic protein fibrils with some amyloid properties. In order to avoid confusion, the Nomenclature Committee of the International Society of Amyloidosis has recommended the use of ‘amyloid-like’ for synthetic fibrils, although this is not fully implemented yet (Westermark *et al*., 2007). Current nomenclature has a list of 27 human and 9 animal fibril proteins, together with a list of 8 inclusion bodies that exhibit some of the properties of amyloid fibrils (Sipe *et al*., 2010).

Amyloidosis is by definition any pathological state associated with the formation of extracellular amyloid deposits. This definition has been generalized to include some intracellular inclusions that are associated with some diseases, as discussed above (Chiti and Dobson, 2006; Sipe *et al*., 2010). A list with some examples of known diseases is given in Table 1.1. No curative treatment is yet available for these amyloid diseases (Dumoulin *et al*., 2005; Groenning, 2010).

Table 1.1 – Human diseases associated with the formation of extracellular amyloid deposits or intracellular inclusions with amyloid-like characteristics.

Adapted from Chiti and Dobson, 2006.

Disease	Aggregating protein or peptide	Number of residues[a]	Native structure of protein or peptide[b]
Alzheimer's disease[c]	Amyloid-β peptide	40 or 42	Natively unfolded
Spongiform encephalopathies[c,e]	Prion protein or fragments thereof	253	Natively unfolded (residues 1-120) and α-helical (residues 121-230)
Parkinson's disease[c]	α-synuclein	140	Natively unfolded
Amyotrophic lateral sclerosis[c]	Superoxide dismutase I	153	All-β, Ig like
Lysozyme amyloidosis[d]	Mutants of lysozyme	130	α+β, lysozyme fold
Type II diabetes[c]	Amylin, also called islet amyloid polypeptide	37	Natively unfolded

[a] Number of residues of the processed polypeptide chains that deposit into aggregates.
[b] According to Structural Classification of Proteins (SCOP).
[c] Predominantly sporadic, although in some cases hereditary forms associated with specific mutations are well documented.
[d] Predominantly hereditary, although in some cases sporadic forms are documented.
[e] Five percent of the cases are transmitted (*e.g.*, iatrogenic).

In each case, a normally soluble protein (like amyloid-β peptide (Aβ) or α-synuclein) self-assembles into β-sheet-rich fibers that ultimately leads cell to death. There are increasing evidences that the prefibrillar intermediates or oligomers are the primary toxic species rather than the mature amyloid fibrils (Aisenbrey *et al.*, 2008; Hebda and Miranker, 2009; Butterfield and Lashuel, 2010). However, being disordered or aggregated is not necessarily a synonym of disease (Figure 1.2). Living systems evolved and apparently some fibrillar assemblies are physiologically useful. The first example of a functional amyloid fiber was demonstrated in *E. coli* and other Gram-negative bacteria, that produce a functional amyloid fiber called curli (Hammer *et al.*, 2008). Others have been found in yeast, fungus and even some human structures, like the p-mel organization in melanosomes. Also, the polypeptide hormones organization when stored in secretory vesicles seem to have an amyloid fibril structure (Chiti and Dobson, 2006; Hammer *et al.*, 2008; Sipe *et al.*, 2010).

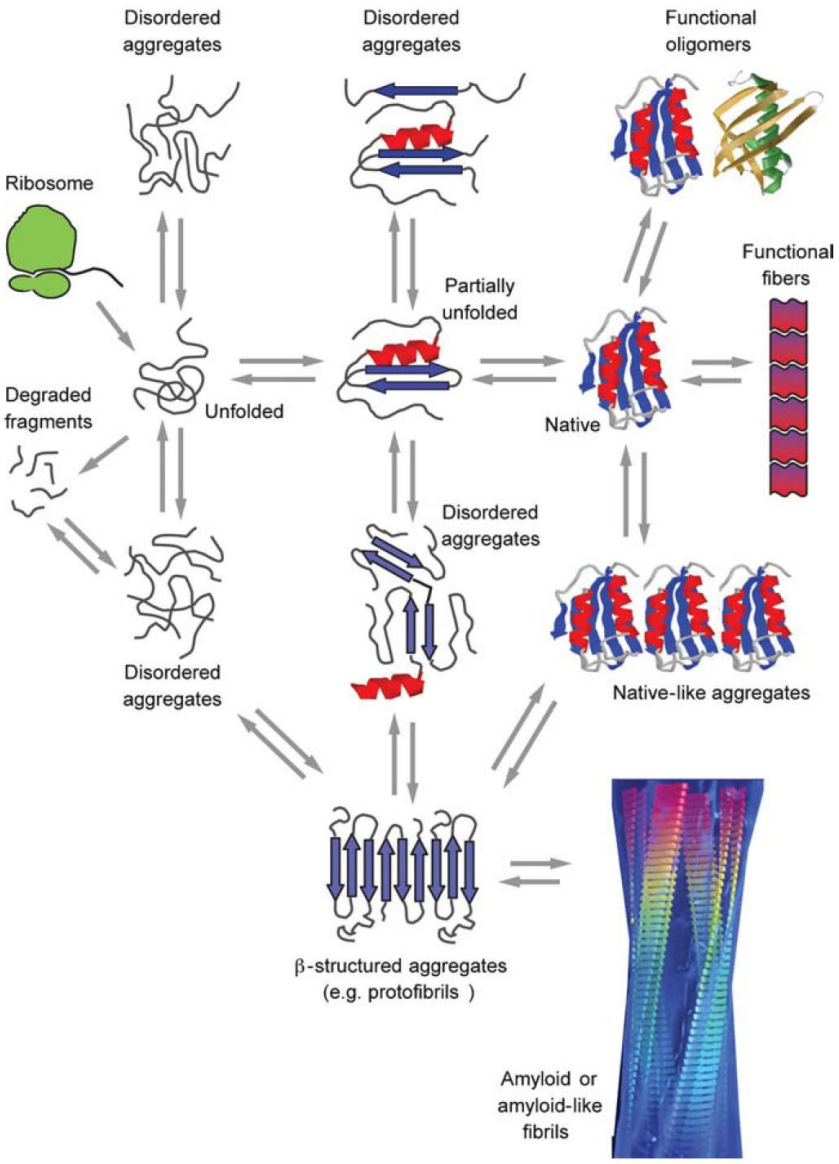

Figure 1.2 – Schematic representation of some of the many conformational states that can be adopted by polypeptide chains.

Polypeptide chains start in an unfolded conformation that can evolve to multiple unfolded or folded states. Not all the aggregated states should be denoted with a disease connotation. Even functional fibers have already been discovered in living systems. Adapted from Chiti and Dobson, 2006.

Some properties of a few characteristic proteins responsible for causing conformational diseases are briefly described next. This will give an insight into the variety of precursors already identified as being causative agents of disease.

Aβ is derived by proteolytic processing from its precursor, β-amyloid precursor protein, and exists as several species of distinct lengths; the most abundant, with 40 residues, is benign while the less abundant variant, with 42 residues, aggregates much faster and is directly related to disease

pathology (Winklhofer *et al.*, 2008). Aβ was shown to accumulate near membranes with charged lipids, which caused an accelerated misfolding into toxic aggregates (Aisenbrey *et al.*, 2008).

The islet amyloid polypeptide (IAPP) can be found within a slender volume near the membrane of insulin secretory granules (Knight *et al.*, 2006). It is a 37-residue peptide hormone normally processed and co-secreted with insulin by the β-cells of the islets of Langerhans (Knight and Miranker, 2004). Amyloid formation by human IAPP in type II diabetes is associated with death of insulin-producing pancreatic islet β-cells (Sparr *et al.*, 2004).

α-synuclein is a small protein (14 kDa), abundant in various regions of the brain and highly conserved. It has an overall low hydrophobicity, a large net charge and its function is not yet fully elucidated (Munishkina *et al.*, 2004). The protein is predominantly unstructured in solution, but it can be divided in three sections: from residues 1-60 is the N-terminus which binds to membrane surfaces and changes its conformation to α-helices; from residues 61-95 is the hydrophobic region which has a high tendency to aggregate into β-sheet-rich amyloid fibrils; residues 96-140 comprise the acidic C-terminus that is unstructured and negatively charged (Thirunavukkuarasu *et al.*, 2008).

1.2.2. Structure of amyloid fibrils

The amyloid precursors do not share a common size, sequence or secondary structure but they form mature amyloid fibrils that present a similar highly organized structure and mechanisms of toxicity (Yonezawa *et al.*, 2002; Chiti and Dobson, 2006). Transmission electron microscopy, atomic force microscopy (AFM), X-ray fiber diffraction, circular dichroism (CD), and more recently solid-state nuclear magnetic resonance (NMR) and single crystal X-ray diffraction analysis (Nilsson, 2009) as well as computational energy minimization procedures and simulations (Smith *et al.*, 1998; Meersman *et al.*, 2010) all contributed to gather structural information about amyloid fibrils. CR birefringence, which can be complemented by CD and Fourier transform infra red spectroscopy, are used to verify β-sheet content (Mishra *et al.*, 2007).

Some common features are accepted to be part of amyloid fibers in general, such as the cross-β X-ray fiber diffraction pattern. Usually they are composed of bundles of 2-6 protofilaments, composed of a core of β-sheets, each with about 2-5 nm in diameter (Munishkina *et al.*, 2004). Depending on the precursor, the β-strands of these sheets can be connected by short loops, or significant portions of the precursor protein may reside outside the fiber core (Hebda and Miranker, 2009). They are usually twisted, unbranched and vary in width. Normally, each filament is displayed in a way that the polypeptide chain forms β-strands that are perpendicular to the long axis

of the fibril while the backbone hydrogen bonds are parallel to the axis (Figure 1.3) (Rochet and Lansbury Jr, 2000; Dumoulin *et al.*, 2005; Groenning, 2010; Biancalana and Koide, 2010). These structures are protease resistant and some molecular probes can bind to intermediates and mature amyloid fibrils, such as the classical markers Thioflavin T (ThT) and CR (Ryan *et al.*, 2008).

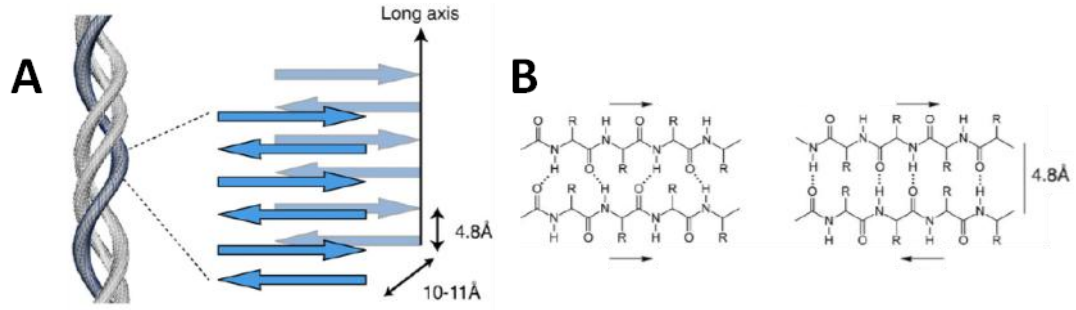

Figure 1.3 – Alignment of polypeptide chains in amyloid fibrils.

(**A**) Schematic representation of a twisted fibril with the polypeptide chains as blue arrows, which are perpendicular to the long axis of the fibril. (**B**) Hydrogen bonds formed between polypeptide chains when displayed parallel or anti-parallel to each other (see the black arrows above the atoms). Adapted from Groenning, 2010 and Biancalana and Koide, 2010.

Using mildly denaturing conditions, the fibrils produced *in vitro* from amyloidogenic proteins or peptides are closely similar to the ones isolated from patients. As an example, the Aβ or the prion protein (Mishra *et al.*, 2011) and α-synuclein (Celej *et al.*, 2008) form fibrils at physiological conditions (such as neutral pH and 37 ºC) but normally require shaking of the solution. Fibrils will adopt the structure that is of lowest free energy and/or the most kinetically accessible (Chiti and Dobson, 2006) and even before molecular structures of amyloid fibrils started to emerge, the idea that there was a significant morphological variation between fibrils formed by the same peptide or protein had already been accepted. These variations may be linked to different arrangements in the position and orientation of the proteins within the fibrils. The deposits found in patients that suffer from any of the amyloid diseases are not only composed by these specific proteins, which normally forms the core of the deposit, but also by other proteins, such as collagen, apolipoprotein E and serum amyloid P component, as well as metal ions or glycosaminoglycans (Kyle, 2001; Chiti and Dobson, 2006; Ryan *et al.*, 2008).

The predisposition to form ordered aggregates is not just associated with disease-causing proteins but to almost any protein when subjected to the appropriate conditions, which are very similar to the ones described above for inducing protein denaturation. A recent study investigated the propensity of 38 different proteins, non disease-related, to form amyloid fibrils, and concluded

that 28 of them formed in fact fibril structures under acidic conditions in the presence of alcohols (Aso *et al*., 2007).

1.2.3. Mechanisms of amyloid fibril formation

Typically, the growth of amyloid fibrils *in vitro* follows a sigmoid kinetic curve that can be described by a nucleation-polymerization pathway, characterized by three stages (Figure 1.4): (*i*) an initial (slow) lag phase, dominated by monomeric constituents that associate into a critical oligomeric nucleus, (*ii*) an elongation phase, when there is a conformational shift to β-sheet and the assembly of monomers into the critical nucleus is now energetically favorable, and (*iii*) a plateau phase, dominated by mature and large amyloid fibrils. The "nucleus" cooperatively and rapidly elongates through monomer addition according to a sigmoidal kinetic curve assembling into protofibrils that will in turn associate to form mature amyloid fibrils. (Munishkina *et al*., 2004; Gorbenko and Kinnunen, 2006; Butterfield and Lashuel, 2010).

The full knowledge of the amyloid formation pathway is far from being totally understood, as this would require structural elucidation of every species and the determination of the kinetics of interconversion of all species on the reaction pathway. It is also difficult to achieve this goal due to the expected large variety of intermediates that are formed transiently and in small quantities that are often too difficult to be detected by the techniques available. This can be really challenging, especially since there is a variety of proteins causative of conformational diseases that may not facilitate or allow the development of a general methodology to isolate and/or to study all the intermediates, independently of their nature.

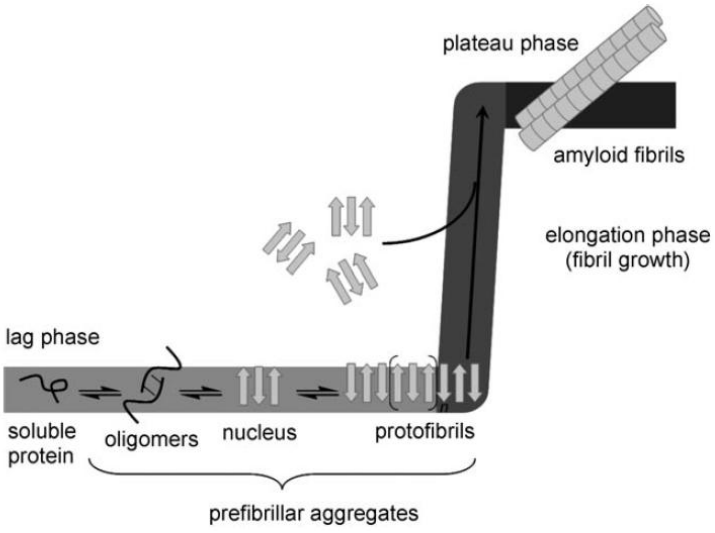

Figure 1.4 – Typical nucleation-polymerization pathway for amyloid fibril formation.
Adapted from Butterfield and Lashuel, 2010.

1.2.4. Biological membranes in amyloidogenesis

Toxicity for living cells is a consequence of the accumulation of the intermediates and amyloid fibrils in amyloidosis. Most recently, it became apparent that the unfolded, metastable intermediates, which exist transiently in the protein aggregation/folding pathways, are the likely origins of pathological behavior (Kinnunen, 2009), probably because they interact with biological membranes. To date, over 10 amyloid systems have been demonstrated to act on biological membranes (Lashuel and Lansbury, 2006) and some are resumed in Table 1.2 (Gorbenko and Kinnunen, 2006).

Table 1.2 – Involvement of membranes in fibril formation by amyloidogenic proteins and peptides.

Cholesterol (Chol), phosphatidic acid (PA), phosphatidylcholine (PC) phosphatidylethanolamine (PE), phosphatidylglycerol (PG), phosphatidylserine (PS), sphingomyelin (SM). Adapted from Gorbenko and Kinnunen, 2006.

Disease	Aggregating protein or peptide	Membrane system	Reference
Alzheimer's disease	Aβ	Total brain lipid bilayers	Yip *et al*., 2001
		PC/PG vesicles	Bokvist *et al*., 2004
	Tau	PS vesicles	Chirita *et al*., 2003
Spongiform encephalopathies	Prion protein	PG, PC, PC/Chol/SM vesicles	Kazlauskaite *et al*., 2003
Parkinson's disease	α-synuclein	PA/PC, PG/PC, PS/PC, PG/PE vesicles	Zhu *et al*., 2003
Systemic amyloidosis	Lysozyme	PC/PS, PC/PG vesicles	Zhao *et al*., 2004
Type II diabetes	IAPP	PG/PC vesicles, liposomes from pancreas lipids	Knight and Miranker, 2004
		PC, PS/PC vesicles, rat insulinoma tumor cells	Sparr *et al*., 2004

The cytotoxicity of the intermediates has been related to the permeabilization and/or disruption of membrane integrity and leakiness of cell membranes, allowing uncontrolled flow of ions into the cell (particularly Ca^{2+}). Sparr and co-workers showed with human IAPP that, in the presence of lipid membranes, the protein aggregates and extracts lipids from the membranes. The extraction of lipids is directly coupled to the process of amyloid formation and to the

permeabilization of the lipid membrane (Sparr *et al*., 2004). In 2005, Quist and co-workers showed that a group of amyloid molecules, namely Aβ(1-40), α-synuclein, IAPP and others, undergo conformational changes in the presence of reconstituted bilayer membranes. They form morphologically compatible ion-channel-like structures, different among them due to the heterogeneity of the peptides, and induce ion-channel activity. These ion channels would destabilize the cell ionic homeostasis and hence induce cell pathophysiology and degeneration in amyloid diseases (Quist *et al*., 2005). Mitochondrial membranes could also be directly affected by the protofibrils. The influx of Ca^{2+} may be sufficient to trigger the permeability transition of the mitochondrial membrane, which leads to the generation of reactive oxygen species and the releasing of cytochrome *c*, which activates apoptotic signals that lead cells to death (Quist *et al*., 2005; Kinnunen, 2009; Hebda and Miranker, 2009).

The nucleation phase of amyloid fibril formation is thermodynamically unfavorable and membranes have been shown to catalyze this process (Hebda and Miranker, 2009). The principal factors responsible for the enhanced formation of fibrils when amyloidogenic proteins/peptides interact with membranes appear to be (*i*) stabilization by membranes of partially folded and flexible aggregation-prone protein confirmations, (*ii*) increase, in a restricted volume, of the local concentration of the protein in the membrane, which in turn favors the interactions among proteins, (*iii*) promotion of particular disposition of the aggregating species relative to a lipid-water interface, (*iv*) variation in the depth of bilayer penetration that affects the nucleation propensity of the protein associated with the membrane and (*v*) the possibility of membranes to serve as templates for protein aggregation (Gorbenko and Kinnunen, 2006; Aisenbrey *et al*., 2008; Hebda and Miranker, 2009). Changes in the physicochemical properties of lipid bilayer associated with pathological processes or aging may increase the binding of proteins to membranes, setting off amyloidogenesis *in vivo* (Gorbenko and Kinnunen, 2006).

The lipidic composition of membranes influence their hydrophobicity, lipid lateral packing density and the net surface charge of the lipid bilayer, largely affecting the interaction between peptides/proteins and the membranes, ultimately shaping all the processes above described. Particularly, negatively-charged phospholipids have been implicated in the enhancement of amyloid fibril formation by amyloidogenic proteins and peptides, although mixtures of other phospholipids (PC and PE) with Chol or SM with Chol have also been seen to promote this formation (Gorbenko and Kinnunen 2006; Kinnunen 2009) (Table 1.2).

More recently, Kinnunen and collaborators proposed that negatively-charged liposomes trigger the formation of amyloid-like assemblies by non-amyloidogenic proteins, like lysozyme,

insulin, myoglobin, transthyretin (TTR), cytocrome *c*, among others, under physiological conditions (Zhao *et al*., 2004). Although presenting different sizes, structures, localizations and functions in cells, all these proteins have cationic residues or cationic amino acid clusters. In this study, the authors used a low lipid/ protein ratio and the buffer solution had a low ionic strength (20 mM HEPES, 0.1 mM EDTA, pH 7.4 buffer); the identification of the fibers consisted on visualizing them by phase contrast microscopy (the authors claim that the fibers became visible after one minute of incubation between the proteins and 1-stearoyl-2-oleoyl-*sn*-glycero-3-phosphocholine/brainPS (8:2 molar ratio) liposomes) and by staining the fibers with CR and with ThT. Since no fibers were seen in the presence of PC only, it appears evident that the presence of negatively charged phospholipids is fundamental in the process of formation of fibers. These investigators proposed that the binding to acidic phospholipids neutralizes the cationic charge in the proteins, facilitating protein-protein interactions (that no longer repulse each other), which in turn promotes protein polymerization and enhances protein fibril formation (Zhao *et al*., 2004). Other studies concerning non-amyloidogenic proteins were later published; some endorse the observations for certain proteins, like lysozyme (Gorbenko *et al*., 2007; Gorbenko and Trusova, 2011) or cytochrome *c* (Alakoskela *et al*., 2006), while others have shown that other non-amyloidogenic peptides/proteins, like endostatin (Zhao *et al*., 2005) and temporins B and L (Mahalka and Kinnunen, 2009) also have this ability to form amyloid-like fibrils in the presence of lipids.

1.3. Lysozyme as a model protein

Lysozyme (EC 3.2.1.17), is the enzyme responsible for the cleavage of the glycosidic linkage β (1-4) between *N*-acetylglucosamine and *N*-acetylmuramic acid in peptidoglycan, the major component of cellular wall in Gram positive bacteria, leading to bacteria death.

Lysozyme amyloid formation has received a considerable attention since in 1993, Pepys and co-workers identified in human lysozyme point mutations associated with hereditary systemic amyloidosis (Pepys *et al*., 1993). Nowadays, different variants have already been identified with one (I56T, F57I, W64R, D67H and T70N) or two (F57I/T70N and T70N/W112R) mutation(s) in the gene that encodes human lysozyme (Figure 1.5) (Dumoulin *et al*., 2005 and 2006; Trexler and Nilsson, 2007). Crystal structures are available for three of them: I56T, D67H and T70N. They closely resemble the wild-type lysozyme (Booth *et al*., 1997; Trexler and Nilsson, 2007); however, the I56T mutant disturbs the interface between α- and β-domain, by introducing a polar side-chain in the hydrophobic protein core, and D67H disrupts the hydrogen bonding arrangement that stabilizes the loop of the β-domain (Booth *et al*., 1997). The results of a comparative study

performed by Dumoulin and co-workers with I56T and D67H mutants suggested that these lysozyme variants have the capacity to form transiently closely similar intermediate species (under physiologically relevant conditions). The two mutations cause a very similar decrease of stability and global cooperativity, despite their different locations and different effects on the native state of the protein, which appears to be the origin of the *in vivo* amyloidogenicity of these two variants of human lysozyme (Dumoulin *et al*., 2005).

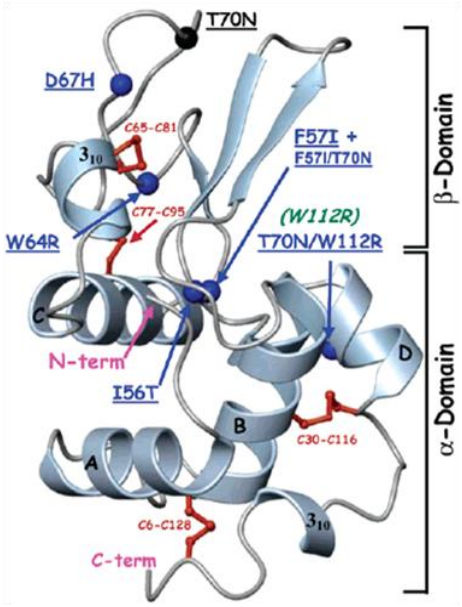

Figure 1.5 – Ribbon diagram of the structure of human wild-type lysozyme showing the locations of the known natural mutations.

The six mutations give rise to seven amyloidogenic variants shown in blue and one non-amyloidogenic variant shown in black. The single point mutant W112R has not yet been detected. Dissulfide bonds are shown in red and the four α-helices in the α-domain are labeled A through D. Adapted from Dumoulin *et al*., 2006.

In 2006, amyloid fibrils formed by human lysozyme at low pH were digested by pepsin and the resulting protease-resistant protein core was identified by mass spectrometry analysis (Frare *et al*., 2006). The data showed that: (*i*) amyloid formation does not require the participation of the entire lysozyme chain, (*ii*) the segment of the protein that appears to form the most stable region of the amyloid core structure, 32–108, includes the β-sheet and helix C of the native protein, and corresponds to the region (approximately residues 31–104) that was previously found to be prone to unfold locally in human lysozyme and its pathogenic variants (I56T and D67H) and (*iii*) that partial unfolding of the native structure of lysozyme is a crucial factor in its conversion to amyloid structure.

Hen egg white lysozyme (HEWL) has been widely used as a model system for protein folding/misfolding studies because it's inexpensive, small, globular and monomeric protein that has

both α- and β-domains and has 60% identity to human lysozyme. It is also very well characterized in functional, structural and stability terms (Yonezawa *et al.*, 2002; Trexler and Nilsson, 2007). HEWL is also an ideal model to study the mechanism of amyloid fibril formation as the variants of human lysozyme forms amyloid fibrils that are related to hereditary systemic amyloidosis (Yonezawa *et al.*, 2002). HEWL has 129 residues comprised in two domains. The α-domain holds the four α-helices of the enzyme, with two 3_{10} helices, and β-domain contains the three β-sheet, a big loop and one 3_{10} helix (Figure 1.6). This protein has 6 tryptophan residues and is strongly stabilized by 4 disulphide bonds (in yellow in the cartoon and light brown in the schematic representation in Figure 1.6, respectively).

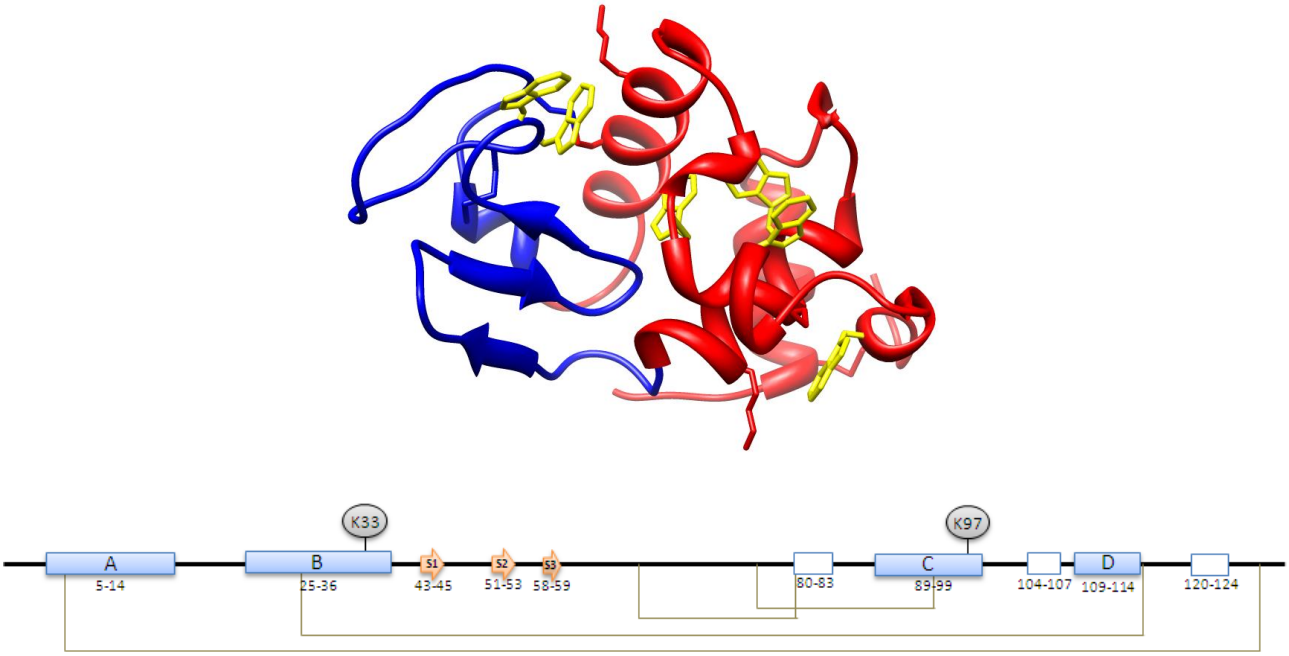

Figure 1.6 - Cartoon representation and schematic secondary structure of HEWL.
The six tryptophan residues are highlighted in yellow and the most reactive lysine residues, K33 and K97, are represented as sticks. α- and β-domain are shown in red and blue, respectively (drawn using UCSF Chimera with PDB ID: 4LZT). Blue boxes represent the four α-helix A-D (filled) and three 3_{10} helical elements (empty), orange filled arrows represent the three β-strands S1-S3 and the connectivity's of the four disulfide bonds C6–C127, C30–C115, C64–C80 and C76–C94 are shown as light brown continuous lines. Grey circles indicate the most reactive K residues.

Some prediction programs indicate that the regions in human lysozyme and HEWL with high aggregation propensity are the same. The aggregation profile of human lysozyme identifies three main "hot spots" corresponding to residues 20–34, 50–62 and 73–104. The equivalent "hot spots" in hen lysozyme comprise residues 24–34, 50–62 and 76 (Groot *et al.*, 2005).

The formation of amyloid fibrils by HEWL *in vitro* has been studied under a variety of denaturing conditions. Krebs and co-workers (Krebs *et al.*, 2000) exploited a variety of conditions,

in particular elevated temperatures, including incubation at 37 ºC and 65 ºC, rapid heating and cooling followed by incubation at 37 ºC, and incubation at low pH (pH 2.0 and 4.0) and neutral pH (pH 7.4) following the addition of organic solvents such as trifuoroethanol. The use of high concentrations of protein, high temperatures and acidic conditions with (Wang *et al.*, 2009; Morshedi *et al.*, 2010) and without stirring (Frare *et al.*, 2004; Mishra *et al.*, 2007; Hill *et al.*, 2009; Meratan *et al.*, 2011) have been frequently reported. Concentrated alcohol solutions have also been investigated (Yonezawa *et al.*, 2002; Holley *et al.*, 2008) as well as studies with the fully reduced lysozyme (Cao *et al.*, 2004). These conditions were found to favor the formation of partially unfolded species that will interact with each other and eventually form amyloid-like fibrils. Partial denaturation of lysozyme appears to be a necessary pre-condition for fibril assembly (Uversky and Fink, 2004); if not, lysozyme monomers have a repulsive effect among them due to the high protein net charge (Hill *et al.*, 2011).

In 2002, Yonezawa and co-workers proposed a pathway for HEWL fibril formation, after studying this process as a function of ethanol and protein concentration using small-angle X-ray scattering experiments, small-angle neutron scattering and CD. They have distinguished several intermediate structures that "evolve" towards fibril formation (Figure 1.7); they were able to distinguish the monomer state, dimer state, the intermediate states of the protofilament formation, the protofilament state (that they've suggested to occur via a nucleation-dependent polymerization pathway), and the intermediate states towards the formation of amyloid fibrils. They have shown that large changes in the secondary structures of HEWL occurred when the dimers were formed, with an increase in β-sheet content (Yonezawa *et al.*, 2002).

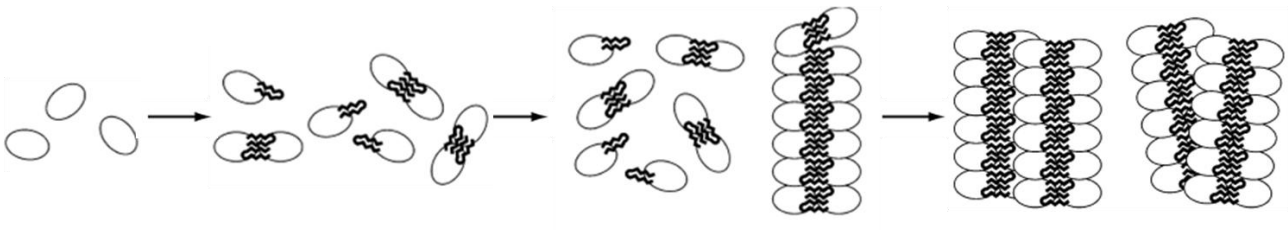

Figure 1.7 – Schematic diagram of the proposed pathway of the amyloid fibril formation of HEWL.

The black zig-zag may denote the hypothetical protrusion induced by ethanol. Since the increase in β-sheet structures was observed during the formation of the dimers, this protrusion may assume the β structure. Adapted from Yonezawa *et al.*, 2002.

Later in 2009, Hill and his team investigated the amyloid fibril formation of HEWL by AFM and dynamic light scattering using approximately 1 mM of protein incubating at pH 2 and 50 ºC,.

They proposed that the amyloid fibril assembly of lysozyme follows a strict hierarchical aggregation pathway, with amyloid monomers, oligomers, and protofibrils forming on-pathway intermediates for assembly into successively more complex structures (Hill *et al*., 2009). A more recent study showed that HEWL assembles into amyloid fibers up to salt concentrations (NaCl) < 350 mM; above this concentration, there is disordered protein precipitation. It was also shown that within low salt concentrations (< 150 mM NaCl) a monomeric assembly prevails involving the nucleation of two filament populations of different length; here, each fibril is composed of three monomeric filaments, and no oligomeric intermediates are detected. With intermediate salt concentrations (150 mM > [NaCl] > 350 mM), oligomeric intermediates are the "building blocks" of fibrils; the assemble of two oligomeric filaments constitutes a fiber (Hill *et al*., 2011). This indeed suggests that there can be a significant morphological variation between fibrils formed by the same peptide or protein, depending on the fibril formation conditions.

Although the human lysozyme and HEWL share only 60 % identity, by understanding the fibril formation pathways of HEWL, including the intermediates involved, a major step forward in the comprehension of amyloid fibril formation would be taken. This information could not only help develop small therapeutic molecules to treat hereditary systemic amyloidosis but would also help unravel the pathways of other disease-causing proteins. For example, it has been stated that the relative sizes and appearance of lysozyme protofibrils and double-stranded fibrils, upon incubation of HEWL in acidic pH and high temperature, share similarities with the morphologies seen in Aβ 1-40 fibrils (Hill *et al*., 2009).

1.4. Some external fluorescent dyes commonly used to study protein stability and aggregation

Whereas the study of native proteins and thermodynamically stable states is usually feasible since it is possible to produce relatively large amounts of these material, it is harder to apply the common used structural techniques to characterize protein aggregates and amyloid fibrils, since the intermediates formed and the final mature aggregates/ amyloid fibrils are normally formed in small quantities and are structurally diverse (Lindgren and Hammarström, 2010). Fluorescence spectroscopy has proved to be very insightful and complementary to more powerful techniques like NMR, electron paramagnetic ressonance and computational approaches to tackle these problems. In fact, fluorescence spectroscopy is one of the most powerful methods to study protein folding, dynamics and interactions. It has also been applied to study membrane structure as well has protein-lipid interactions.

Fluorescence has several advantages that make it an appealing method to use. Almost all proteins have intrinsic fluorophores, which allow the study of local and global changes in the protein conformation upon varying its environment. When proteins are not intrinsically fluorescent or when individual residues cannot be easily followed, it is possible to label proteins with extrinsic fluorophores by chemical modification and mutagenesis. An external probe is likely to have a similar behavior for many proteins and its optimal wavelengths are less likely to be protein-dependent (Munishkina and Fink, 2007; Matulis *et al.*, 2005). Fluorescence spectroscopy has low sample requirements (pM-nM), quick assay times (Mishra *et al*., 2011) and normally a high signal-to-noise ratio; it is also possible to perform ensemble-average measurements (e.g. in a cuvette), follow a single-molecule (fluorescence correlation spectroscopy (FCS)) and do imaging (in a microscope) that gives us spatial information about the sample under study. The fluorescence emission lifetime is usually within the nanosecond range which is convenient to study fast protein conformational changes (Munishkina and Fink, 2007).

In addition to intrinsic fluorophores, a variety of compounds have been developed to function as extrinsic fluorescent dyes. They can be applied in different fields of protein analysis such as characterization of conformational variants or folding intermediates, measurements of surface hydrophobicity and detection of aggregates or fibrils (Hawe *et al.*, 2008). Valuable information about protein structure, unfolding and aggregation can come from the usage of extrinsic fluorescent dyes as they are highly sensitive and versatile tools for protein characterization. Fluorescent dyes can be covalently attached to proteins, *e.g.* via the ε-amino group of lysine or the α-amino group of the N-terminus (*eg*: Alexa Fluor 488 carboxylic acid, succinimidyl ester (A488 SE) Figure 1.8 A) or the thiol group of cysteine, or interact noncovalently with proteins, *e.g.* via hydrophobic or electrostatic interactions (for example 8-anilino-1-naphthalenesulfonic acid (1,8-ANS) or Nile Red (NR), Figure 1.8 B and C, respectively).

Several different probes have been used to monitor the unfolding process of proteins and to learn more about the intermediates formed, including NR, Sypro Orange (SO), dapoxyl sulfonic acid, 4,40-dianilino-1,10-binaphthyl-5,50-disulfonic acid and 1,8-ANS (Sinisterra and Finerty, 2009). The basis for the use of extrinsic dyes for protein characterization comes from the fact that the interaction of the dye with proteins will normally change the preferred relaxation pathway, for example, from radiationless processes to fluorescence emission. Most dyes present low quantum yields in solution that increases upon their binding to hydrophobic patches exposed by the unfolding process or to fibrils (Hawe *et al.*, 2008). Dyes are largely employed to follow fibrillation kinetics assays due to their different characteristics depending on the medium inserted. The signal reported when following their fluorescence emission resembles a sigmoid profile, which reflects the

sigmoid behavior expected in a nucleation-polymerization pathway. The different times reported in each phase depend on the conditions employed to study the fibrillation assay. In a first lag phase, no major variations of parameters can be seen since there are no fibrils in solution and most dyes do not bind to the intermediates formed. In the exponential growth of the fibrils, the fluorescence emission is greatly increased, since the dyes can detect and bind to the species formed in this phase. By the end, a plateau of the signal is reached, which is due to the saturation of the species present.

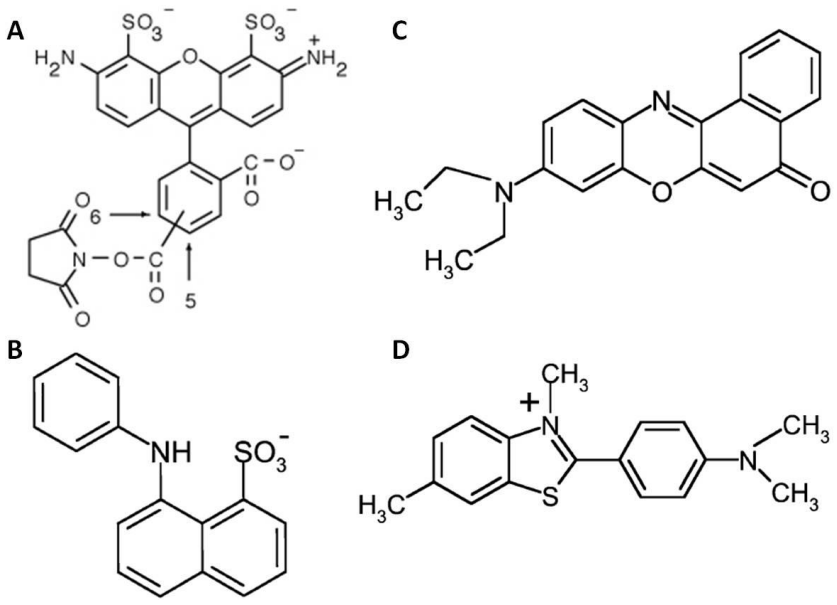

Figure 1.8 - Fluorescent dyes used in the study of proteins.

Different fluorescent dyes can be used to study proteins. Some are used to label covalently proteins like (**A**) A488 SE while others interact noncovalently with proteins, like (**B**) 1,8-ANS and (**C**) Nile Red. (**D**) Thioflavin T is the dye of excellence to probe amyloid structures.

Some properties of the dyes that will be used throughout the work are briefly described next.

1,8-ANS (Figure 1.8 B) is a fluorescent dye that binds with high affinity to hydrophobic surfaces of native or partially unfolded proteins. It belongs to a family of naphthalene derivates with substituted aniline groups. The emission maximum of 1,8-ANS undergoes a blue shift and fluorescence intensity increases significantly upon binding to low polarity regions of a protein surface (Haugland, 2005). The first descriptions of its use were made in the 1950's, namely the study of its interactions with apomyoglobin and apohemoglobin (Hawe *et al.*, 2008). Hydrophobic and electrostatic interactions have been pointed out as the binding mechanism of 1,8-ANS to proteins, but the predominant interaction appears to be ion pairing. This occurs between the negatively charged groups of 1,8-ANS with positively charged amino acids of proteins and van der

Waals interactions are required to stabilize the ion pairs (Hawe *et al.*, 2008). 1,8-ANS is widely used to study the denaturation behavior and thermal stability of proteins (Matulis *et al.*, 2005), unfolding/dissociation processes of multimeric proteins, to identify molten globular states (Haugland, 2005; Hawe *et al.*, 2008) and protein aggregation and prefibrillar/fibrilar states in amyloid kinetic assays (Bolognesi *et al.*, 2010; Lindgren and Hammarström, 2010). However, it has been reported that protein structure can suffer local rearrangements in order to accommodate the dye (Haugland, 2005). It is thus necessary to be aware of conclusions taken exclusively from the use of this dye.

This dye can undergo a twisted internal charge transfer (TICT), which explains the low fluorescence intensity in water and the consequent increase upon binding to hydrophobic surfaces. When a fluorophore contains both an electron donor and an electro acceptor group, which in this case are an electron-donating amino-aryl group and the sulfonated naphthalene system, respectively, upon excitation, there can be an increase in the charge separation within the fluorophore. The polarity of the solvent will dictate which state has the lowest energy. If the solvent is polar the species with the charge separation becomes the one that has the lowest energy state, whereas in a nonpolar solvent, the species without charge separation may have the lowest energy. In the 1,8-ANS case, there is a subsequent twist of the molecules but this is not always needed to the occurrence of internal charge transfer (Lakowicz, 2006; Hawe *et al*., 2008).

NR (Figure 1.8 C) is usually presented as a probe to be used to localize and quantitate lipids, particularly neutral lipid droplets within cells, and that is selective for neutral lipds and suitable for staining lysosomal phospholipid inclusions (Haugland, 2005). NR was indeed used to stain lipid droplets by fluorescence microscopy and flow cytofluorometry in the 80's (Greenspan and Fowler, 1985), and these authors stated that it acts as a hydrophobic probe in which the florescence maxima exhibit a blue-shift proportional to the hydrophobicity of the environment. However, soon after, Sackett and Wolff employed it to probe the formation of hydrophobic surfaces during aggregation and unfolding of proteins (Sackett and Wolff, 1987).

NR is an uncharged, heterocyclic and hydrophobic dye, which is soluble in organic solvents but has poor solubility in water (~1 μM), which makes it almost nonfluorescent in water (Sutter *et al.*, 2007; Mishra *et al.*, 2011). Therefore, it has the tendency to partition into hydrophobic phases. It is a photochemically stable dye whose fluorescence maximum varies, depending on the polarity of the environment. Decreasing polarity leads to a substantial blue shift of the absorption and emission maxima, as well as a marked increase of quantum yield and fluorescence lifetime, which

is explained by TICT, similar to what is verified in 1,8-ANS. In NR, the electron transfer is from the diethylamino group to the aromatic system (Hawe *et al*., 2008; Tajalli *et al*, 2008).

NR has been used to detect proteins in electrophoretic gels (Steinberg *et al*., 1996), for monitoring aggregation of β-galactosidase (Sutter *et al*., 2007) and unfolding of bovine serum albumin (Anand *et al*., 2011). Also, it has been demonstrated to be a versatile dye for detection and characterization of amyloid fibrils grown *in vitro* from bovine insulin, HEWL, TTR, human Aβ1-42 and human prion protein 90-231 in neutral and acid pH. It was also shown to be sensitive to the local structure of the proteins that surround the dye, since it presents different wavelength emission maxima and apparent affinity for the different proteins (Mishra *et al*., 2011).

SO was initially design to detect and stain proteins, noncovalently, in electrophoretic gels, in nanogram levels. It was presented as an alternative to silver, which also stained nucleic acids and bacterial lipopolysaccharides, and to some other fluorescent probes which required covalent labeling (Steinberg *et al*., 1996). It was then employed in high-throughput screening methods, designed to analyze multiple samples with small amounts of material. These assays are based on the increase in fluorescence intensity of the dye SO when bound to hydrophobic areas/regions of thermally unfolded proteins (Lo *et al*., 2004, Hawe *et al*., 2008). Although its structure and molar extinction coefficient are still not publically available (Layton and Hellinga, 2010), SO has been successfully employed to identify optimum formulation conditions for crystallization and purification of proteins, with respect to pH, buffer, excipients and ligands, and to collect thermal denaturation data and characterize binding affinity constants by thermal shift (Lo *et al*., 2004; Hawe *et al*., 2008; Sinisterra and Finerty, 2009; Layton and Hellinga, 2010). Probes like SO come to suit the urge on developing a number of economical and straightforward techniques that allow protein stabilities to be determined, as well as to identify small molecule compounds or inhibitors that interact with the purified proteins. They might serve as starting points for drug/ligand discovery and to improve protein purification and crystallization (Matulis *et al.*, 2005; Sinisterra and Finerty, 2009; Layton and Hellinga, 2010).

The most used fluorescent probe to detect amyloid fibrils is ThT (Figure 1.8 D). This dye is composed by two rings, a benzylamine and a benzathiole ring linked by a carbon bond (Stsiapura *et al*., 2008; Kumar *et al*., 2008; Biancalana and Koide, 2010; Groenning, 2010). ThT was introduced in 1959 by Vassar and Culling to stain amyloid fibrils in tissue sections/histology (Biancalana and Koide, 2010). It was right away compared to CR as being far superior to demonstrate the presence of amyloid. ThT displays an enhanced fluorescence emission when bound to fibrils and a shift in the emission maximum from 445 to 482 nm (Groenning, 2010). The basis for this difference comes

from the fact that ThT functions as a molecular rotor (Stsiapura *et al.*, 2008); when the dye is in aqueous solutions, the two rings rotate freely across the carbon bond that links them and this rotation quenches the molecule excited state. When bound to structures that limit this rotation, the fluorescence quantum yield increases since the loss of excitation by the non-radiative decay process (rotation) is not available (Kumar *et al.*, 2008; Biancalana and Koide, 2010; Groenning, 2010).

The enhanced fluorescence emission is the key element in the usage of this dye to follow amyloid fibril formation. With the increase of structural models for amyloid fibrils, several groups tried to rationalize the binding of ThT to such entities. It is widely accepted that amyloid fibrils share a cross-β architecture and fibril-ThT interactions are explained via the binding of ThT molecules aligned parallel to the long axis of the fiber (Figure 1.9).

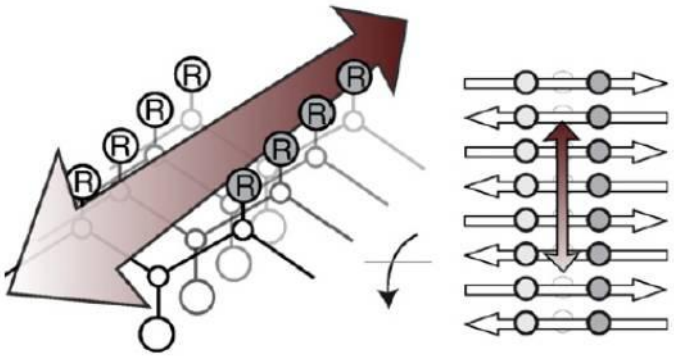

Figure 1.9 – Model proposed to explain the binding of Thioflavin T to amyloid fibrils.
ThT molecules (purple arrow) aligned parallel to the long axis of the fiber, interacting with the polypeptide chains. Adapted from Biancalana and Koide, 2010.

ThT does not affect fibrillation kinetics (or only to a limit extent) (Groenning, 2010). Although considered to be specific for amyloid fibers, several reports show fluorescence enhancement of ThT upon binding to native proteins (*e.g.* AchE), dimers, trimers, large aggregates of β-lactoglobulin, early oligomers formed during the fibrillation of TTR or Aβ, DNA or sodium dodecyl sulfate (SDS) (Kumar *et al.*, 2008; Hawe *et al.*, 2008). These observations highlight the need to confirm if ThT binds to the initial material, if it is going to be used to follow fibrillation kinetics. ThT fluorescence has already been proven to be pH-dependent, upon binding to fibrils of insulin, lysozyme, TTR, human prion protein, and Aβ 1-42, with a 10-fold decrease in intensity upon lowering the pH (Mishra *et al.*, 2011). So different conditions, namely different pH, ionic strength, ThT concentration and amyloid fibril origin (different proteins and different morphologys) must be carefully compared (Groenning, 2010).

1.5. Objectives and thesis organization

An important research line over the last couple of years at the host laboratory has been trying to elucidate whether negatively-charged liposomes can, in fact, trigger the formation of amyloid-like assemblies by non-amyloidogenic proteins under conditions close to physiological, as first proposed by Kinnunen´s group (Zhao *et al*., 2004). In order to elucidate this question, HEWL was chosen as a model non-amyloidogenic protein and its interaction with liposomes prepared with a variable anionic lipid content was studied in great detail using mainly steady-state and time-resolved fluorescence measurements. First, A488 SE was covalently conjugated to lysozyme (Lz-A488) to study its partition behavior towards POPC large unilamellar vesicles (LUVs) containing variable mol% of POPS using FCS. This study confirmed that lysozyme binding to negatively charged liposomes is dominantly driven by electrostatic interactions (Melo *et al*., 2011). Secondly, the variation of Lz-A488 fluorescence properties as a function of total lipid concentration allowed identifying three consecutive stages in lysozyme interaction with acidic lipid vesicles. In this study, it was shown that the critical parameter controlling the photophysical properties of Lz-A488 was the surface coverage of the anionic liposomes by the conjugated protein (Melo *et al.*, 2012).

The results obtained in these experiments, briefly described above, raised the important issue whether the fluorescence properties of the fluorophore Alexa 488 are able to report conformational transitions undergone by lysozyme. This question was first addressed here by monitoring the thermal denaturation of Lz-A488 at both pH 2.2 and 7.4 using fluorescence spectroscopy (both steady-state and time-resolved fluorescence measurements were made). The thermal unfolding of lysozyme is a topic thoroughly studied in the literature, both experimentally and computationally (Arnaudov and Vries, 2005; Lee *et al.*, 2006; Meersman *et al.*, 2010), providing an adequate framework to compare and interpret the fluorescence data obtained in these thermal unfolding studies.

The impact of lysozyme fibrillation on the fluorescence properties of Lz-A488 was also studied by carrying out fibrillation assays at acidic pH and elevated temperature (pH 2.2. and 57 ºC), using two different lysozyme concentrations, namely 0.2 and 1.0 mM. These conditions have already been shown to promote the misfolding and aggregation of lysozyme into amyloid-like fibrils after incubation for some days under quiescent conditions (Frare *et al.*, 2004; Mishra *et al.*, 2007; Hill *et al.*, 2009; Meratan *et al*., 2011). In these studies, the ability of Lz-A488 to form mixed fibrils with lysozyme was first evaluated by performing different fluorescence measurements (both

steady-state and time-resolved fluorescence intensity and anisotropy measurements, and fluorescence imaging). Then, the influence of Lz-A488/lysozyme mixing ratio (1/2, 1/8, 1/40, 1/100 and 1/200) on both the kinetics of lysozyme fibrillation and the structural properties presented by the isolated mature mixed lysozyme fibrils were investigated. Controls assays were carried out in parallel by monitoring lysozyme fibrillation using two amyloid-specific fluorescent probes, ThT and NR. Some additional studies were also performed with NR to characterize its binding affinity to mature isolated lysozyme fibrils using both steady-state and time-resolved fluorescence measurements.

Finally, a fluorescence partition study of ThT towards POPC LUVs containing variable mol% of POPS was carried out. In addition, the ability of ThT spectroscopic properties to detect amyloid-like fibrils in the presence of anionic lipid membranes was addressed by performing competition binding assays of ThT and lysozyme/ mature lysozyme amyloid fibrils and POPC LUVs containing 20mol% of POPS.

2. Materials and Methods

2.1. Materials

Lysozyme (EC 3.2.1.17) from chicken egg white was purchased from Sigma. 1-Palmitoyl-2-oleoyl-*sn*-glycero-3-phosphocholine (POPC) and 1-palmitoyl-2-oleoyl-*sn*-glycero-3-phosphoserine (POPS) (Figure 3.1) were obtained from Avanti Polar Lipids.

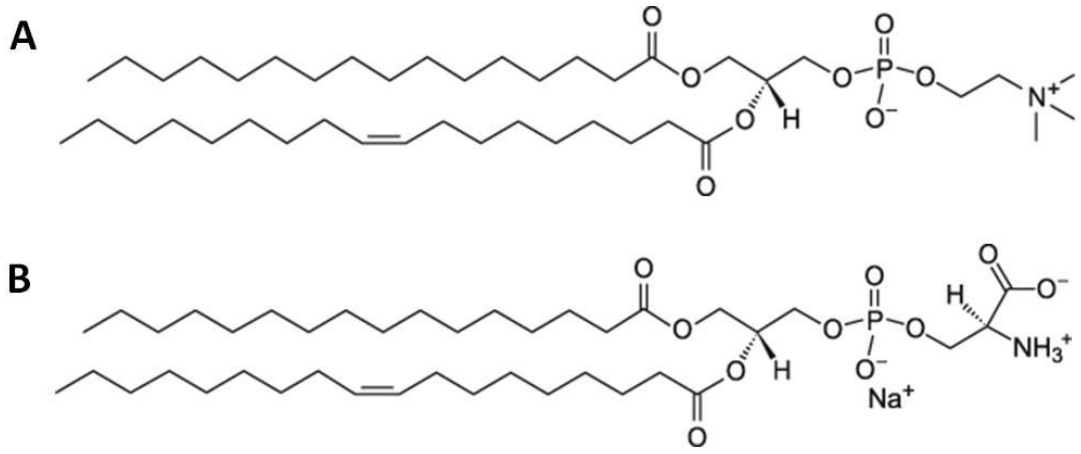

Figure 3.1 - Chemical structures of the phospholipids used in this study.

A - 1-Palmitoyl-2-oleoyl-*sn*-glycero-3-phosphocholine (POPC). **B -** 1-palmitoyl-2-oleoyl-*sn*-glycero-3-phosphoserine (POPS). Adapted from http://avantilipids.com/ (last consulted on 4/8/2012).

The fluorescent probes Alexa Fluor 488 carboxylic acid, succinimidyl ester (mixed isomers, dilithium salt) (A488 SE), NR, 1,8-ANS (Figure 1.8) were obtained from Molecular Probes, Invitrogen. ThT (Figure 1.8) and SO were obtained from Sigma-Aldrich. Tris (tris(hydroxymethyl)aminomethane), potassium hydroxide, ethylenediamine-*N,N,N',N'*-tetraacetic acid (EDTA) and the organic solvents chloroform, methanol and dimethylsulphoxide (DMSO), of spectroscopic UVasol grade, were obtained from Merck. HEPES (4-(2-hydroxyethyl)-1-piperazineethanesulfonic acid), glycine and hydroxylamine were purchased from Sigma-Aldrich. Unless otherwise stated, all other chemicals were purchased from Sigma-Aldrich and used as provided.

The main buffer systems used in this work were (*i*) 20 mM HEPES-KOH, 0.1 mM EDTA, pH 7.4 (HEPES-KOH buffer, pH 7.4), (*ii*) 50 mM glycine, pH 2.2 (glycine buffer, pH 2.2) and (*iii*) 50 mM Tris-HCl, pH 7.4 (Tris-HCl buffer, pH 7.4). The buffer solutions were prepared using ultrapure water produced using a Milli-Q system (>18 MΩ·cm) (Q-Gard 1 Millipore) and were

always filtered with 0.22 μm cellulose acetate filters (Millipore) or with 0.2 μm nylon membrane filters (Sartorius) prior to use.

The stock solutions of the different fluorescent probes were prepared and quantified spectrophotometrically according to the conditions summarized in Table 3.1. The stock solution of NR in methanol was filtered before its spectrophotometric quantification and was kept at 4 ºC. The ThT stock solution was always freshly prepared and filtered using 0.22 μm cellulose acetate filters prior to use.

Table 3.1 - Conditions employed in the preparation and quantification of the different extrinsic dye stock solutions used in this work.

Fluorescent probe	*M*r (g/mol)	Concentration/ solvent of the stock solution	Spectrophotometric quantification		
			λ (nm)	ε ($M^{-1}cm^{-1}$)	Reference
Nile Red	318.37	0.5 mM in methanol	552	4.5×10^4	Haugland, 2005
1,8-ANS	299.34	1.2 mM in: - Glycine buffer, pH 2.2 or - HEPES-KOH buffer, pH 7.4	350	5.0×10^3	Shcharbin *et al*., 2007
Thioflavin T	318.86	1.0 mM in: - Glycine buffer, pH 2.2 or - Tris-HCl buffer, pH 7.4	412	3.6×10^4	Foderá *et al*., 2008

2.2. Fluorescent labeling of lysozyme

Fluorescent labeling of lysozyme on its amine groups with A488 SE was carried out essentially according to the instructions provided by the manufacturer (Haugland, 2005). Briefly, the A488 SE was dissolved in DMSO and added slowly, drop by drop, into 0.75 mM lysozyme in 0.1 M sodium bicarbonate buffer, pH 8.3 under constant stirring. The covalent labeling reaction was allowed to proceed in the dark for 2 h at room temperature using a dye-to-protein molar ratio (D/P) of 2 in the reaction mixture. The labeling reaction was stopped using 1.2 M hydroxylamine freshly prepared at pH 8 - 8.5, followed by a further incubation for 1 h at room temperature. The reaction mixture was then centrifuged at 10 000 × *g* for 10 min at room temperature (centrifuge Sigma 2K15). Lz-A488 was separated from unreacted free probe by gel filtration chromatography using a

Sephadex G-25 (Sigma) column (30.5 cm × 1.6 cm) equilibrated in HEPES-KOH buffer, pH 7.4. Approximately 1 mL fractions were collected manually and characterized spectrophotometrically to determine the labeling ratio of Lz-A488 present in each fraction. The concentrations of A488, $[D]$, and protein, $[P]$, present in each sample, respectively, and its final labeling stoichiometry D/P were calculated using the following equations (Brinkley, 1992; Haugland, 2005):

$$[D] = \frac{Abs_{Dye}^{\lambda_{max}}}{\varepsilon_{Dye}^{\lambda_{max}}} \quad \text{Eq. 3.1}$$

$$CF = \frac{\varepsilon_{Dye}^{280}}{\varepsilon_{Dye}^{\lambda_{max}}} \quad \text{Eq. 3.2}$$

$$[P] = \frac{\left[Abs_{F}^{280} - Abs_{Dye}^{\lambda_{max}} \cdot CF)\right]}{\varepsilon_{P}^{\lambda_{280}}} \quad \text{Eq. 3.3}$$

$$D/P = [D]/[P] \quad \text{Eq. 3.4}$$

where $\varepsilon_{Dye}^{\lambda_{max}}$ and $Abs_{Dye}^{\lambda_{max}}$ are the molar absorption coefficient and absorbance of A488 at its maximum absorption wavelength, λ_{max}, respectively ($\varepsilon_{Dye}^{\lambda_{max}}$= 7.1 × 10^4 $M^{-1}cm^{-1}$ (Haugland, 2005)), $\varepsilon_{P}^{\lambda_{280}}$ and Abs_{F}^{280} are the molar absorption coefficient of lysozyme and the absorbance of each fraction at 280 nm, respectively ($\varepsilon_{P}^{\lambda_{280}}$= 37 680 $M^{-1}cm^{-1}$ (Pace *et al.*, 1995)), and CF is a correction factor that takes into account the contribution of the dye to the sample absorbance at 280 nm (CF = 0.11 for A488; Haugland, 2005). The more concentrated Lz-A488 fractions that presented similar labeling ratios were pooled together and kept at 4 ºC until used. The labeling procedure was repeated once and very similar D/P values were obtained in each case ($(D/P)_1$= 0.69 ± 0.04 (*n*= 3) and $(D/P)_2$= 0.71 ± 0.06 (*n*= 2), respectively).

Some experiments (lysozyme thermal denaturation and fibrillation studies (*vide infra*)) were conducted at pH 2.2. Therefore, Lz-A488 was first dialyzed against glycine buffer, pH 2.2 at room temperature using a mini dialysis kit from Amersham Biosciences (porous membrane cut-off of 8 kDa) to exchange the sample buffer. When necessary, Lz-A488 pooled fractions were concentrated using Amicon® Ultra-15 filter units (cut-off 3 kDa (Millipore)) spun at 5 000 × g and 4 ºC (centrifuge Eppendorf 5804 R). The final Lz-A488 concentrations obtained after these procedures

were always confirmed spectrophotometrically using the molar absorption coefficients presented above.

2.3. Thermal denaturation of lysozyme and A488-fluorescently labeled lysozyme

The thermal stability of Lz-A488 was studied by both steady-state and time-resolved fluorescence measurements at both pH 2.2 and 7.4. Lz-A488 was diluted to 1 μM in glycine buffer, pH 2.2 or HEPES-KOH buffer, pH 7.4, respectively. The samples were introduced in 1 cm × 1 cm fluorescence quartz cuvettes (Hellma Analytics) and their steady-state fluorescence emission spectra were measured as a function of temperature using a spectrofluorimeter containing a Peltier-controlled thermostated cell support. The cuvette temperature was scanned automatically between 20 and 90 ºC (± 0.2 ºC) with 1 ºC increments and allowing 3 minute equilibration at each temperature. The samples were continuously stirred using small magnetic stirrer bars. Control samples containing 0.68 μM of the free dye in each buffer were studied in parallel. The samples were excited at 480 nm and their emission spectra were measured between 490 and 600 nm. The fluorescence intensity decay was also measured as a function of temperature, using λ_{exc}= 340 nm and λ_{em}= 515 nm. In addition, two different extrinsic probes, 1,8-ANS and SO, were used to detect the thermally-induced lysozyme unfolding at each pH. In the first case, the thermal denaturation of 1 μM lysozyme in the presence of 20 μM of 1,8-ANS was followed at both pH 2.2 and 7.4; in the second case, the thermal unfolding of 1 μM lysozyme in the presence of SO (5 × concentration of S5692 Sigma-Aldrich) was studied at pH 7.4. The 1,8-ANS containing samples were excited at 350 nm and their emission spectra were measured between 400 and 650 nm; the SO containing samples were excited at 470 nm and their emission spectra were measured between 480 and 750 nm.

2.4. Kinetics of lysozyme amyloid fibril formation

Lysozyme amyloid fibril formation was initiated by incubating either 0.2 or 1.0 mM lysozyme in glycine buffer, pH 2.2 at 57 ºC (Figure 3.2). Each stock solution of lysozyme was previously centrifuged at 18 320 × *g* for 90 min to ensure that no aggregates remained in solution. At different time intervals, lysozyme stocks were mixed by vortexing for 5 s and an aliquot of 4 μL was withdrawn and mixed with either NR or ThT, to a final volume of 800 μL. The final concentrations in the analyzed samples were 1 or 5 μM protein (on a monomer basis) (obtained

from 0.2 and 1 mM lysozyme stock solutions, respectively) and 2.9 μM NR (in glycine buffer, pH 2.2) or 8.6 μM of ThT (in Tris-HCl buffer, pH 7.4). In parallel, variable mixtures of Lz-A488 and unlabeled lysozyme were prepared using different molar ratios and final total protein concentrations (Table 3.2 and Figure 3.2). These were further treated to form amyloid fibrils in a way similar to that described above (incubation at pH 2.2 and 57 ºC for several days). Again, after vortexing for 5 s the fibrillation mixture under study, an aliquot of 4 μL was withdrawn at different time intervals and diluted 200-fold with glycine buffer, pH 2.2. The final protein concentrations (on a monomer basis) present in each sample obtained at different time points are also summarized in Table 3.2.

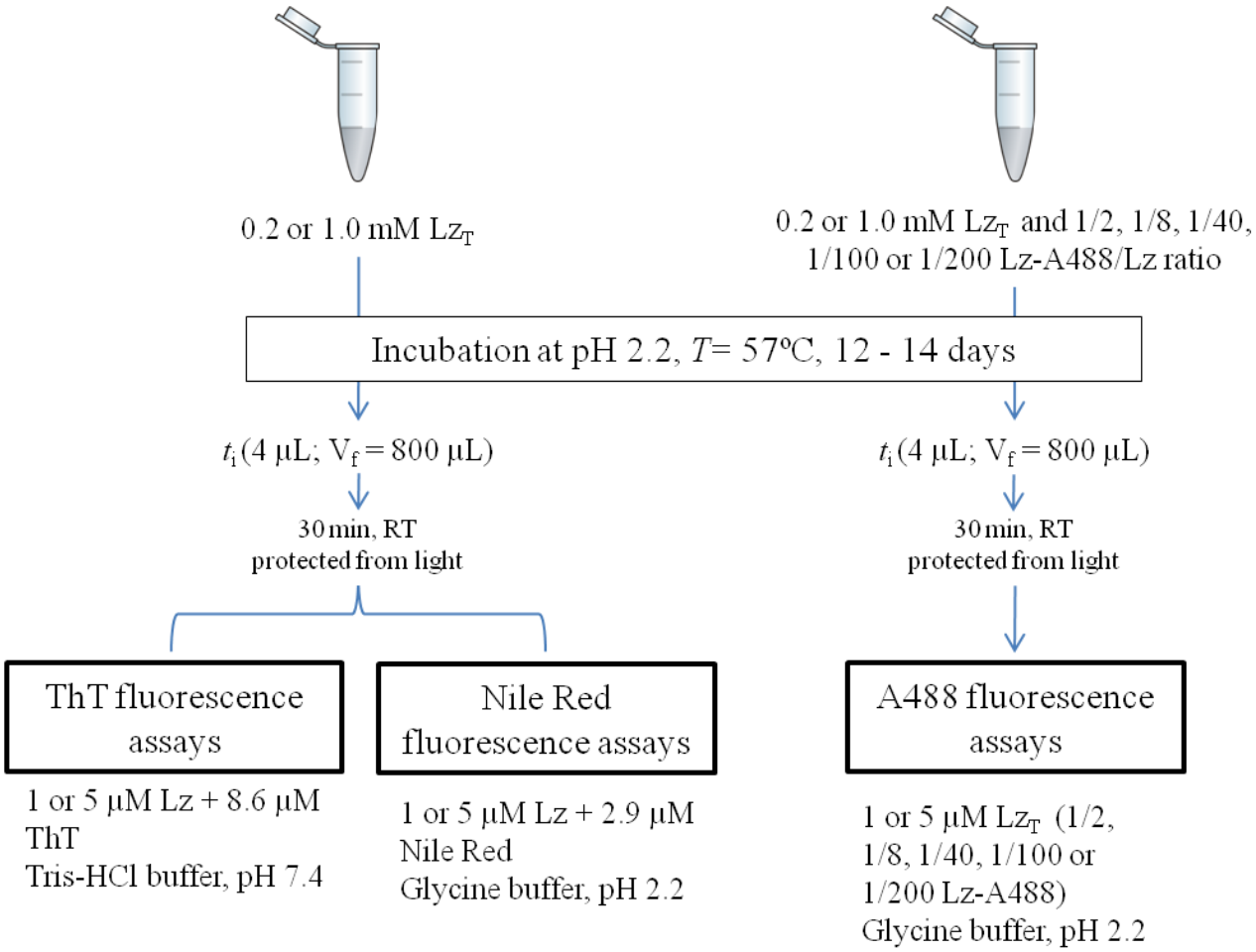

Figure 3.2 - Schematic representation of the experimental procedure used in the study of lysozyme amyloid fibril formation.

Each sample was kept for 30 min at room temperature before measuring their fluorescence emission spectra and steady-state fluorescence anisotropies at 25 ºC using 0.5 cm × 0.5 cm fluorescence quartz cuvettes (Hellma Analytics) (Table 3.3). Time-resolved fluorescence measurements (fluorescence intensity and anisotropy decays) of these samples were also made at 25

ºC (Table 3.3). When necessary, the samples were kept at 4 ºC protected from light before doing these measurements.

Table 3.2 - Total protein, labeled (Lz-A488) and unlabeled lysozyme (Lz) concentrations used in the fibrillation kinetic assays performed at pH 2.2 and 57 ºC.

Variable molar ratios of labeled/unlabeled lysozyme were used during the incubation of lysozyme mixtures in each fibrillation experiment. The final total protein and labeled lysozyme concentrations present in each aliquot obtained at different time points are expressed on a monomer basis.

$[Lz]_T$ (mM)	Incubation fibrillation mixture			Analyzed sample	
	[Lz-A488] (mM)	[Lz] (mM)	Lz-A488/Lz molar ratio	$[Lz]_{total}$ (µM)	[Lz-A488] (µM)
0.2	0.100	0.100	1/2	1	0.500
	0.025	0.175	1/8		0.125
1.0	0.025	0.975	1/40	5	0.125
	0.010	0.990	1/100		0.050
	0.005	0.995	1/200		0.025

Table 3.3 - Excitation and emission wavelengths used in the steady-state and time-resolved fluorescence measurements performed with each sample obtained at different time points during the study of lysozyme fibrillation kinetics at pH 2.2 and 57 ºC.

Fluorescent dye	Fluorescence emission spectra		Steady-state anisotropy measurements		Time-resolved fluorescence measurements	
	λ_{exc} (nm)	λ_{em} (nm)	λ_{exc} (nm)	λ_{em} (nm)	λ_{exc} (nm)	λ_{em} (nm)
Alexa 488	480	490 - 600	495	515	460	515
Thioflavin T	450	470 - 600	450	480	450	480
Nile Red	552	565 - 800	562	636	565	650

2.5. Isolation of mature lysozyme amyloid fibrils

After an incubation period not shorter than 12 days, mature lysozyme amyloid fibrils were isolated by centrifugation (18 320 x *g*, 3 x 60 min). The concentration of protein remaining in the supernatants were determined using the above stated extinction coefficient for lysozyme at 280 nm. The fibril concentration was determined (on a monomer basis) by subtracting the amount of protein in the supernatants from the final amount of lysozyme expected to be present at the end of the fibrillation kinetics and taking into account the final volume in their ressuspension (Meratan *et al.*, 2011).

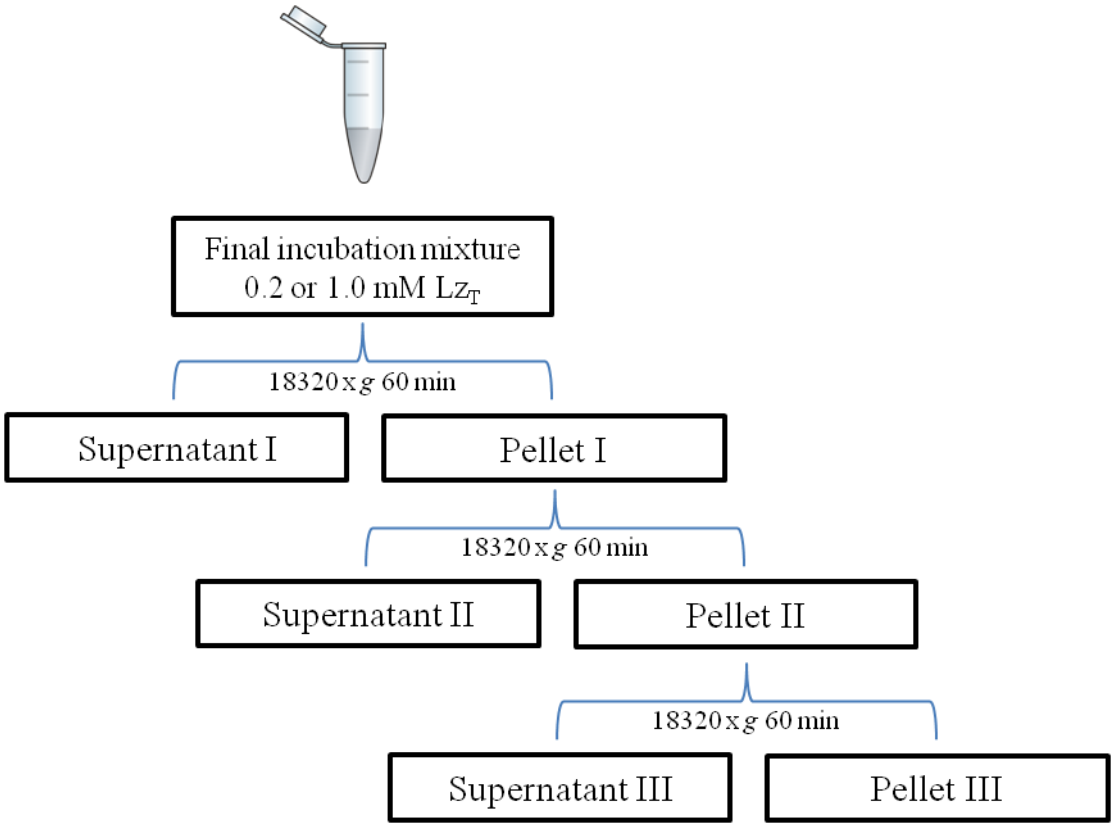

Figure 3.3 – Schematic representation of the protocol used to obtain mature lysozyme fibrils.

The final pellet III was ressuspended in glycine buffer, pH 2.2 and corresponds to the mature isolated lysozyme fibrils. The amount of lysozyme present in each supernatant was quantified spectrophotometrically at 280 nm and subtracted from the final amount of lysozyme expected to be present at the end of the fibrillation kinetics, in order to calculate the final fibril concentration on a monomer basis.

2.5.1. Nile Red binding to mature lysozyme amyloid fibrils

The changes in NR fluorescence properties upon its binding to lysozyme fibrils were used to determine the equilibrium dissociation constant of the dye from amyloid fibrils in glycine buffer, pH 2.2. The same concentration of NR (2.9 μM) was added to freshly and independently prepared fibril samples, ranging from 0 to 115 μM total protein concentration (on a monomer basis). After an incubation time of 30 min at room temperature, the steady-state and time-resolved fluorescence measurements were performed as indicated in Table 3.3.

Considering that NR binding sites in amyloid fibrils are independent of each other, the equilibrium dissociation constant of the dye from lysozyme amyloid fibrils, K_d, is determined as follows (Celej *et al.*, 2008):

$$K_d = \frac{([P]_t - [NR]_b) \times [NR]_f}{[NR]_b} \quad \text{Eq. 3.5}$$

where $[NR]_f$ and $[NR]_b$ are the concentrations of Nile Red free and bound to the fibrils, respectively, $[P]_t$ is the total lysozyme concentration (on a monomer basis) and $([P]_t - [NR]_b)$ represents the concentration of free binding sites. An unitary stoichiometry was considered in describing the binding of the dye to the protein ($NR_f + P \rightleftharpoons NR_b$) since it is difficult to implement more sophisticated thermodynamic techniques to determine the number, nature and distribution of dye-binding sites on the fibrils. Taking into account the mass balance equations:

$$[P]_t = [P]_f + [P]_b \quad \text{Eq. 3.6}$$

$$[NR]_t = [NR]_f + [NR]_b \quad \text{Eq. 3.7}$$

and

$$x_b = \frac{[NR]_b}{[NR]_t} \quad \text{Eq. 3.8}$$

the following Eq. 3.9 is obtained:

$$x_b = \frac{([P]_t + K_d + [NR]_t) - \sqrt{([P]_t + K_d + [NR]_t)^2 - 4 \times [P]_t \times [NR]_t}}{2 \times [NR]_t} \quad \text{Eq. 3.9}$$

The bound molar fraction of the dye, x_b, was calculated by analyzing the fluorescence anisotropy decays of NR obtained in the presence of increasing amounts of lysozyme fibrils according to an associative model (see section 3.2.1.3). Eq. 3.9 was than fitted to the experimental data of x_b *versus* $[P]_t$ by a non-linear least-squares regression method using K_d as the fitting parameter.

2.6. Interaction of lysozyme and mature lysozyme amyloid fibrils with anionic lipid membranes

2.6.1. Preparation of large unilamellar vesicles

LUVs containing POPC mixtures with 10, 20 or 30 mol% POPS were prepared by means of the extrusion technique (Mayer *et al.*, 1986). Stock solutions of POPC and POPS (with approximately 18 mM) were prepared in chloroform and stored at -20ºC and the exact concentrations of these solutions were determined using phosphate analysis (McClare, 1971). Adequate volumes of each phospholipid stock solution were mixed in a round-bottom flask and a thin lipid film was formed by drying the solvent out using a gentle N_2 flow and then further evaporated overnight under an oil pump vacuum. Phospholipid mixtures were hydrated with HEPES-KOH buffer, pH 7.4 and repeatedly vortexed until all lipid was removed from the flask wall. The lipid dispersions were equilibrated by freeze-thaw cycles using liquid nitrogen and a 50 ºC water bath. They were then extruded 31 times through polycarbonate membranes of 100-nm pore size (Nucleopore) using a miniextruder device (Avanti Polar Lipids) with 1001RN syringes (Hamilton). The resulting stock solution was stored at 4 ºC and the lipid vesicles were used within 2 days of preparation.

2.6.2. Thioflavin T partition to anionic lipid membranes

The increase in ThT quantum yield upon its partitioning to POPC LUVS prepared with variable mol% of POPS (10, 20 and 30 mol%) was used to determine the dependence of its membrane partition coefficient with the mol% of anionic phosphoslipid included in the lipid vesicles. A stock solution of ThT in HEPES-KOH buffer, pH 7.4 was freshly prepared before the assay and a constant concentration of 9 µM of ThT was added to LUVs suspensions prepared

independently ranging from 0 to 6 mM total phospholipid concentration. After an incubation time of 1 h at room temperature, the fluorescence emission spectra of ThT was measured between 465 and 700 nm using λ_{exc} = 450 nm. Adequate controls (with the same concentrations of lipid but without ThT) were also prepared in parallel and their fluorescence intensities were subtracted from the corresponding sample.

The mole-fraction ThT partition coefficient, K_p, is an equilibrium constant described as:

$$K_p = \frac{\frac{n_{ThT,L}}{n_L + n_{ThT,L}}}{\frac{n_{ThT,W}}{n_W + n_{ThT,W}}} \quad \text{Eq. 3.10}$$

where n_W and $n_L$are the moles of water and lipid, and $n_{ThT,i}$ are the moles of ThT present in each phase (i=W, aqueous phase; i=L, lipid phase). However, and like in most experimental conditions, $n_W \gg n_{ThT,W}$ and $n_L \gg n_{ThT,L}$ (to avoid deviations from ideal behavior), the definition is simplified to:

$$K_p = \frac{\frac{n_{ThT,L}}{n_L}}{\frac{n_{ThT,W}}{n_W}} \quad \text{Eq. 3.11}$$

The fluorescence intensity of ThT measured will be a sum of the fluorescence intensity of the fraction of ThT present in water and in lipid:

$$I = x_W^{ThT} \cdot I_W^{ThT} + x_L^{ThT} \cdot I_L^{ThT} \quad \text{Eq. 3.12}$$

where $I_W^{ThT}$and $I_L^{ThT}$are the limiting intensity of ThT in water and lipid, respectively, and $x_W^{ThT}$and $x_L^{ThT}$are the molar fractions of ThT in water and lipid, respectively. Considering the mass balance $[ThT]_T = [ThT]_W + [ThT]_L$ and the simplified formulation of the partition coefficient, K_p was determined by fitting Eq. 3.13 to the experimental data obtained at each mol% of POPS by a non-linear least-squares regression method using OriginPro 8 software:

$$\frac{\Delta I}{\Delta I_{max}} = \frac{K_p \cdot [L]_{ac}}{[W] + K_p \cdot [L]_{ac}} \quad \text{Eq. 3.13}$$

where $\Delta I = I - I_W^{ThT}$and $\Delta I_{max} = I_L^{ThT} - I_W^{ThT}$, $[L]_{ac}$ is the accessible lipid concentration (half of the total lipid concentration used in each sample) and $[W]$ is the molar concentration of water (55.5 M at 25

ºC, Santos *et al.*, 2003). A multi-curve fit of the experimental data by Eq. 3.13 was performed by linking ΔI_{max} during the fitting of the three experimental data sets.

2.6.3. Competitive binding of Thioflavin T to mature lysozyme amyloid fibrils and anionic lipid membranes

To evaluate the ability of ThT to detect amyloid fibrils in the presence of anionic lipid membranes, competition binding assays of ThT and lysozyme/ mature lysozyme amyloid fibrils and POPC LUVs containing 20 mol% of POPS to ThT were carried out at room temperature. Briefly, lysozyme or pre-formed lysozyme fibrils, ranging from 0 to 6 μM total protein concentration (on a monomer basis) were added to a fixed concentration of 0.86 mM POPC:POPS 80:20 LUVs. After 1 hour incubation of the LUV-protein mixtures at room temperature, 9 μM ThT was added to each sample. The fluorescence emission intensity of ThT in each sample was then measured between 470 and 600 nm using λ_{exc} = 450 nm after a further incubation period of 30 min. Control samples containing the same concentrations of dye and protein but without lipids were also measured.

2.7. Instrumentation

2.7.1. UV-visible Spectroscopy

UV-visible absorption measurements were carried out at room temperature using a Shimadzu MPC-3100 spectrophotometer (Shimadzu Scientific Instruments). Typically, the absorption spectra were measured in 1 cm x 1 cm or 1 cm x 0.4 cm path length quartz cuvettes (Hellma Analytics) using a bandwidth and sampling interval of 1 nm.

2.7.2. Fluorescence spectroscopy

2.7.2.1. Steady-state fluorescence measurements

Fluorescence measurements were usually performed in a right-angle geometry using 0.5 cm × 0.5 cm width quartz cuvettes and an SLM-AMINCO 8100 spectrofluorometer (SLM Instruments Inc.). This apparatus, which has double excitation and emission monochromators, is fitted with automated rotating Glan-Thompson polarizers and was operated in “photon counting” mode. The light source was a 450-watt Xe arc lamp and the reference was a Rhodamine B quantum counter

solution. The sample temperature was controlled with a water circulating bath from Julabo (model F25). The excitation and emission wavelengths employed in each experiment are described in their respective section of Materials and Methods. Background intensities were always taken into account and subtracted from the measured sample intensities.

The steady-state fluorescence anisotropy, $< r >$, is defined by:

$$< r > = \frac{I_{VV} - G \cdot I_{VH}}{I_{VV} + 2\,G \cdot I_{VH}} \qquad \text{Eq. 3.14}$$

and was obtained by measuring the vertically (parallel, I_{VV}) and horizontally (perpendicular, I_{VH}) polarized components of the fluorescence emission with the excitation polarized vertically. G is an instrumental factor ($G = I_{HV}/I_{HH}$) that corrects for bias in the transmissivity between vertically and horizontally polarized components of the emission introduced by the detection system.

The thermal denaturation studies of lysozyme and Lz-A488 were performed in a HORIBA Jobin Yvon Fluorolog-3-22 spectrofluorometer using 1 cm × 1 cm width quartz cuvettes because this apparatus is equipped with a FI-3751 thermoelectric temperature controller (Wavelength Electronics) which allows programming temperature ramps and automatic data acquisition. This apparatus, which has double excitation and emission monochromators, is fitted with automated rotating Glan-Thompson polarizers and was operated in "photon counting" mode. The light source was a 450-watt Xe lamp and the reference was a silicon diode. The excitation and emission wavelengths employed in each experiment are described in their respective section of Materials and Methods.

2.7.2.2. Time-resolved fluorescence measurements

Time-resolved fluorescence intensity measurements with picosecond resolution were obtained by the time-correlated single-photon timing technique (TCSPT) (Lakowicz, 2006). In some cases, the excitation source was a mode-locked Tsunami titanium:sapphire laser (Spectra Physics) pumped by a Nd.YVO_4 diode laser (model Milennia Xs from Spectra Physics). The exit pulses of this laser present a temporal duration below 100 fs and a continuously tunable output emission over a broad range of near IR wavelengths (λ= 700 – 1000 nm). Its repetition rate was reduced from 80 to 4 MHz by a pulse selector (Angewand Physik and Electronik). Finally, an excitation wavelength of 450 or 460 nm was obtained by frequency doubling using a second harmonic generation system. For excitation at 565 nm, a cavity dumped (3.7 MHz repetition rate)

dye laser of Rhodamine 6G (Coherent 701-2), synchronously pumped by a mode-locked Vanguard 2000-HM532, DPSS green laser (Spectra Physics) was used. Excitation at 340 nm was achieved by frequency doubling this laser system.

The fluorescence intensity decays, $I^{exp}(t)$, were measured with an emission polarizer set at the magic angle (54.7º) relative to the vertically polarized excitation beam. This condition is used to avoid the effects of rotational diffusion and/or anisotropy on the intensity decay (Lakowicz, 2006). The fluorescence was detected by a Hamamatsu R-2809U microchannel plate photomultiplier at the desired wavelength that was selected using a Jobin-Yvon HR320 monochromator in combination with an adequate cut-off filter to avoid interference from Rayleigh-scattered light. The instrument response function (IRF) was recorded as excitation light scattered by a Ludox solution (silica, colloidal water solution from Aldrich). The data were collected in a multichannel analyzer with a time window of 1024 channels, at typically 4 - 20 ps/channel and up to 50 000 and 20 000 counts in the peak channel of the IRF and decay curves, respectively. In some cases, the two components of the fluorescence, polarized parallel, $I_{VV}(t)$) and perpendicular, $I_{VH}(t)$ to the plane of polarization of the excitation beam, were recorded sequentially by alternating the orientation of the emission polarizer every 15, 30 or 60 s. For our setup system, the instrumental *G* factor is expected to be 1 because the polarized fluorescence light components were depolarized before the entrance slit of the monochromator.

Data analysis

The fluorescence intensity decay curves, $I(t)$, were described by a sum of discrete exponential terms:

$$I(t) = \sum_{i=1}^{n} \propto_i \cdot \exp(-t/\tau_i) \qquad \text{Eq. 3.15}$$

where α_i and τ_i are, respectively, the amplitude and the lifetime of the *i*th decay component of fluorescence. Briefly, the kinetic parameters describing each curve (amplitudes, α_i and lifetimes, τ_i) were obtained by iteratively convoluting the empirical function above with the instrumental response function, $IRF(t)$):

$$I_{calc}(t) = I\,(t) \otimes IRF(t) \qquad \text{Eq. 3.16}$$

and fitting $I_{calc}(t)$ to the experimental data, $I_{exp}(t)$ using a non-linear least squares regression method. The usual statistical criteria, namely a reduced χ_G^2 value < 1.3 and a random distribution of weighted residuals and autocorrelation plots, were used to evaluate the goodness of the fits (Lakowicz, 2006). Sometimes, the fit was greatly improved by including an extra very short-lived lifetime component (typically fixed at 5 ps) that allows taking into account the detection of any scattered excitation. Data analysis was performed using the TRFA Data Processing Package version 1.4 (Scientific Software Technologies Centre, Belarusian State University) which allows calculating automatically the confidence interval corresponding to one standard deviation for each fitted parameter (Lakowicz, 2006).

The amplitude-weighted and intensity-weighted mean fluorescence lifetimes, $\langle\tau\rangle_1$ and $\langle\tau\rangle_2$, respectively, were calculated according to:

$$\langle\tau\rangle_1 = \sum_{i=1}^{n} \propto_i \cdot \tau_i \qquad \text{Eq. 3.17}$$

$$\langle\tau\rangle_2 = \frac{\sum_{i=1}^{n} \propto_i . \tau_i{}^2}{\sum_{i=1}^{n} \propto_i \cdot \tau_i} \qquad \text{Eq. 3.18}$$

The anisotropy decay functions, $r(t)$, were described by:

$$r\,(t) = \sum_{i=1}^{n} \beta_i \cdot exp\,(-t/\phi_i) + r_\infty \qquad \text{Eq. 3.19}$$

where β_i and ϕ_i are the initial anisotropy or normalized amplitude and the rotational correlation time of the *i*th decay component of anisotropy, respectively, and r_∞ is the residual anisotropy, containing information about the restriction of the depolarizing processes. In most cases, the time-resolved anisotropy decays were globally analysed using the TRFA Data Processing Package version 1.4 using a two-step procedure. First, the fluorescence decay parameters were obtained by iterative convolution of Eq. 3.15 with the IRF and fitting to the experimental data calculated as:

$$I_m(t) = I_{VV}\,(t) + 2 \cdot G \cdot I_{VH}\,(t) \qquad \text{Eq. 3.20}$$

using a nonlinear least-squares regression methods as previously described. Then, the anisotropy decay parameters were determined by simultaneous iterative convolution of $I_{VV}(t)$ and $I_{VH}(t)$:

$$I_{\mathrm{VV}}(t) = \frac{I(t)}{3}[1 + 2 \cdot r(t)] \qquad \text{Eq. 3.21}$$

$$I_{\mathrm{VH}}(t) = \frac{I(t)}{3}[1 - r(t)] \qquad \text{Eq. 3.22}$$

with the IRF and globally fitting to the experimental parallel and perpendicular polarized components of the fluorescence, $I_{\mathrm{VV}}^{exp}(t)$ and $I_{\mathrm{VH}}^{exp}(t)$, respectively (Lakowicz, 2006), after fixing the fluorescence decay parameters to the values obtained after the first step.

The steady-state fluorescence anisotropy, <*r*>, was used to check the time-resolved data by calculating a *G* factor according to Lakowicz (2006):

$$G = \left(\frac{1 - \langle r \rangle}{1 + 2\langle r \rangle}\right) \cdot \frac{\int_0^\infty I_{\mathrm{VV}}^{exp}(t) \cdot dt}{\int_0^\infty I_{\mathrm{VH}}^{exp}(t) \cdot dt} \qquad \text{Eq. 3.23}$$

As expected, the *G* factors obtained were always very close to 1. To further confirm the adequacy of the fit, the steady-state fluorescence anisotropy was calculated using the parameters obtained from the time-resolved analysis by separate integration of the numerator and denominator of the following equation over time and compared with the experimental steady-state anisotropy value obtained for each sample:

$$\langle r \rangle_{calc} = \frac{\int_0^\infty I(t) \times r(t)\, dt}{\int_0^\infty I(t)\, dt} \qquad \text{Eq. 3.24}$$

An associative model was fitted to the fluorescence anisotropy decays obtained when studying NR binding to lysozyme fibrils using homemade software that uses a nonlinear least-squares reconvolution method based on the Marquardt algoritm (courtesy of Prof. Mário Nuno Berberan Santos).

2.7.2.3. Confocal fluorescence microscopy

Confocal fluorescence microscopy (CFM) of mature lysozyme amyloid fibrils were obtained by placing an aliquot of samples containing A488 or pre-stained with ThT or NR on glass slides (Thermo Fisher Scientific) with 22 x 30 mm cover slips (Thermo Fisher Scientific).

Spatial resolved fluorescence images of the mature fibrils were acquired using an epifluorescence confocal microscope (Leica TCS SP5 from Leica Microsystems) and detected using R9624 photomultiplier tubes (Microsystems). Excitation lines provided by an Ar laser were focused into the sample by an apochromatic water immersion objective (HCX PL Apochromat 63×, 1.2 numerical aperture (NA) (Zeiss)). The emission was detected after passing through a dichroic mirror. A 111.4 µm diameter pinhole placed in front of the image plane blocked out-of-focus signals. The 458 and 514 nm Ar laser lines were used to excite the samples containing mature lysozyme fibrils stained with ThT and NR, respectively (the emission was collected between 470 and 600 nm and between 550 and 690 nm, respectively); the 488 nm Ar laser line was used to excite lysozyme fibrils containing Lz-A488 at variable molar ratios and the emission was collected between 510 and 600 nm.

2.7.2.4. Fluorescence lifetime imaging microscopy

Fluorescence lifetime imaging microscopy (FLIM) was performed using a Becker & Hickl setup in combination with a Leica TCS SP5 inverted microscope (Leica Microsystems). 2-photon excitation (TPE) pulses were generated by a Ti:Sapphire laser (Spectra-Physics Mai Tai BB, 710-990 nm). Pulse trains of 80 MHz (100 fs pulse duration) were produced. The excitation light was directly coupled into the microscope and focused into the sample using a water immersion objective HCX PL Apochromat 63×, NA 1.2. 780 nm TPE was used to excite ThT-stained amyloid fibrils; the emitted light was discriminated from the excitation light by a dichroic beamsplitter (FF665-Di01 (Semrock)) and a short pass dichroic filter (FF01-680/SP (Semrock)). The emission light from the samples was further selected with a 470-500 nm band pass filter and recorded using a PMC-100-4 cooled high speed PMT detection head for photon counting coupled to the X1-port of the microscope. The emitted photons were processed by a Becker & Hickl SPC 830 module that addresses simultaneously the *xy* location of the collected photons. Typically, images were collected with a frame size of 64 × 64 pixels at a scan rate of 400 Hz per frame; the average count rate was 10^3-10^4 counts/s and 250 s of scanning time was used for image acquisition.

Complete fluorescence intensity decays were calculated using a binning of 1 (*i.e.* for each nine pixels: one central pixel and the eight surrounding pixels in a square lattice) and a

biexponential model was fitted by iterative re-convolution with the IRF using the SPCImage software (Becker & Hickl). Typically, a threshold (*i.e.* minimum number of photons in the peak of the fluorescence curve) of 150 was considered in the fitting procedure. The images were pseudocolor-coded according to the amplitude-weighted mean lifetime (Eq. 3.17) of the pixels. In case of the lifetime histogram, the frequency is intensity-weighted, *i.e.* pixels with higher total number of counts have a stronger contribution to the histogram because they are statistically more meaningful.

3. Results and Discussion

3.1. The effect of pH on Lz-A488 fluorescence properties and thermal stability

Lysozyme is an intrinsically fluorescent protein with 6 tryptophan residues (W28, W62, W63, W108, W111 and W123, Figure 1.6). However, 80% of its fluorescence is due to only 2 of these residues (W62 and W108) and they both present a low quantum yield (Imoto *et al.*, 1972). Therefore, lysozyme has been previously covalently conjugated to A488 SE at the host laboratory to increase the sensitivity of the fluorescence assays performed with this protein, in general, and to be able to carry out FCS measurements, in particular (Melo *et al.*, 2011). The A488 fluorophore (Figure 1.8 A) was chosen because it presents several important and desirable properties, namely it is water soluble, has a high photostability and quantum yield, is pH insensitive from pH 4-10 (Haugland, 2005) and has a high fundamental anisotropy (r_0~ 0.38 (Rusinova *et al.*, 2002)). As one of the main goals of this study was to evaluate how well the fluorescence properties of A488 can report conformational alterations undergone by Lz-A488, we started our work by performing thermal denaturation studies of A488-fluorescently labeled lysozyme at both pH 2.2 and 7.4. These two pH values were selected because whereas the protein-lipid interaction studies are most commonly performed at a neutral pH (Zhao *et al.*, 2004; Gorbenko *et al.*, 2007), lysozyme fibrillation kinetics is usually studied *in vitro* using an acidic pH/ elevated temperature and a high protein concentration (Arnaudov and Vries, 2005; Mishra *et al.*, 2007; Meratan *et al.*, 2011). The first step of this study was therefore to study the effect of pH on the photophysics of this fluorophore and on the rotational dynamics of the fluorescently-labeled protein in solution at room temperature.

3.1.1. The fluorescence properties of native Lz-A488 are similar at pH 2.2 and 7.4 at room temperature

Among the commonly used reagents to label amines, active esters, in which are included the succinimidyl esters (*e.g.*, A488 SE, Figure 1.8 A), are the preferred chemistry for conjugates as they produce amide bonds as stable as peptide bonds (Banks and Paquette, 1995).

Lysozyme was covalently labeled with A488 SE at pH 8.3 and separated from unreacted free probe by gel filtration chromatography as illustrated in Figure 3.1 A. The first peak of the chromatogram corresponded to A488-fluorescently labeled lysozyme, while the free dye started to elute after ~ 45 mL. Each collected fraction was characterized spectrophotometrically to determine its dye and protein concentrations and the more concentrated Lz-A488 fractions that presented

similar labeling ratios were pooled together and kept at 4 ºC until used. The labeling procedure was repeated once and very similar D/P values were obtained in both cases ((D/P) ~ 0.70).

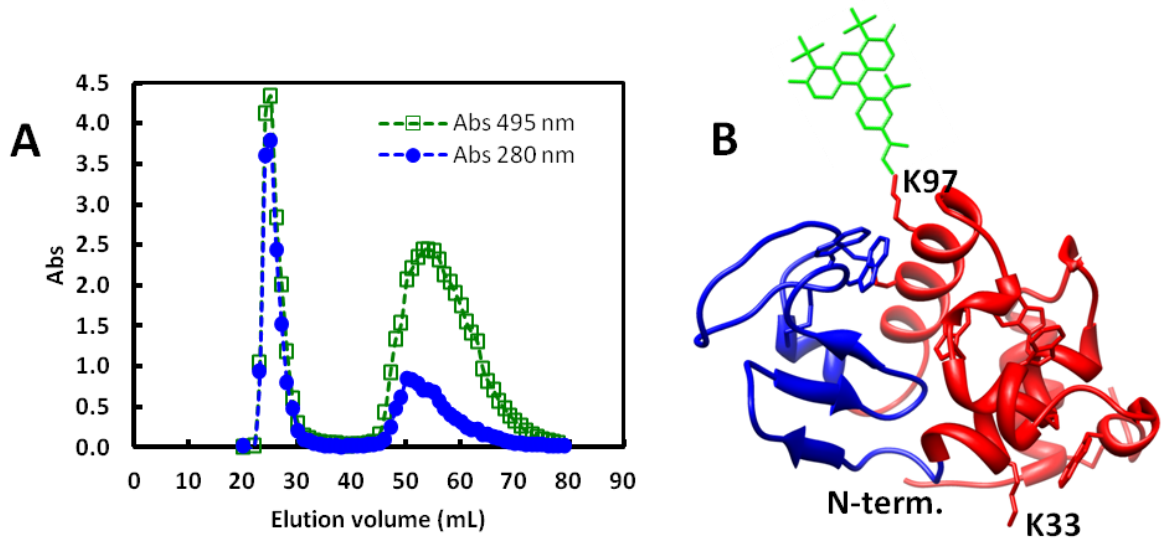

Figure 3.1 - A488-fluorescently labeled lysozyme was separated from free dye by gel filtration chromatography at pH 7.4.

(**A**) Gel filtration chromatography with Sephadex G-25 was used to separate Lz-A488 from free dye (first and second peaks in the chromatogram, respectively). The eluent was HEPES-KOH buffer, pH 7.4. The absorbance of each sample was measured at both 280 nm (blue circles) and 495 nm (green squares). The absorbance scale has arbitrary units. (**B**) Cartoon drawn using UCSF Chimera with PDB ID: 4LZT, representing lysozyme labeled with A488 at residue K97 (one of its most probable labeling sites (Suckau *et al.*, 1992))

It is known that the succinimidyl group reacts with the free base form of aliphatic amines to form stable carboxamides. On HEWL, there are six ε-amino groups of lysine and the *N*-terminal amine. However, K97 and K33 are considered to be the preferably labeling residues at the labelling conditions used (pH 8.3), since the reactivities of K residues on this protein have been previously shown to be primarily dependent on their relative surface accessibilities (Suckau *et al.* 1992). In fact, the major modification sites of lysozyme detected in several studies were K97 and K33, followed by the amino group on the N-terminus and K1 (Suckau *et al.*, 1992; Schnaible and Przybylski, 1999; Teske *et al.*, 2007). Therefore, the first two residues are also the best candidates for the modification site of the protein with the A488 dye given the fact that the conjugation reaction is based on the same chemistry (Teske *et al.*, 2007).

After covalently-labeling lysozyme with A488, the effect of pH on its fluorescence emission properties was characterized in buffer solution at room temperature by both steady-state and time-resolved fluorescence measurements. As a control, a parallel study was performed with the free dye.

The modification of lysozyme with the Alexa dye was confirmed by fluorescence spectroscopy. A 2 nm red-shift was detected in the emission spectra of Lz-A488 as compared to the free dye at each pH value studied (Table 3.1). In addition, the emission spectra obtained for both Lz-A488 and A488 at pH 2.2 were red-shifted 5 nm as compared to the ones measured at pH 7.4 (Table 3.1). Nevertheless, the shape of the spectra remained essentially invariant. The maximum excitation and emission wavelengths obtained for Lz-A488 were in agreement with the values presented by other proteins conjugated to A488 (IgG antibody and Factor VIIa (Haugland, 2005; Rusinova *et al.*, 2002)), as for the free A488 dye (Rusinova *et al.*, 2002; Choi *et al.*, 2011).

Table 3.1 - Maximum excitation and emission wavelengths, λ_{exc}^{max} and λ_{em}^{max} , respectively, and steady-state fluorescence anisotropies, <*r*>, measured for 1.25 μM A488 and 2.6 and 2.1 μM Lz-A488 at pH 2.2 and 7.4, respectively.

Samples were measured in glycine buffer, pH 2.2 or HEPES-KOH buffer, pH 7.4 at room temperature. All the spectra were measured at magic angle conditions. Anisotropy values are presented as mean ± the standard deviation (SD) of ten measurements.

Sample	pH	λ_{exc}^{max} [a] (nm)	λ_{em}^{max} [b] (nm)	<*r*> [c]
A488	2.2	497	517	0.011 ± 0.005
	7.4	492	512	0.013 ± 0.005
Lz-A488	2.2	497	519	0.214 ± 0.006
	7.4	493	514	0.200 ± 0.006

[a] λ_{em} = 540 nm; excitation and emission bandwidths of 2 and 8 nm, respectively;

[b] λ_{exc} = 480 nm; excitation and emission bandwidths of 2 and 8 nm, respectively;

[c] λ_{exc} = 495 nm; λ_{em} = 515 nm; excitation and emission bandwidths of 2 and 4 nm, respectively;

The fluorescence intensity decays of free A488 dye were well described by a mono-exponential function, presenting a lifetime of 4.0 ns at both pH studied (Table 3.2 and Figure 3.3). These values are close to the ones previously described by the manufacturer (τ= 4.1 ns (Haugland, 2005)) and reported in the literature (τ= 4 ns and τ= 3.8 ± 0.1 ns, both at pH 7, described by Chen *et al.*, 2010 and Choi *et al.*, 2011, respectively). In contrast, the fluorescence decay kinetics of the A488 dye covalently attached to lysozyme was best fitted to a sum of three exponentials in buffer

solution at pH 2.2 and 7.4 (Table 3.2 and Figure 3.3). At 25 ºC, the native Lz-A488 exhibited a nearly mono-exponential fluorescence intensity decay with a main lifetime component of 3.6 – 3.7 ns (fractional amplitude ~ 0.6 – 0.7). The fractional amplitudes of the short- and intermediate-lived species detected (τ_1~ 0.1 – 0.2 ns and τ_2~ 1.7 - 2 ns) were about 0.1 – 0.2 and 0.2, respectively (Table 3.2). In principle, the complex fluorescence decay could result from different lysozyme molecules being labeled at distinct sites (ground-state heterogeneity) and/or due to local structural fluctuations of the polypeptide backbone of the native enzyme.

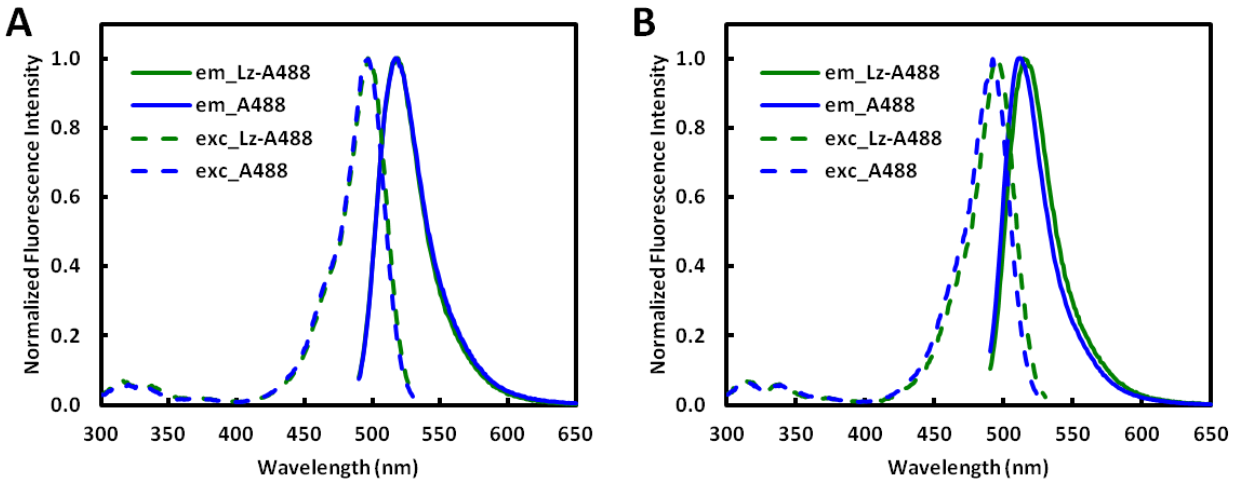

Figure 3.2 - Fluorescence excitation and emission spectra of Lz-A488 and A488 at (A) pH 2.2 and (B) pH 7.4.

Lz-A488 and A488 spectra are represented green and blue, respectively. Emission and excitation spectra are continuous and dotted lines, respectively. For additional details, see the legend of Table 3.1.

Finally, and in order to evaluate if Lz-A488 had partially unfolded at pH 2.2 as compared to pH 7.4, its nanosecond rotational dynamics was also measured in buffer solution at both pH. Time-resolved fluorescence anisotropy measurements provide information on both the amplitude of motion, β_i, and the time scale, ϕ_i, on which this motion occurs. As expected, the A488 fluorophore rapidly depolarized its fluorescence emission to 0 at both pH values (Figure 3.4), presenting a fast rotational correlation time of ~ 0.15 ns (Table 3.3) in agreement with its low molecular weight. This behavior is responsible for the low steady-state fluorescence anisotropy measured for the free dye in solution, $\langle r \rangle = 0.011 \pm 0.005$ (pH 2.2) and $\langle r \rangle = 0.013 \pm 0.005$ (pH 7.4) (Table 3.1).

Table 3.2 - Mean fluorescence lifetimes and intensity decay parameters from 1.25 μM A488 and 2.6 and 2.1 μM Lz-A488 at pH 2.2 and 7.4.

The fluorescence emission kinetics were measured using λ_{exc}= 460 nm and λ_{em}= 515 nm. α_i , normalized amplitudes; τ_i, fluorescence lifetimes; $<\tau>_1$ and $<\tau>_2$, amplitude-weighted and intensity-weighted mean fluorescence lifetimes, respectively. The goodness-of-fit was judged by the χ_G^2 value. Values in brackets are the errors of the recovered parameters estimated as the lower and upper bound of the joint confidence interval calculated for a 67% probability level. For additional details, see the legend of Table 3.1.

Sample	pH	α_1	τ_1 (ns)	α_2	τ_2 (ns)	α_3	τ_3 (ns)	$<\tau>_1$ (ns)	$<\tau>_2$ (ns)	χ_G^2
A488	2.2	1.00	4.1 [4.1,4.1]					4.1	4.1	1.09
	7.4	1.00	4.0 [4.0,4.0]					4.0	4.0	1.15
Lz-A488	2.2	0.24	0.11 [0.09,0.11]	0.20	1.7 [1.5,1.8]	0.56	3.6 [3.6,3.6]	2.9	3.4	1.15
	7.4	0.10	0.19 [0.16,0.22]	0.24	2.0 [1.7,2.1]	0.66	3.7 [3.6,3.7]	2.9	3.4	1.12

On the other hand, two rotational correlation times were necessary to describe the anisotropy decay of Lz-A488 in both buffer solutions (Figure 3.4 and Table 3.3). Since the long rotational correlation time (ϕ_2= 5.6 ns (Table 3.3)) was significantly longer than the short one (ϕ_1~ 0.1 – 0.2 ns (Table 3.3)), the total anisotropy can be interpreted as a product of two independent depolarizing processes: the first one (fast) due to segmental, rapid restricted movements of the covalently linked flurophore and the second one (slow) due to global rotation of the protein (Lakowicz, 2006; Pastor *et al.*, 2007):

$$r(t) = r_{slow}(t) \times r_{fast}(t) \qquad \text{Eq. 3.1}$$

where

$$r_{slow}(t) = \exp\left(-\frac{t}{\phi_{\text{global}}}\right) \qquad \text{Eq. 3.2}$$

and

$$r_{fast}(t) = r(0)\left[(1 - S_{seg}^2) \times \exp\left(-\frac{t}{\phi_{\text{segmental}}}\right) \times S_{seg}^2\right] \quad \text{Eq. 3.3}$$

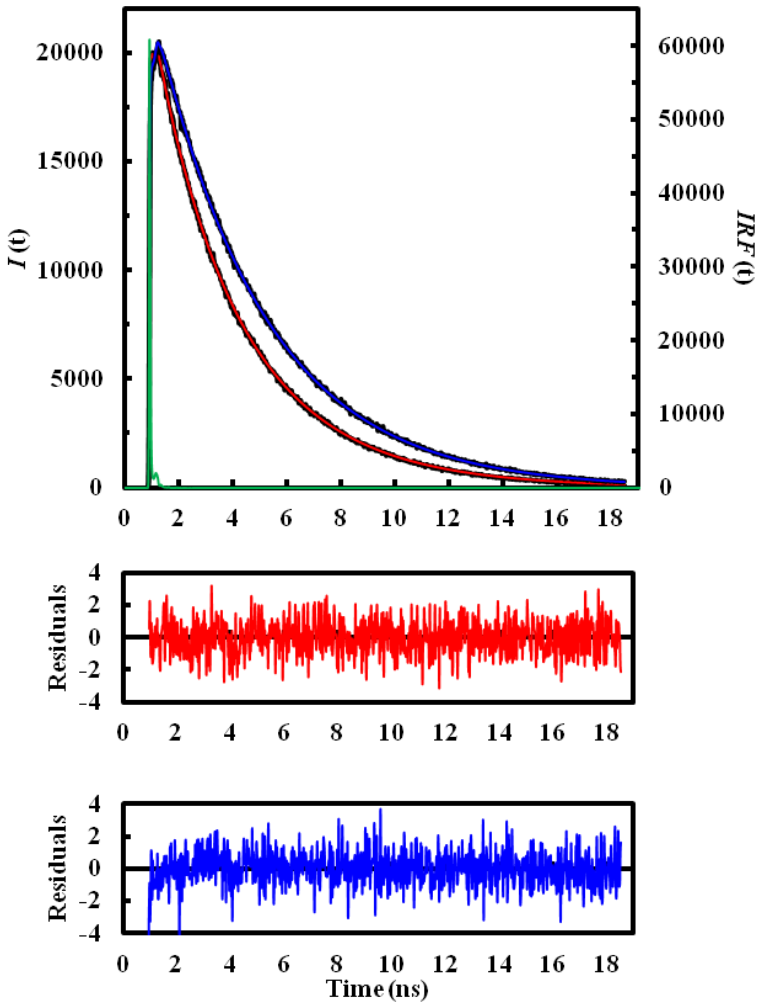

Figure 3.3 – Fluorescence intensity decays from 1.25 μM A488 and 2.1 μM Lz-A488 at pH 7.4.
The red and blue lines are the best fits of Eq. 3.15 to the experimental data from Lz-A488 and free A488 at pH 7.4, respectively. The fits obtained for pH 2.2 are very similar (not shown, see Table 3.2. for values). The green line is the instrumental response function, IRF(*t*), of the laser system. For additional details, see the legend of Table 3.2.

S_{seg} is an order parameter that characterizes the restricted range of internal angular fluctuations of the protein segment containing the covalently-bound dye (Figure 3.4 inset). It can be calculated using Eq. 3.4, being β_i the fractional anisotropies that decay with correlation times ϕ_i, which were empirically fitted to the decays (Pastor *et al.*, 2007):

$$S_{seg}^2 = \frac{\beta_2}{\beta_1 + \beta_2} \quad \text{Eq. 3.4}$$

On the other hand, the short and long rotational correlation times obtained from the fit are related to ϕ_{global} and $\phi_{segmental}$ by Eq. 3.5 and Eq. 3.6, respectively:

$$\phi_2 = \phi_{global} \qquad \text{Eq. 3.5}$$

$$\phi_1 = \frac{\phi_{global} \times \phi_{segmental}}{\phi_{global} + \phi_{segmental}} \qquad \text{Eq. 3.6}$$

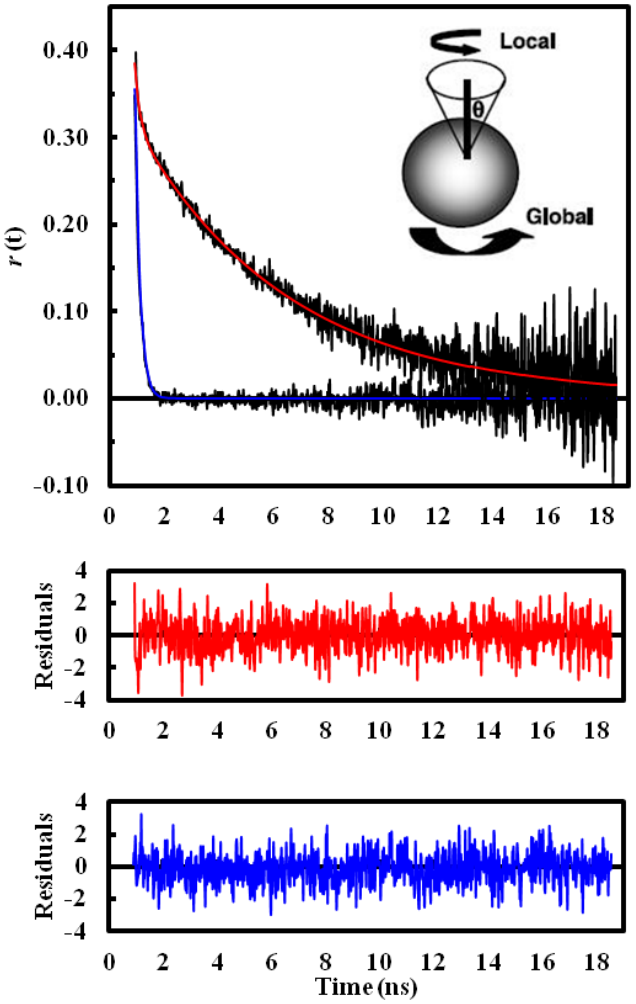

Figure 3.4 – Fluorescence anisotropy decays from 1.25 µM A488 and 2.1 µM Lz-A488 at pH 7.4.

The red and blue lines are the best fits of Eq. 3.19 to the experimental data from Lz-A488 and free A488, respectively. For additional details, see the legend of Table 3.3. **Inset:** Local and global rotational motions detected when a fluorophore is linked covalently to a protein assuming a wobbling-in-cone model. $\boldsymbol{\theta}$ is the cone semi-angle, the maximum rotation allowed for the fluorophore. Adapted from Mukhopadhyay *et al.*, 2006.

Table 3.3 - Fluorescence anisotropy decay parameters from 1.25 μM free A488 and 2.6 and 2.1 μM Lz-A488 at pH 2.2 and 7.4, respectively.

The anisotropy decays were measured using λ_{exc}= 460 nm and λ_{em}= 515 nm. β_i, fractional amplitudes; ϕ_i, rotational correlation time; r(0)= β_1 + β_2. $<r>_{calc}$ was calculated according to Eq. 3.24. For additional details, see the legend of Table 3.2.

Sample	pH	r(0)	β_1	ϕ_1 (ns)	β_2	ϕ_2 (ns)	χ^2_G	$<r>_{calc}$
A488	2.2	0.36	0.36	0.15 [0.15,0.15]			1.16	0.013
	7.4	0.36	0.36	0.15 [0.15,0.16]			1.04	0.013
Lz-A488	2.2	0.39	0.06	0.10 [0.06,---]	0.33	5.6 [5.4,5.7]	1.04	0.211
	7.4	0.39	0.07	0.16 [0.12, ---]	0.31	5.6 [5.5,5.8]	1.22	0.200

Note that since $\phi_2 \gg \phi_1$, then $\phi_2$can be pointed as the ϕ_{global} (Eq. 3.5). The value obtained for ϕ_{global} = 5.6 ns (Table 3.3) can be compared with the theoretical prediction for the rotation of native lysozyme considered as a rigid hydrated sphere according to Eq. 3.7 (Lakowicz, 2006):

$$\phi = \frac{\eta \times M_r}{R \times T}(\bar{v} + h) \qquad \text{Eq. 3.7}$$

where η is the solvent viscosity (1 cP), M_r is the relative molecular mass of lysozyme (14 300), R is the ideal gas constant (R= 8.314 J K^{-1} mol^{-1}) , T is the absolute temperature (T= 295 K), $\bar{v}$ is the partial specific volume of the protein and h its hydration. Assuming 20% hydration and $\bar{v}$= 0.74 cm^3/g, the correlation time for the overall lysozyme rotation is calculated to be 5.2 ns, which is in close agreement to the experimental value (ϕ = 5.6 ns (Table 3.3)) and indicates that the lysozyme is properly folded at both pH values. This was expected since previous studies (using CD) indicated that the secondary and tertiary structures of the native protein did not change significantly in acidic solution up to pH 0.64 (Frare *et al*., 2004).

The segmental correlation time ($\phi_{segmental}$= 0.11 e 0.16 ns, pH 2.2. and 7.4, respectively) reflects an average of the fast localized motions of the covalently-bound fluorescent dye. The range of angular displacement of these motions can be derived from S_{seg} assuming a "wobbling-in-cone"

model (Kinosita *et al.*, 1977), in which a vector associated with the chromophore (in our case, the transition dipole moment) is assumed to move freely within a cone with fixed semi-angle (Figure 3.4 inset). From this model, the semi-angle θ_{seg} of the cone within which the segment containing the covalently-attached dye freely rotates is given by (Czeslik *et al.*, 2003):

$$\cos\theta_{seg} = \frac{1}{2}\left[\left(8 \times S_{seg} + 1\right)^{\frac{1}{2}} - 1\right] \qquad \text{Eq. 3.8}$$

An angle of θ_{seg} = 19.1º and 21.5º was obtained for the dye covalently-bound to lysozyme in buffer at pH 2.2 and 7.4, respectively, suggesting that this segment experiences relatively little angular displacement with respect to the protein as a whole during the fluorophore excited lifetime. The constraints on the local motions of the dye are due to the short covalent linkage between the dye and the macromolecule (Figure 1.8 A) and steric hindrances caused by the protein surface, as well as to possible electrostatic interactions between the negatively charged dye and the protein. Altogether, the overall tumbling motion of Lz-A488 in buffer solution dominates the depolarization of its fluorescence emission, being responsible for its relatively large steady-state value measured at both pH (<*r*>= 0.214 ± 0.006 (pH 2.2) and <*r*>= 0.200 ± 0.006 (pH 7.4) (Table 3.1)).

The apparent "zero-time" anisotropy, $r(0) = \beta_1 + \beta_2 = 0.39$ measured for Lz-A488 is close to the value measured for A488 in a rigid environment (100% glycerol at -10 ºC), r_0= 0.376 ± 0.003 (Rusinova *et al.*, 2002), assuring that no very fast movements of the dye covalently-bound to the native protein were missed in the anisotropy analysis.

Summarizing, lysozyme was successfully covalently tagged with A488. Its fluorescence emission properties were found to be essentially identical in buffer solution at room temperature at both pH 2.2 and 7.4. In addition, time-resolved fluorescence anisotropy decays indicated that the protein is properly folded in both conditions and that the covalently-bound dye experiences a restricted range of internal angular fluctuations during its excite-sate fluorescence lifetime.

3.1.2. Lysozyme is more thermally unstable at pH 2.2 than at pH 7.4

The next step of this work was to compare the thermal denaturation profiles of Lz-A488 obtained at pH 2.2 and 7.4 in order to evaluate the ability of the covalently-conjugated fluorophore A488 to report conformational changes undergone by the fluorescently-labeled lysozyme under known destabilizing conditions. In this section, the thermal denaturation data obtained for Lz-A488

at both pH using fluorescence spectroscopy will be first described; complementary studies made with lysozyme and the extrinsic dyes 1,8-ANS and SO will be presented next.

3.1.2.1. Thermal denaturation study of Lz-A488 at pH 7.4

The thermal stability of 1 µM Lz-A488 was measured by fluorescence spectroscopy. Upon increasing the solution temperature at pH 7.4, the intensity of its steady-state fluorescence emission spectra progressively decreased, gradually at the beginning and then steeper (Figure 3.5 A). From 20 to 90 ºC, there is an overall decrease in Lz-A488 fluorescence intensity of about 80%, whereas the intensity of the 0.7 µM free probe decreases only ~20% within the same temperature range (Figure 3.5 B). Simultaneously, the maximum emission wavelength of Lz-A488 and free A488 were essentially temperature-independent (λ_{em}^{max}= (519 ± 1) nm for Lz-A488 and (514 ± 1) nm for A488 (Figure 3.5 D)). Note that these values are slightly different from the previous ones presented in Table 3.1 since the apparatus used to measure the spectra was different (see section 2.3).

Within the 20 - 60 ºC temperature interval the fluorescence emission intensities of both free and conjugated dye decrease in parallel only 10%. Above 60 ºC, the tertiary structure of the enzyme begins to unfold and a cooperative transition was observed for the labeled protein only (Figure 3.5 C). Assuming a two-state model, we retrieve a T_m of 73.5 ºC for Lz-A488 at pH 7.4, where T_m is defined as the midpoint in a thermal ramp and represents the temperature where the free energy of the native and non-native forms is equivalent (Matulis *et al.*, 2005). Based on data obtained by other authors by both experimental and computational methods (Meersman *et al.*, 2010), the secondary and tertiary structures of lysozyme at neutral pH are generally maintained within the interval of 20 and 64 ºC. This is in agreement with what was verified experimentally (Figure 3.5 C). The unfolding then progresses first by loosing sheet structures in lysozyme β-domain, along with a small part of the helical structure of α-domain, and then a generally loss of tertiary structure. The authors also indicated that above 80 ºC lysozyme's unfolding is irreversible. This observation can explain why after reaching 90 ºC and cooling down the solution to 25 ºC, it was not possible to recover the initial value of Lz-A488 fluorescence intensity (data not shown).

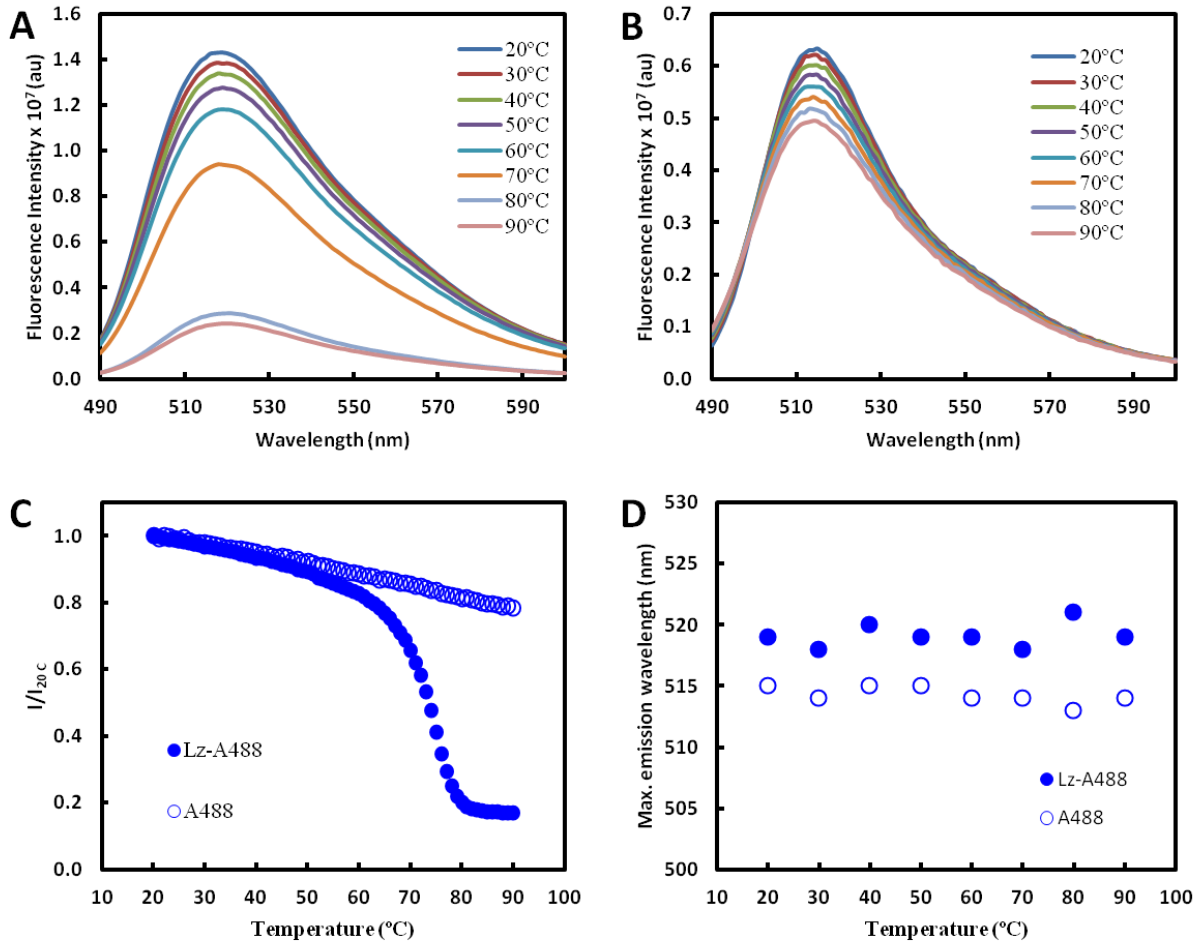

Figure 3.5 - Thermal unfolding of Lz-A488 monitored by steady-state fluorescence spectroscopy at pH 7.4.

Temperature dependence of the steady-state fluorescence emission spectra from (**A**) 1 µM Lz-A488 and (**B**) 0.7 µM free A488 dye at pH 7.4. The emission spectra were measured using λ_{exc}= 480 nm. Variations of (**C**) the normalized maximum fluorescence intensities to their values at 20 ºC and (**D**) of the maximum emission wavelengths of Lz-A488 (closed circles) and free A488 (open circles) with the temperature.

At pH 7.4, all the fluorescence decay profiles of Lz-A488 obtained at different temperatures were adequately described by a tri-exponential function (Figure 3.6). At 25 ºC, the native Lz-A488 exhibited an intensity decay with a main lifetime component of τ_3= 3.6 ns and a short- and intermediate-lived species of τ_1~ 0.25 ns and τ_2~ 2 ns with fractional amplitudes of 69%, 7% and 24%, respectively (Figure 3.6 A and B). The long and intermediate fluorescence lifetimes of Lz-A488 decreased almost linearly with the temperature, whereas the short fluorescence lifetime was essentially temperature-insensitive (Figure 3.6 B). Figure 3.6 A further shows that until reaching the temperature when Lz-A488 starts to unfold (*T*~ 60 ºC), the long-lived fluorescent lifetime is the major component of its fluorescence decay. Above this temperature, the populations of both τ_1 and τ_2 are significantly enhanced until reaching plateau values of 34% and 40% at 90 ºC, respectively.

As a result of both these changes, the amplitude-weighted mean fluorescence lifetime of Lz-A488 decreased from 3.0 to approximately 1.4 ns upon heating the solution from 25 to 90 ºC (Figure 3.6 C). As for the free dye, its fluorescence lifetime decreased from approximately 4.0 to 3.6 ns within the same temperature interval (Figure 3.6 C) due to an increasing contribution with the temperature of the non-radiative processes involved in A488 returning from its excited sate to the ground-state.

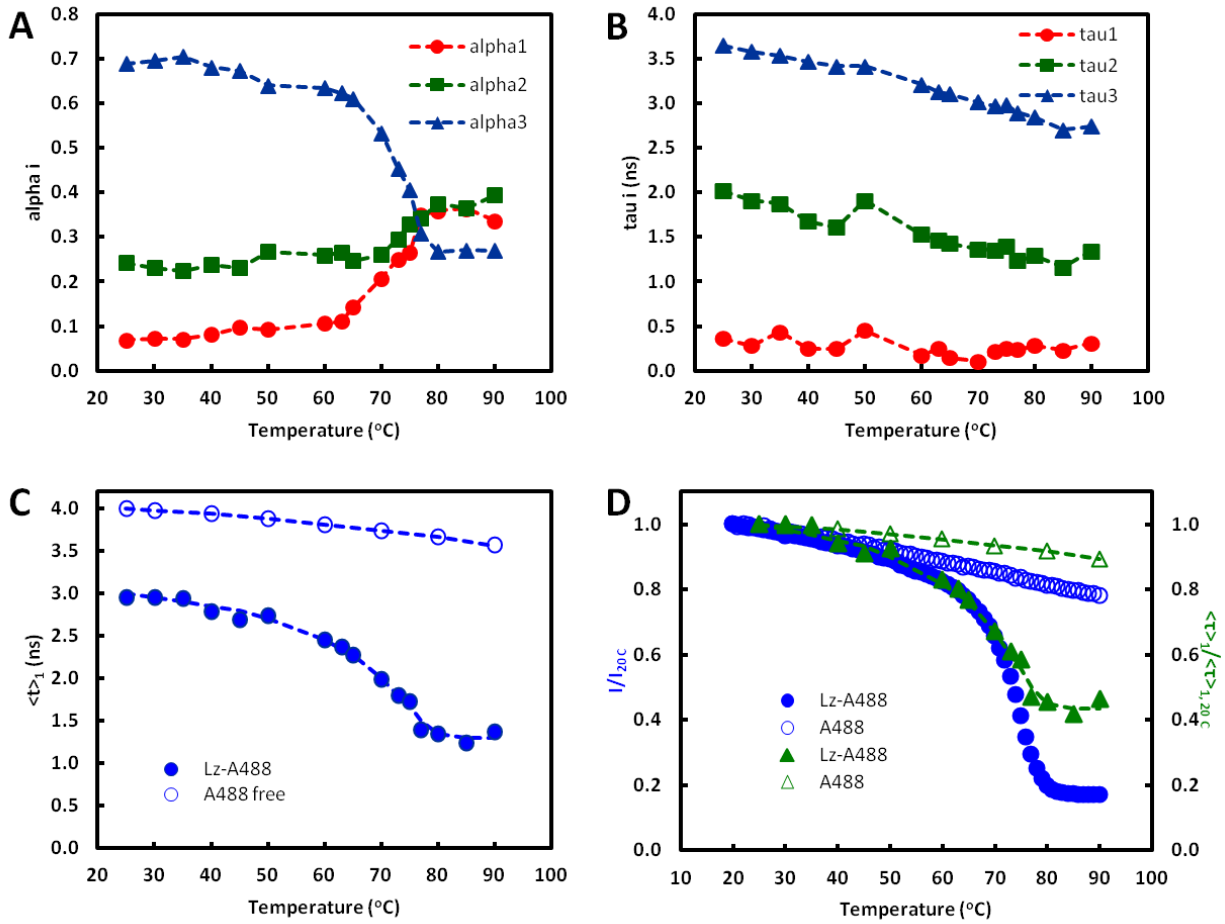

Figure 3.6 - Thermal unfolding of Lz-A488 monitored by time-resolved fluorescence spectroscopy at pH 7.4.

The fluorescence emission kinetics were measured using λ_{exc}= 340 nm and λ_{em}= 515 nm. Temperature dependence of the (**A**) fractional amplitudes and (**B**) lifetime components obtained for 1 µM Lz-A488 at pH 7.4. Variations of **(C)** the amplitude-weighted mean fluorescence lifetimes and **(D)** the normalized fluorescence intensities (blue circles) and amplitude-weighted mean fluorescence lifetimes (green triangles) of 1 µM Lz-A488 and 0.7 µM free A488 with the temperature. The dashed lines are just a guide to the eye.

The observation above that the long-lived fluorescence lifetime of Lz-A488 was the dominant component of its fluorescence intensity decay only when the enzyme retained a natively-structured conformation is consistent with a temperature-dependent quenching mechanism affecting

the conjugated protein. This quenching can be rationalized in terms of a photoinduced electron transfer (PET) mechanism (Doose *et al.*, 2009) (Figure 3.7) from an electron donor present in several possible adjacent amino acid residues to the covalently-conjugated dye A488. This quenching mechanism has been proposed before in quenching studies of free Alexa dyes in solution by different amino acids (Chen *et al.*, 2010; Sun *et al.*, 2011) and for different A488-fluorescently-labeled proteins (apomyoglobin, Chen *et al.*, 2007; cytochrome *c*, Choi *et al.*, 2011). Specifically, Chen *et al.* (2010) found that the fluorescence of A488 can be quenched by several amino acids, mainly by tryptophan and tyrosine (strong quenchers) and by histidine and metionine (weak quenchers). Within a 8 Å radius, at least 1 tyrosine and 4 tryptophan residues, and 1 metionine and 2 tryptophan residues are nearby residues K97 and K33, respectively, in the native lysozyme. Moreover, A488 can rotate freely within a cone with a semi-angle of 19-21.5º in Lz-A488 (discussed previously), increasing its probability of interaction with nearby amino acid residues. Therefore, we conclude that upon heating the solution, partial unfolding of lysozyme must allow for the establishment of van der Waals contacts between these amino acid residues and the dye attached to the protein, resulting in an efficient quenching of its fluorescence by a PET-based mechanism. This is expected to cause an increased population of Lz-A488 molecules that present a much shorter excited-state lifetime or that even are non-fluorescent, as it was observed (Figure 3.6 A and C).

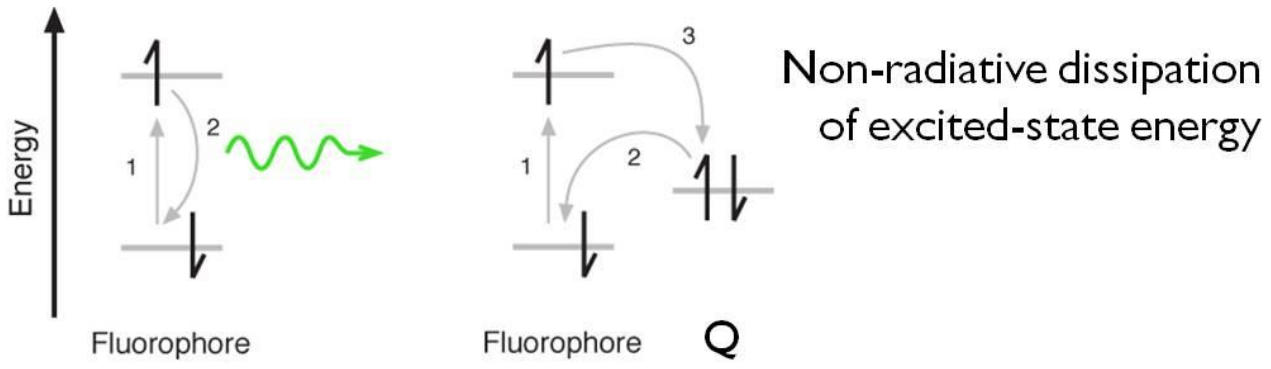

Figure 3.7 – Representative scheme of fluorescence quenching by a photoinduced electron transfer mechanism.

(A) When a fluorophore is excited (1), an electron goes from the ground-state to the first excited state (S1). When it returns to the first state (2), part of the energy is released via radiative processes, namely fluorescence (green arrow). **(B)** In photoinduced electron transfer, the fluorophore is excited (1) and the electron goes to S1. A nearby quencher (Q) donates one of its electrons (2) to the ground-state of the fluorophore preventing the excited electron to return to the ground-state. There is a non-radiative dissipation of the excited-state energy and no emission of fluorescence occurs. Adapted from http://labrigger.com/blog/tag/calcium-imaging/ (last consulted on 11/9/2012).

3.1.2.2. pH strongly influences the thermal denaturation of Lz-A488

Both the steady-state and time-resolved fluorescence measurements made for Lz-A488 and A488 as a function of temperature were repeated at pH 2.2 (Figure 3.8 A). The fluorescence properties of Lz-A488 at this pH presented a very similar behavior in general to the one described above for pH 7.4. The main difference detected was that the thermal denaturation profile obtained for Lz-A488 at pH 2.2 was almost 20 ºC-shifted to lower temperatures relatively to the ones measured at pH 7.4 (Figure 3.8 B). In fact, a much lower T_m of 55 ºC was measured for Lz-A488 at this acidic pH as compared to pH 7.4. This result is in agreement with the literature (for HEWL at pH 2, T_m = 54.8 ºC (Arnaudov and Vries, 2005) and at pH 7, T_m = 75 ºC (Lee *et al.*, 2006)) and confirms the strong destabilization of lysozyme at low pH probably due to electrostatic repulsions between the accumulated positive charges in the enzyme. For pH values below 4.0, Machuqueiro and Baptista (2008) have already detected a destabilization of lysozyme secondary structure, being its β-domain the less stable. It should be noted, however, that this structural perturbation of Lz-A488 at acidic pH does not affect its rotational dynamics significantly at room temperature as it was discussed above.

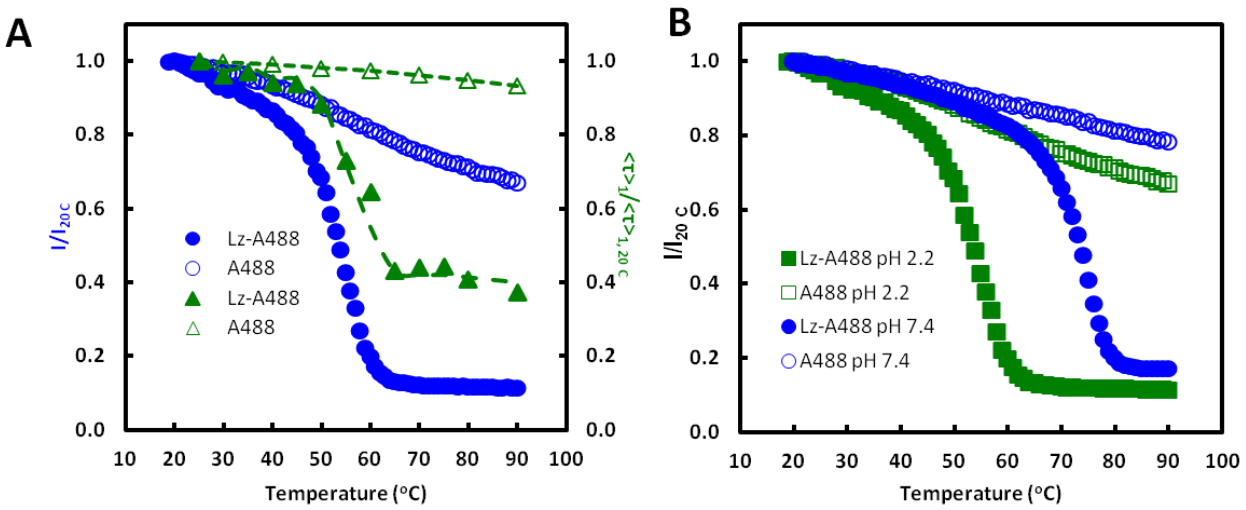

Figure 3.8 - Thermal unfolding of Lz-A488 is influenced by pH.

(**A**) Variation of the normalized fluorescence intensities and amplitude-weighted mean fluorescence lifetimes of 1 µM Lz-A488 and 0.7 µM free A488 with the temperature at pH 2.2. The dashed lines are just a guide to the eye. (**B**) Comparison of the thermal denaturation profiles obtained for Lz-A488 at pH 2.2 and 7.4. For more details, see the legend of Figure 3.6.

3.1.2.3. Using 1,8-ANS and Sypro Orange to detect lysozyme thermal unfolding

Finally, the extrinsic dyes 1,8-ANS and SO were used in independent control assays to confirm the alterations undergone by the tertiary structure of lysozyme upon heating the solution at both pH 2.2 and 7.4. Both these probes are commonly used to collect protein thermal denaturation data because they bind to organized hydrophobic clusters on proteins that become widely accessible to the solvent when proteins unfold, increasing their fluorescence quantum yields (Hawe *et al.*, 2008; Layton and Hellinga, 2010).

At pH 7.4, the fluorescence intensity of 5x SO in the presence of 1 µM of lysozyme did not vary significantly with the temperature within the interval 20 – 60 ºC. For temperatures higher than 60 ºC, the fluorescence intensity of the probe progressively increased, peaking at 74 ºC, close to the T_m value determined above for Lz-A488 at this pH (Figure 3.9 A). Concomitantly, the maximum emission wavelength of SO shifted from approximately 630 nm to ~ 620 nm for temperatures higher than 65 ºC (data not shown). SO could not be used at pH 2.2 due to alterations registered in its absorption spectra at this pH and since its structure is not publically available, it was decided to employ 1,8-ANS to monitor the thermal unfolding of lysozyme at this pH instead. As it is shown in Figure 3.9 B, the fluorescence intensity of this probe in the presence of 1 µM of lysozyme increased almost two-fold when the temperature was varied between 45 and 65 ºC at pH 2.2, reporting the formation of partially unfolded conformations of lysozyme (molten globules) with a high amount of hydrophobic area exposed to the solvent within this temperature range. At pH 2.2 1,8-ANS presented a blue shift from 540 nm (until 40 ºC) to 524 nm after the denaturation of lysozyme. At pH 7.4 this was not observed and the maximum emission wavelength of this dye remained between 513 and 516 nm at all temperatures (data not shown). At pH 7.4, 1,8-ANS binding to lysozyme was much less effective, probably due to the establishment of less strong electrostatic interactions between the anionic probe and the cationic protein at this pH.

The fluorescence intensity of the dyes increases on protein unfolding because they present a higher quantum yield when bound to hydrophobic regions that are normally exposed upon protein unfolding (Lo *et al.*, 2004). Unfolded intermediates may have sizable nonpolar patches on their surface, namely hydrophobic residues that were buried in the native protein, which lead to hydrophobic interactions between protein and dye (Munishkina *et al.*, 2004). However, after reaching the peak (Figure 3.9), the fluorescence intensity of the dyes starts to decrease. Some explanations have been put forward in the literature to explain this behavior: Munishkina and co-workers suggest that these organized hydrophobic patches are absent in the fully unfolded state

(Munishkina *et al.*, 2004); in Lo work, the authors state that there is aggregation of the denatured protein–dye complexes (Lo *et al.*, 2004); particularly for SO, in Layton and Hellinga work is explained that the decrease in the fluorescence intensity has been attributed primarily to protein aggregation and irreversible interaction of the dye with the denatured protein. However, further observations discredited these hypotheses and this behavior was attributed to intrinsic properties of the dye photophysics, consistent with the temperature dependence of SO fluorescence in low-dieletric solvents (Layton and Hellinga, 2010).

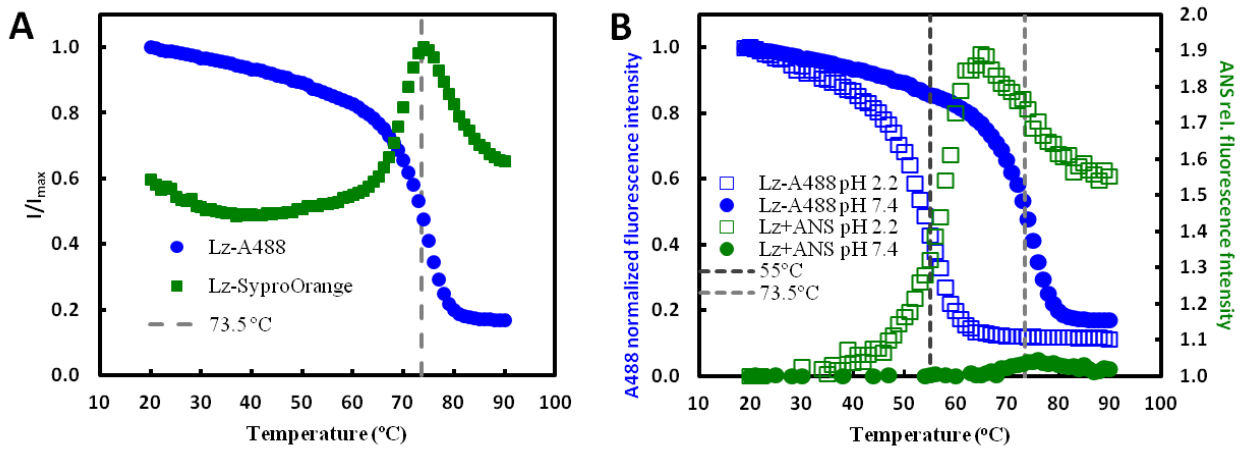

Figure 3.9 - Thermal unfolding of lysozyme monitored by Sypro-Orange (at pH 7.4) and 1,8-ANS (at pH 7.4 and 2.2).

Variation with the temperature of the normalized fluorescence intensities of (**A)** 5x concentrated SO at pH 7.4 (green squares) and (**B**) 20 µM of 1,8-ANS in the presence of 1 µM of lysozyme at both pH 2.2 (open green squares) and 7.4 (closed green circles). The fluorescence intensities presented are from different emission wavelengths: 620 nm for SO, 530 and 515 nm for 1,8-ANS at pH 2.2 and 7.4, respectively. Fluorescence data obtained for 1 µM Lz-A488 in the same conditions are also plotted (blue symbols, see the legend of Figure 3.8 for further details). Dashed vertical lines indicate the T_m values determined for Lz-A488 at pH 2.2 (dark grey, T_m= 55 ºC) and pH 7.4 (light grey, T_m= 73.5 ºC).

In conclusion, in this section we showed that A488 can be used as a sensitive reporter for unfolding transitions of lysozyme due to its sensitivity to a PET-based quenching mechanism. The partial unfolding of lysozyme probably allows van der Waals contacts between the fluorophore molecule and nearby amino acids residues, previously shown to quench free Alexa 488 (Chen *et al.*, 2010; Sun *et al.*, 2011).

3.2. Lysozyme amyloid fibril formation at pH 2.2 and 57 ºC

3.2.1. Nile Red has a moderate binding affinity to mature isolated lysozyme amyloid fibrils at pH 2.2

Traditionally, ThT is the fluorophore of choice to easily monitor amyloid fibril processes *in vitro* (Groenning, 2010; Biancalana and Koide, 2010). It is a cationic fluorophore (Figure 1.8 D) that is known to have a very low quantum yield in water solutions and in the presence of native and denatured proteins and their amorphous aggregates, but to form a highly fluorescent complex with amyloid and amyloid-like fibrils (Groenning, 2010; Biancalana and Koide, 2010). However, poor binding of ThT to amyloid aggregates and fibrils at pHs under 3 is described in the literature, since it is a charged molecule and its binding properties are different at acidic and neutral pH (Lindgren *et al.*, 2005; Mishra, *et al.*, 2007 and 2011). NR is an uncharged aromatic dye (Figure 1.8 C) that has been used earlier as an alternative red fluorescent probe for monitoring amyloid formation at acidic pH (Mishra *et al.*, 2011). In this section, we first confirm the preparation of mature lysozyme fibrils grown at pH 2.2 and 57 ºC under quiescent conditions by their fluorescence detection with ThT at pH 7.4. We then present the steady-state and time-resolved fluorescence measurements made to study NR binding to mature lysozyme fibrils at pH 2.2 that further validate its use as a versatile amyloidotropic dye for detection and characterization of amyloid fibrils grown *in vitro* from HEWL.

3.2.1.1. Preparation and detection of mature lysozyme fibrils using Thioflavin T

The conditions chosen to carry out lysozyme fibrillation assays *in vitro* were acidic pH (pH= 2.2) and elevated temperature (T= 57 ºC). These conditions closely match the T_m previously established for lysozyme at this pH (T_m~ 55 ºC, Arnaudov and Vries, 2005 (Figure 3.8)) and have been used earlier (Meratan *et al.*, 2011). At this pH and temperature, lysozyme is submitted to denaturing conditions that will promote its unfolding. Consequently, the unfolded intermediates formed will interact with each other, eventually originating lysozyme fibrils at long incubation times. After an incubation period of 12 days at pH 2.2 and 57 ºC under quiescent conditions, mature lysozyme fibrils were isolated by three consecutive centrifugation steps (Figure 3.3) and quantified spectrophotometrically at 280 nm as previously described in section 2.5. To confirm that lysozyme fibrillation was effective under the experimental conditions used, mature isolated lysozyme amyloid fibrils were stained with ThT at pH 7.4 and examined by CFM. Fibril clusters up to several

micrometers in length were easily visualized in the samples prepared as it is exemplified in Figure 3.10 A.

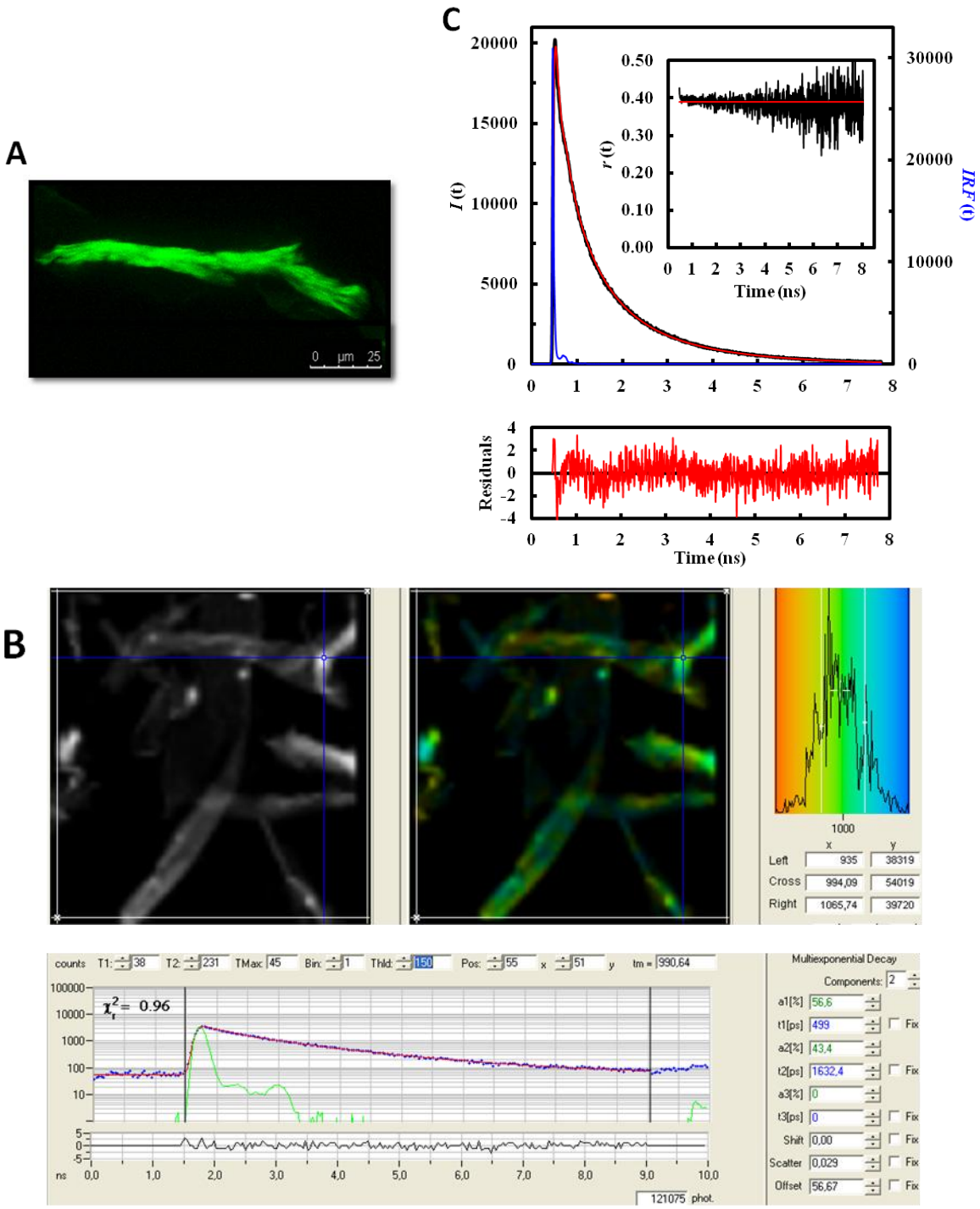

Figure 3.10 – Mature isolated lysozyme fibrils investigated with Thioflavin T.

Mature lysozyme fibrils pelleted by centrifugation were stained with ThT at pH 7.4 and imaged by (**A**) CFM and (**B**) FLIM. Ensemble-averaged (cuvette) measurements were also made. (**C**) Fluorescence intensity decay of ThT stained fibrils. The best fit to the experimental data was obtained using three exponentials: α_1= 0.44; τ_1= 0.13 ns; α_2= 0.36; τ_2= 0.67 ns; α_3= 0.20; τ_3= 1.89 ns; χ^2= 1.23; $\langle\tau\rangle_1$= 0.68 ns). **Inset:** ThT fluorescence anisotropy decay measured for the same sample. The concentrations of lysozyme fibrils (on a monomer basis) and ThT were 73.4 and 8.6 µM, respectively.

In addition, ThT-stained amyloid fibrils were also characterized by FLIM. The amplitude-weighted mean fluorescence lifetime of ThT had a uniform spatial distribution on these structures ($<\tau>_1$= 0.99 ns (Figure 3.10 B)), being very similar to the value measured in an ensemble-average (cuvette) assay ($<\tau>_1$= 0.68 ns (Figure 3.10 C)). The difference between these two values must be due to the distinct instrumentation used in their determination, as well as to the programs used in the analysis of the time-resolved data and the data itself. Whereas in ensemble-average assays (cuvette measurements) about 20 000 counts were collected in the peak channel of the decay curves, in FLIM measurements there were usually less than 2 000 counts collected at each pixel. This influences the accuracy of the lifetime value determined as well as the number of exponentials needed to fit the decays. ThT belongs to the class of molecular rotors and the significant increase of its fluorescence lifetime/quantum yield when incorporated in amyloid and amyloid-like fibrils is caused by restriction of torsional oscillations of the ThT rings (Figure 1.8 D) relative to each other (Biancalana and Koide, 2010) . The fluorescence emitted by the ThT molecules bound to the fibrils did not depolarize during its mean fluorescence lifetime ($r(t)$~ 0.4, inset of Figure 3.10 C). This result can be explained considering that ThT is almost non-fluorescent in aqueous solution and that this probe is strongly immobilized upon its intercalation between the β-sheets of the very long lysozyme amyloid fibrils formed under these conditions. A similar high value of anisotropy was reported by Celej and co-workers while studying the aggregation of α-synuclein by time-resolved fluorescence anisotropy (Celej *et al*., 2008).

3.2.1.2. Nile Red binding to mature lysozyme fibrils at pH 2.2 – steady-state and time-resolved fluorescence measurements

NR binding to mature isolated lysozyme fibrils was studied by both steady-state and time-resolved fluorescence measurements. Upon increasing the concentration of lysozyme fibrils, there was a pronounced blue-shit of the dye's maximum emission wavelength, from near 655 nm (expected for NR molecules in water (Tajalli *et al.*, 2008)) to approximately 630 nm (Figure 3.11 A). This behavior is typically observed when the dye molecules present in aqueous solution bind to hydrophobic or apolar sites (Sutter *et al*., 2007). Simultaneously, its steady-state fluorescence emission intensity (data not shown) and anisotropy increased. The free dye in solution presents an anisotropy of $<r>_f \sim 0.09 \pm 0.02$ (n= 3) that progressively augmented reaching a plateau value of $<r>_b \sim 0.344 \pm 0.007$ for concentrations of fibers above 28 μM (Figure 3.11 A).

All the fluorescence decay profiles obtained for NR in the presence of variable amounts of fibers were adequately described by a tri-exponential function (Figure 3.11 B and C).

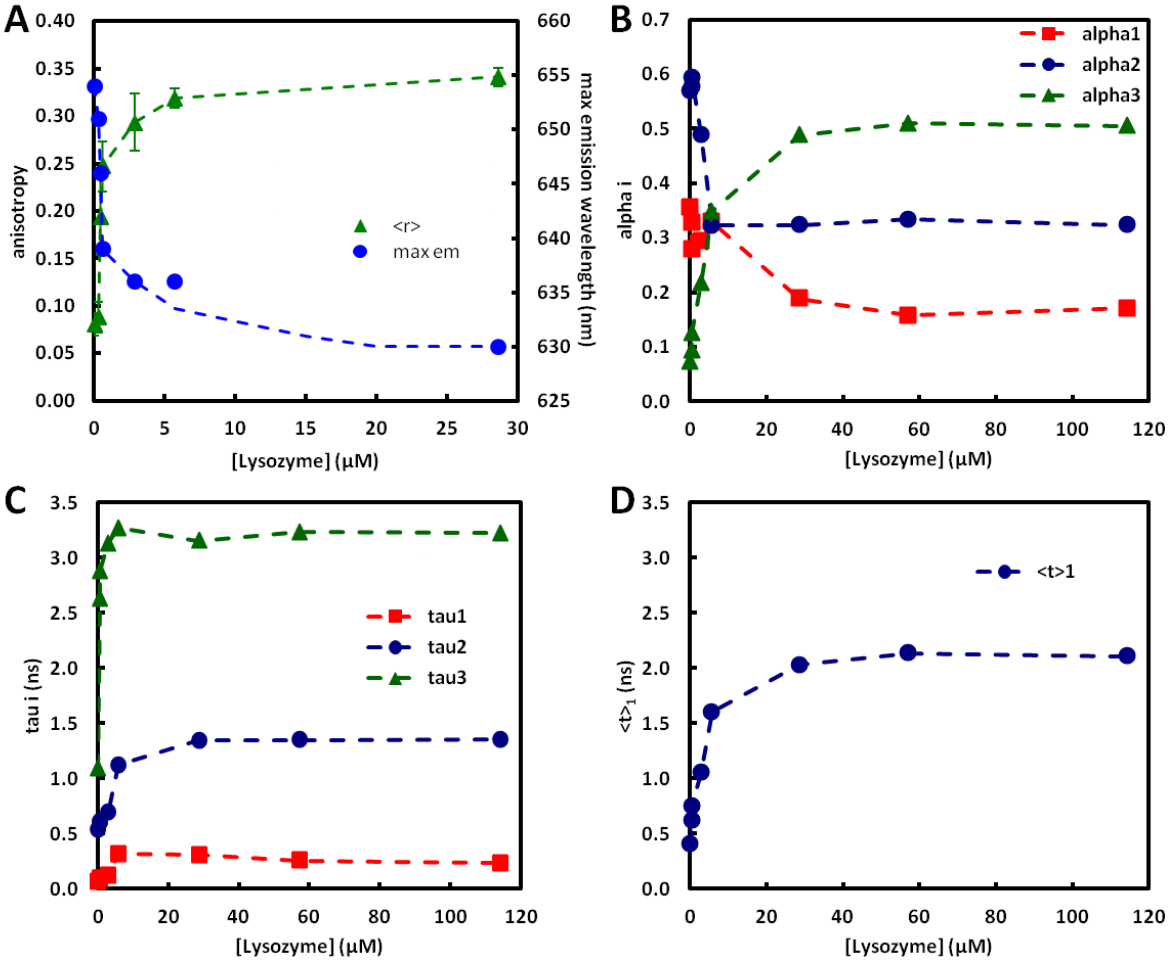

Figure 3.11 – Characterization of Nile Red binding to mature lysozyme amyloid fibrils at pH 2.2 using steady-state and time-resolved fluorescence measurements.

(**A**) The emission spectra and steady-state fluorescence anisotropy were obtained using λ_{exc} = 552 nm and λ_{em} = 570-800 nm and λ_{em} = 636 nm, respectively. Fluorescence anisotropy values are presented as mean ± SD of ten measurements. (**B**) Fractional amplitudes, (**C**) lifetime components and (**D**) $\langle\tau_1\rangle$ (calculated with Eq. 3.17) of 2.9 μM NR as a function of lysozyme fibril concentration (expressed on a monomer basis). The fluorescence decay profiles were obtained using λ_{exc} = 565 nm and λ_{em} = 650 nm and were all adequately described by a tri-exponential function (Eq. 3.15). The dashed lines are just a guide to the eye.

The free dye in solution presented an amplitude-weighted mean fluorescence lifetime of $\langle\tau\rangle_{1f}$= 0.48 ns (α_{1f}= 0.240 ± 0.008; τ_{1f}= 0.076 ns [0.066, 0.081]; α_{2f}= 0.713 ± 0.072; τ_{2f}= 0.56 [0.54;0.56] ns; α_{3f}= 0.047 ± 0.014; τ_{3f}= 1.4 [1.3;1.5] ns; the lifetime values were linked in the analysis (*n*= 3)) that increased approximately 5-fold to $\langle\tau\rangle_{1b}$= 2.1 ns) (α_{1b}= 0.16 ± 0.01; τ_{1b}= 0.25 ± 0.02 ns; α_{2b}= 0.33 ± 0.01; τ_{2b}= 1.350 ± 0.001 ns; α_{3b}= 0.507 ± 0.003; τ_{3b}= 3.230 ± 0.002 ns (*n*= 2)) for protein concentrations higher than 28 μM (Figure 3.11 D). These results are in agreement with previous works where NR was used to study aggregates of β-galactosidase (Sutter *et al.*, 2007). These authors also needed to use three lifetime components when analyzing the intensity decays of

NR in the presence of different samples of β-galactosidase and they emphasized the fact that it was not possible to relate particular lifetimes to free and protein-bound state of NR.

The fluorescence signal originated from NR-stained mature lysozyme amyloid fibrils at pH 2.2 was strong enough to allow for their imaging using CFM. Figure 3.12 shows several fibrillar bundles that present variable morphologies (shapes and sizes), which reflect that a complex mixture of entities is present in solution by the end of the incubation period. Protein fibrillation is a complex process: multiple species are formed in solution, which originate protofilaments that finally associate to form the mature fibrils (Yonezawa *et al*., 2002). The small and thinnest bundles seen may correspond to associations between these protofilaments and/or this variety of species may have been amplified by the fact that the fibrils are pelleted by centrifugation and further re-suspended in buffer by vortexing the sample, which can lead to fragmentation of some structures. Altogether, these results confirm the potential of NR for monitoring real time fibril growth using fluorescence microscopy (Mishra *et al*., 2011).

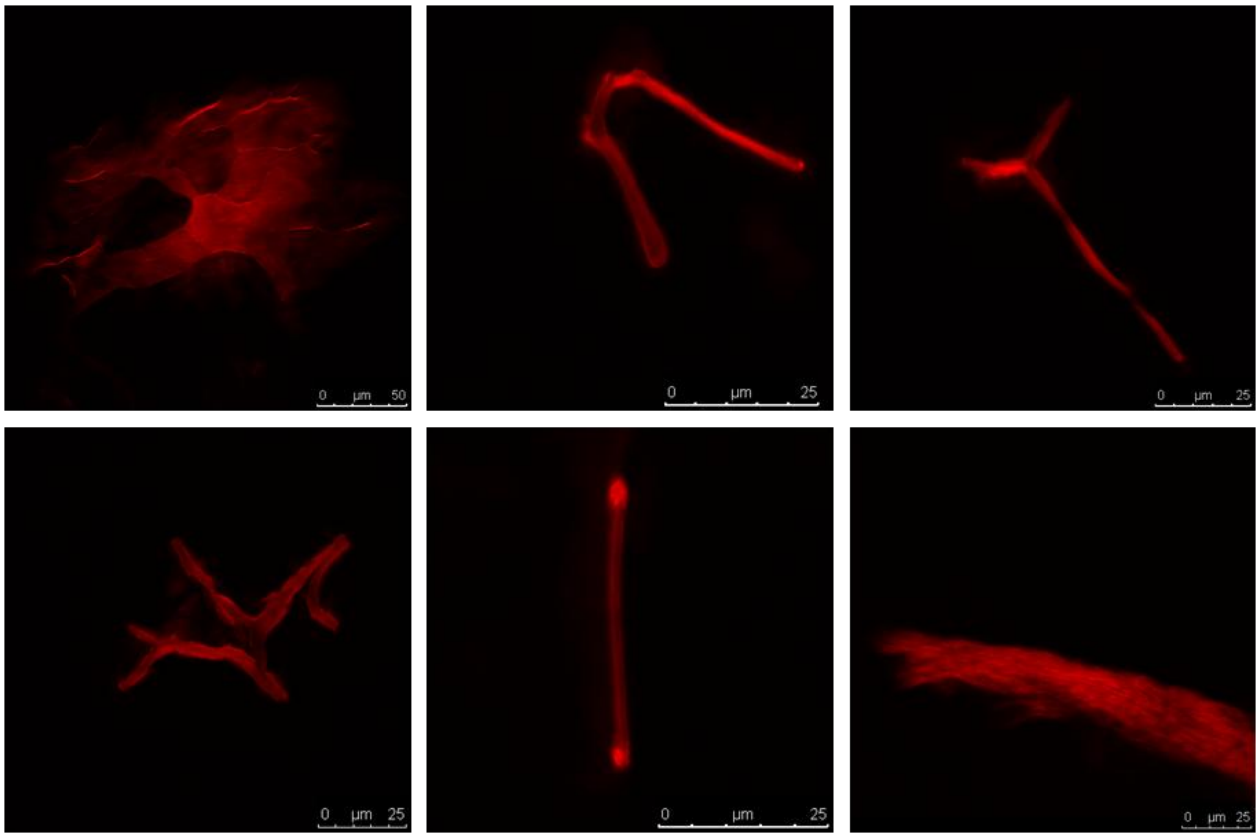

Figure 3.12 – A wide diversity of mature lysozyme fibrils were imaged by confocal fluorescence microscopy after staining with Nile Red.

Lysozyme fibrils pelleted by centrifugation were stained with NR at pH 2.2 and imaged by CFM. The concentrations of lysozyme fibrils (on a monomer basis) and NR were 76.6 and 2.9 μM, respectively.

Finally, NR binding to mature lysozyme fibrils was also studied quantitatively by time-resolved fluorescence anisotropy measurements. The time-resolved anisotropy of the free dye in solution decayed mono-exponentially with a rotation correlation time of ~ 0.14 ns, rapidly depolarizing its fluorescence emission to 0 (Figure 3.13 and Table 3.4). For lysozyme fibril concentrations above 0.43 μM, the anisotropy of NR was essentially constant over time ($r(t)$ ~ 0.35) and for the intermediate fibril concentrations studied its anisotropy decays presented a "dip-and-rise" behavior (Figure 3.13).

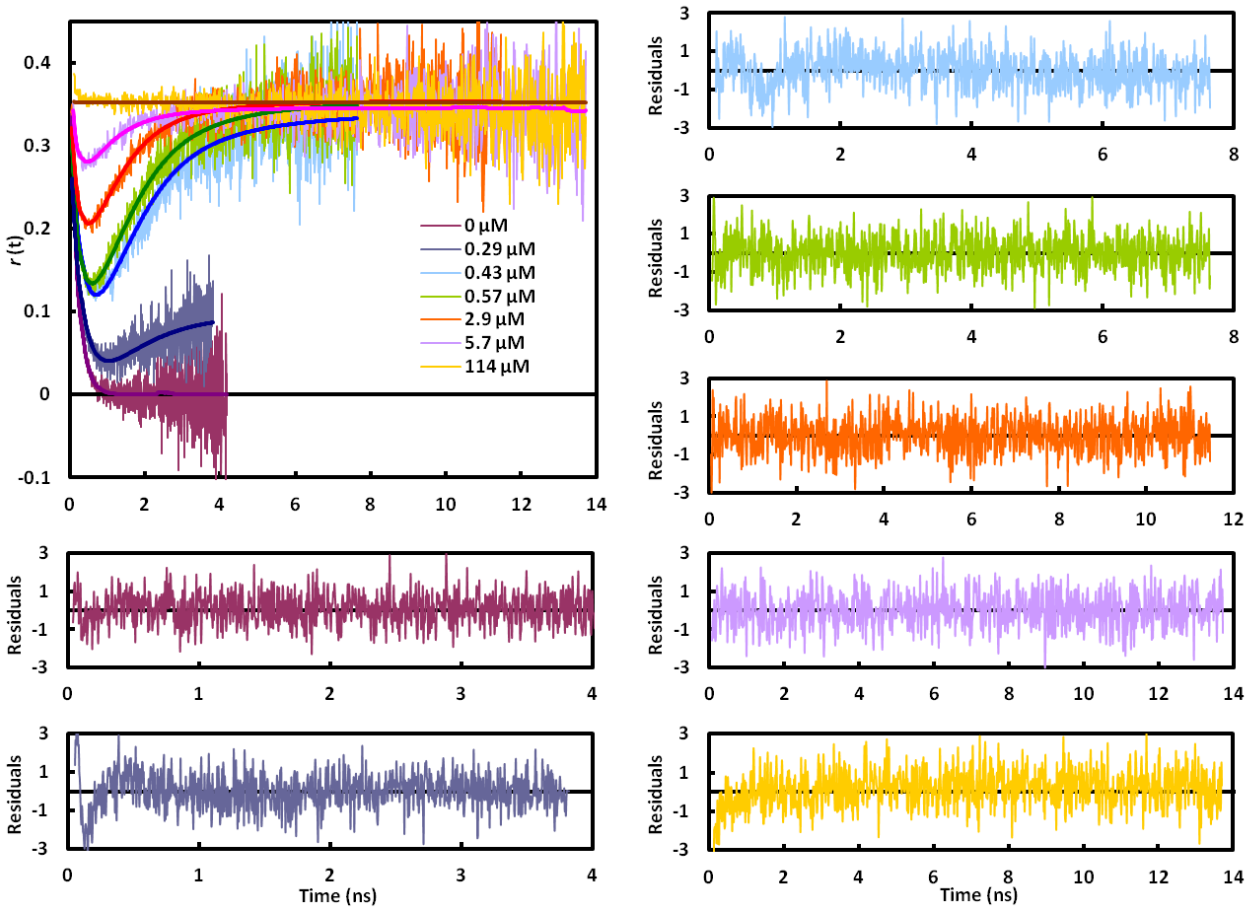

Figure 3.13 - Fluorescence anisotropy decays of 2.9 μM Nile Red in the presence of increasing concentrations of mature lysozyme fibrils at pH 2.2.

The fluorescence anisotropy decays were fitted according to an associative model (see the text and Table 3.4 for more details). The analyses were performed using a nonlinear least-squares reconvolution method based on the Marquardt algorithm implemented on Microsoft Office ® Excel 1997-2003 (courtesy of Prof. Mário Nuno Berberan Santos).

The curious behavior observed can be explained by admitting that NR is present in each sample in equilibrium between two different environments (free in solution and bound to the fibrils) that confer very different fluorescent and rotational properties to the fluorescent dye (Figure 3.14):

- free NR molecules have a short mean fluorescence lifetime ($<\tau>_{1f}$~ 0.48 ns) and a very fast rotational correlation time (ϕ_f~ 0.14 ns), thus, they rapidly depolarize their fluorescence emission;

- NR molecules bound to the fibrils are much more fluorescent ($<\tau>_{1b}$~ 2.1 ns) and their rotational dynamics is strongly hindered due to their binding to the large macromolecular structures ($r(t)$ ~ 0.35).

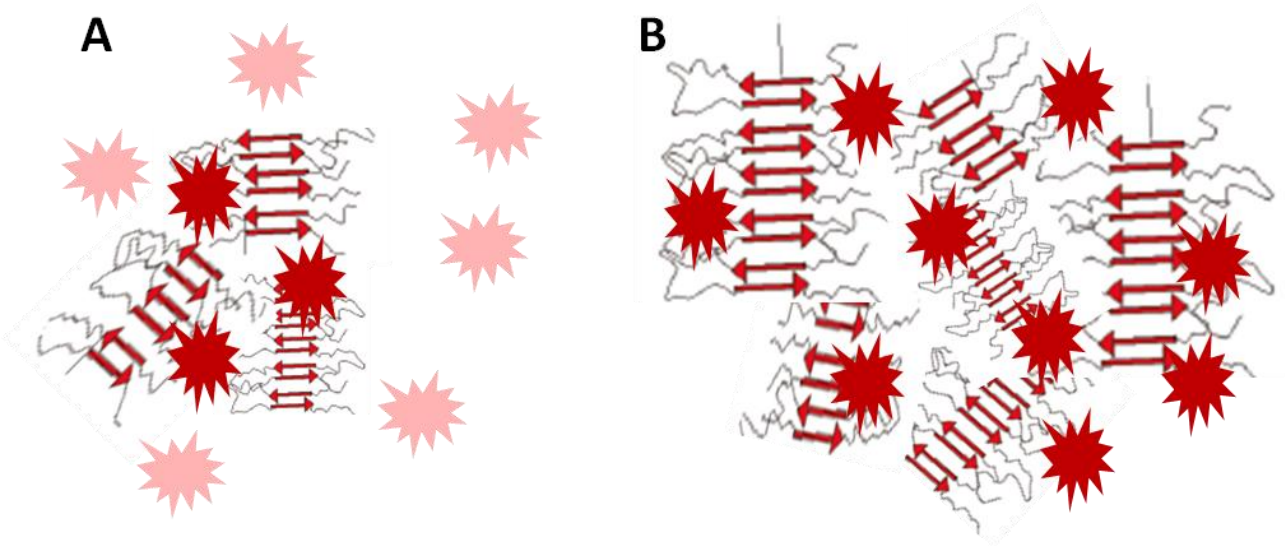

Figure 3.14 – Schematic representation of Nile Red binding to mature lysozyme fibrils.

(**A**) When a small amount of lysozyme fibrils is present in solution, there is an equilibrium between NR molecules that stay free in solution (pink stars) and that bind to the fibrils (red stars); (**B**) when a large amount of lysozyme fibrils is present in solution, essentially all NR molecules available are bound to lysozyme fibers.

3.2.1.3. Analysis of Nile Red fluorescence anisotropy decays using an associative model

According to the discussion above, the fluorescence anisotropy decays of NR were analyzed with an associative model. The fluorescence anisotropy of a sample is an intensity-weighted average of the anisotropies of each species present in the sample (Lakowicz, 2006). Therefore, at any time following excitation, the time-resolved fluorescence anisotropy of NR can be written as:

$$r(t) = f_f(t) \times r_f(t) + f_b \times r_b(t) \qquad \text{Eq. 3.9}$$

where $f_{\mathrm{f}}(t)$ and $r_{\mathrm{f}}(t)$ and $f_{\mathrm{b}}(t)$ and $r_{\mathrm{b}}(t)$ are the fractional intensities and anisotropy decays of NR free and fibril- bound molecules, respectively.

These parameters can be calculated from the following equations:

$$f_f(t) = \frac{x_f \times I_f(t)}{x_f \times I_f(t) + x_b \times I_b(t)} \quad \text{Eq. 3.10}$$

and

$$f_b(t) = \frac{x_b \times I_b(t)}{x_f \times I_f(t) + x_b \times I_b(t)} \quad \text{Eq.3.11}$$

where x_{f} and x_{b} are the free- and bound molar fractions of NR in solution , and $I_{\mathrm{f}}(t)$ and $I_{\mathrm{b}}(t)$ are their respective fluorescence intensities. The rotational dynamics of the free dye in solution was described by a single fast rotational correlation time, ϕ_{f}:

$$r_f(t) = \beta_f \times \exp(-\frac{t}{\varphi_{\mathrm{f}}}) \quad \text{Eq. 3.12}$$

whereas the bound molecules were admitted to be essentially immobile on the time scale used in the time-resolved fluorescence measurements:

$$r_b(t) = r_\infty \quad \text{Eq. 3.13}$$

Both the fluorescence intensity decays from the free, $I_{\mathrm{f}}(t)$, and bound, $I_{\mathrm{b}}(t)$, NR molecules were considered to be well described by a sum of three exponentials:

$$I_f(t) = \sum_{i=1}^{3} \propto_{i\,f} \times \exp\left(-\frac{t}{\tau_{i\,f}}\right) \quad \text{Eq. 3.14}$$

and

$$I_b(t) = \sum_{i=1}^{3} \propto_{i\,b} \times \exp(-\frac{t}{\tau_{i\,b}}) \quad \text{Eq. 3.15}$$

Eq. 3.9 shows that since NR free has a shorter mean fluorescence lifetime than the bound molecules, its fractional contribution to the intensity decay of the sample decreases more rapidly with time than the emission from the NR bound molecules. At longer times, the fluorescence emission from the sample becomes dominated by the bound NR molecules with its larger

anisotropy. Therefore, at some point, the value of $r(t)$ starts to increase, giving rise to the "dip-and-rise" behavior described earlier (Figure 3.13).

Eq. 3.9 was fitted to the experimental $r(t)$ data by a nonlinear least squares regression method using x_{f} ($x_{\mathrm{f}} = 1 - x_{\mathrm{b}}$) (Eq. 3.10), β_{f} and ϕ_{f} (Eq. 3.12) and r_∞ (Eq. 3.13) as fitting parameters. The functions describing the intensity decays were fixed to the values obtained for the free dye in solution and in the presence of a saturating concentration of fibrils (values presented in section 3.2.1.2). The experimental NR time-resolved anisotropy data was adequately described by this associative model as it is shown in Figure 3.13. Table 3.4 summarizes the results obtained from the fits; the results obtained are self-consistent as the mean values retrieved for ϕ_{f} and r_∞ were ϕ_{f}= (0.181 ± 0.037) ns for the first 6 fibril concentrations studied and r_∞= 0.347 ± 0.007 for the last 7 anisotropy decays, validating the associative model used in data analysis.

Table 3.4 - Analysis of NR fluorescence anisotropy decays obtained at pH 2.2 in the presence of increasing concentrations of mature lysozyme fibrils according to an associative model.

Anisotropy decays were measured using λ_{exc}= 565 nm and λ_{em}= 650 nm. The concentrations of lysozyme fibrils are expressed on a monomer basis and the concentration of NR was fixed to 2.9 μM in each assay.

[Fibrils] (μM)	x_b	β_{f}	ϕ_{f} (ns)	r_∞	χ^2_G
0	0	0.344 ± 0.007	0.142 ± 0.005	-	0.65
0.29	0.135	0.292 ± 0.006	0.239 ± 0.008	0.099 ± 0.002	0.89
0.43	0.152	0.321 ± 0.021	0.212 ± 0.021	0.341 ± 0.002	0.88
0.57	0.188	0.310 ± 0.011	0.171 ± 0.012	0.356 ± 0.001	0.84
2.9	0.374	0.303 ± 0.018	0.170 ± 0.024	0.355 ± 0.001	0.82
5.7	0.660	0.4 [a]	0.151 ± 0.058	0.346 ± 0.001	0.79
29	0.957	0.4 [a]	0.2 [a]	0.341 ± 0.001	0.97
57	0.995	0.4 [a]	0.2 [a]	0.339 ± 0.001	0.96
114	0.995	0.4 [a]	0.2 [a]	0.353 ± 0.001	0.97

[a] this value was fixed during the analysis.

The plotting of the NR bound fraction, x_b, as a function of total protein concentration defines a saturation curve and can be used to determine the affinity of NR binding to the amyloid lysozyme fibrils at pH 2.2, by fitting Eq. 3.9 to the experimental data. Using a non-linear least-squares regression method, K_d= (2.0 ± 0.4) μM was obtained (Figure 3.15).

To decrease the error associated to these measurements, it is necessary to exploit more protein concentrations, especially within the range of 0 to 20 μM of mature lysozyme fibrils. Despite the error, it is possible to conclude that NR presents a moderate binding affinity to lysozyme amyloid fibrils in aqueous solution at pH 2.2.

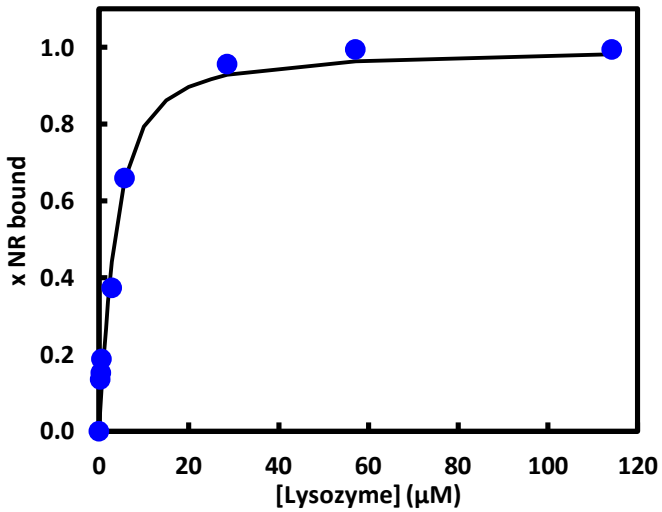

Figure 3.15 – Determination of Nile Red binding affinity to mature lysozyme fibrils at pH 2.2. Eq. 3.9 was fitted to the data of NR bound molar fraction as a function of lysozyme fibril concentration (solid line: K_d= (2.0 ± 0.4) μM). Lysozyme fibril concentrations are expressed on a monomer basis. The concentration of NR used was 2.9 μM (for more details see Table 3.4).

In conclusion, after confirming the formation of mature lysozyme fibrils under the conditions used in this study (acidic pH and elevated temperature) by CFM, the ability of NR to be used as fluorescent reporter of amyloid fibril formation was further explored. The steady-state fluorescence anisotropy of NR was found to be a very reliable parameter to detect the presence of lysozyme fibrils in solution. Furthermore, the analysis of the time-resolved fluorescence anisotropy decays of NR according to an associative model, which were obtained in the presence of increasing concentrations of lysozyme fibrils, allowed the determination of its binding affinity (K_d= (2.0 ± 0.4) μM) to the mature isolated lysozyme amyloid fibrils at pH 2.2.

3.2.2. Concentration-dependence of lysozyme amyloid fibril formation kinetics – a comparative study of Thioflavin T and Nile Red

After successful confirmation that the experimental conditions chosen lead to the growth of mature lysozyme fibrils as described in the literature, we studied the concentration-dependence of lysozyme amyloid fibrillation kinetics under acidic pH and elevated temperature. Two different lysozyme concentrations (0.2 and 1.0 mM) were incubated at pH 2.2 and 57 ºC and the use of the 'standard' fluorescent probes ThT and NR to monitor their fibrillation kinetics was compared. Both these lysozyme concentrations were previously demonstrated to form fibrils (Mishra *et al.*, 2007). Aliquots from the incubated samples were withdrawn for at least 12 days and mixed with assay solutions containing 8.6 μM of ThT (in Tris-HCl buffer, pH 7.4) or 2.9 μM of NR (in glycine buffer, pH 2.2). The final protein concentrations in the analyzed samples were 1 or 5 μM (on a monomer basis) (obtained from 0.2 and 1.0 mM lysozyme stock solutions, respectively (Figure 3.2)). These assays will be further used as controls for the studies that will be presented in the next section, where the fluorescence properties of A488 will be explored as a sensitive probe for detecting lysozyme amyloid fibril formation *in vitro*.

1.0 and 0.2 mM lysozyme amyloid fibril formation followed a sigmoidal growth curve with an approximately 4- and 6-days lag phase, respectively, before an increase in the fluorescence intensity of ThT was detected (Figure 3.16 A). This behavior is characteristic of a nucleation-dependent polymerization mechanism (Butterfield and Lashuel, 2010). During the lag phase, the protein starts to unfold and several partially unfolded monomeric intermediate species are formed in solution. These intermediates interact with each other, associating and dissociating until a thermodynamically unfavorable conversion of monomers into a β-enriched oligomeric "nucleus" occurs. Up to this point, ThT fluorescence intensity remains low as the intermediates present in solution do not bind the dye. The "nuclei" formed will then assemble into higher-order protofibrils through fast addition of monomers. This results in exponential fibril growth as this is now an energetically favorable process. The fluorescence intensity of ThT increases steeply during this phase as ThT shows enhanced fluorescence upon binding to amyloid fibrils (Figure 3.16 A). Finally, the signal reaches a plateau value because fibril formation reached an equilibrium state. It should be noted that these measurements are typically more erratic at the last days of incubation, particularly when a high protein concentration is used (blue and red squares, Figure 3.16 A). At these time points, large mature fibrils are suspended in solution and it is difficult to guarantee that each aliquot withdrawn from the incubation mixtures samples has the same amount of material. Finally, the lower plateau value obtained for the ThT fluorescence intensity when fibril formation was initiated using 0.2 mM as compared to 1.0 mM lysozyme is due to both a lower overall fibril

formation yield (see Table 3.7 in section 3.2.3.2) and the presence of lower final protein concentrations (1 *versus* 5 μM, respectively) in the assay mixtures.

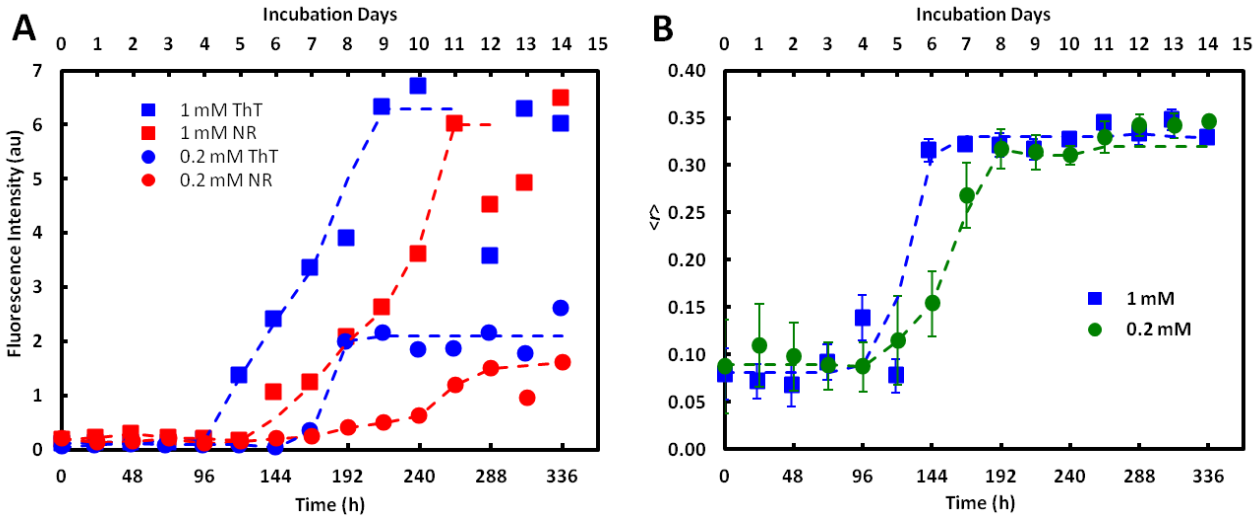

Figure 3.16 - Lysozyme fibrillation kinetics evolves with a sigmoidal behavior at pH 2.2 and 57 ºC.

(**A**) Kinetics of lysozyme amyloid formation was monitored by NR (red symbols) and ThT (blue symbols). The values presented are the integrated areas of the emission spectra of ThT from 470-600 nm (λ_{exc}= 450 nm) and of NR from 565-800 nm (λ_{exc}= 552 nm). (**B**) NR steady-state fluorescence anisotropy was measured at different time points (λ_{exc}= 562 nm; λ_{em}= 636 nm). Two different protein concentrations were used in the incubation mixtures: 0.2 (green circles) and 1.0 mM (blue squares), respectively. The dashed lines are just a guide to the eye.

The kinetic trajectories obtained using ThT and NR fluorescence intensities do not overlap exactly as the lag phases detected using NR are ~ 1 day longer as compared to ThT and the growth phases do not seem as abrupt as the ones detected with ThT (Figure 3.16 A). These results were confirmed by performing time-resolved fluorescence measurements with the samples containing NR. As it is shown in Figure 3.17, until day5 and day6 for 1.0 and 0.2 mM lysozyme solutions, respectively, the amplitude-weighted mean fluorescence lifetime of NR is essentially constant ($<\tau>_1$~ 0.5 ns), and very similar to the value presented by the free dye in aqueous solution (Figure 3.11). The increase of NR lifetime components (particularly τ_3 from ~1.5 to 3.2 ns) after day5 and day6 for 1.0 and 0.2 mM lysozyme solutions, respectively, causes an increase in its mean fluorescence lifetime up to ~2.0 ns, reporting the presence of lysozyme fibrils in solution after these incubation periods.

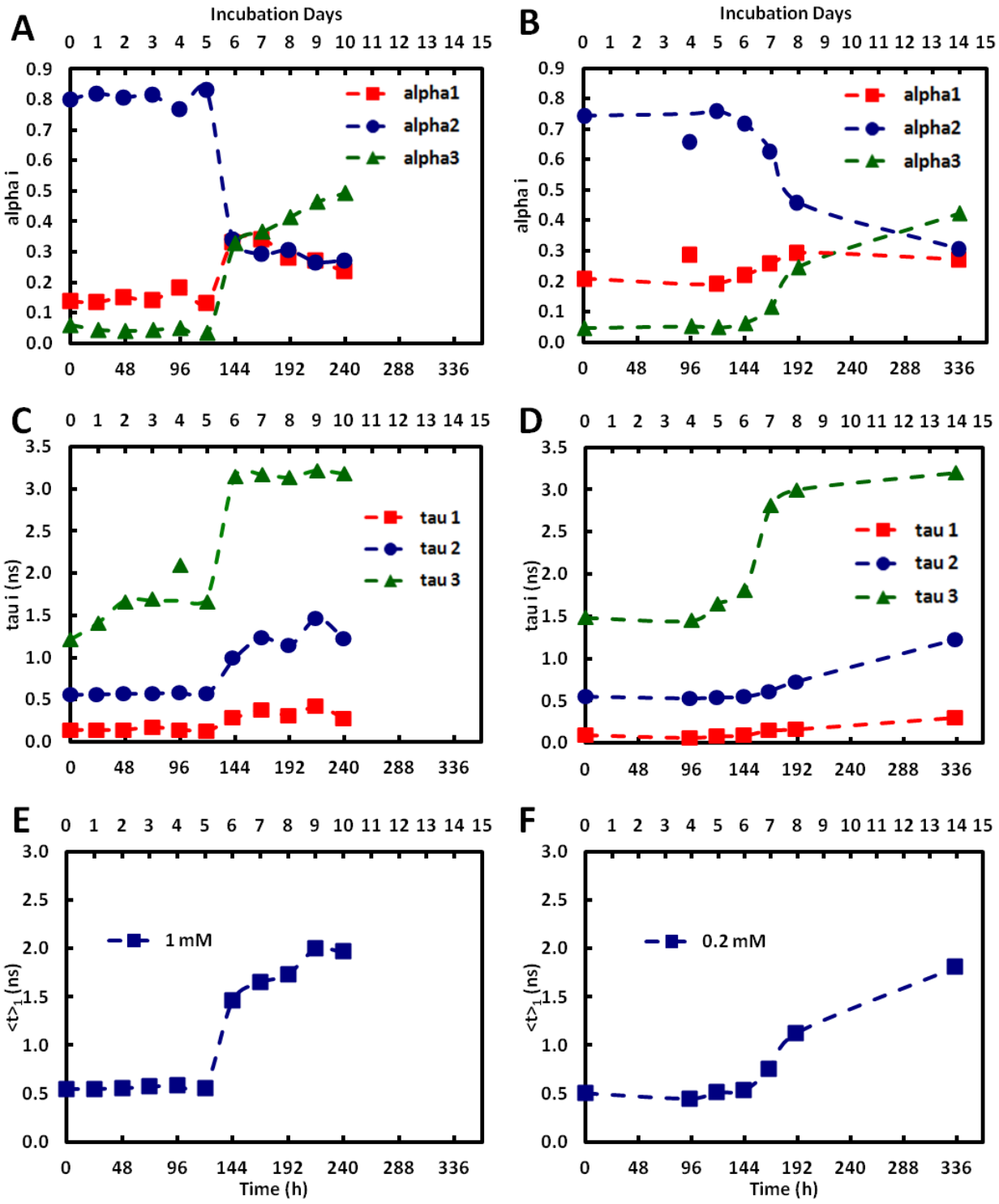

Figure 3.17 – Kinetics of lysozyme amyloid fibril formation (pH 2.2 and 57 °C) monitored by time-resolved fluorescence intensity measurements with 2.9 µM of Nile Red.

(**A** and **B**) fractional amplitudes, (**C** and **D**) lifetime components and (**E** and **F**) amplitude-weighted mean fluorescence lifetime of 2.9 µM NR at different time points during the fibrillation reactions of (**A**, **C** and **E**) 1.0 and (**B**, **D** and **F**) 0.2 mM lysozyme. The dashed lines are just a guide to the eye. The fibrillation took course for 14 days, although not all the time-points were investigated.

To complement these results, steady-state and time-resolved fluorescence anisotropy measurements of Nile Red-containing samples were also performed. During the lag phases of lysozyme kinetics, the steady-state anisotropy of NR presented a low value, identical to the one measured for the free dye in solution (<*r*>= 0.09 ± 0.02 (*n*= 3)) (Figure 3.11 A). The NR anisotropy decay measured at these early times depolarized rapidly in solution to 0, as it is exemplified in Figure 3.18 A for t0/ 0.2 mM lysozyme. At longer incubation times, the characteristic "dip-and-rise" behavior discussed earlier was detected in the fluorescence anisotropy decays of NR (exemplified in Figure 3.18 A for t6 and t7/ 0.2 mM lysozyme). Simultaneously, the steady-state anisotropy of NR in these samples increased until reaching plateau values of <*r*>~ 0.33 ± 0.01 (Figure 3.16 B).

The fluorescence anisotropy decays of NR obtained at different time points were analyzed with the associative model described above (section 3.2.1.3). Again, this simple model could adequately describe the experimental data obtained during the fibrillation kinetics of lysozyme and the values recovered from the fittings for the fast rotational correlation time presented by the free dye ($\phi_f = 0.15 \pm 0.04$ ns (day 6-14; *n*= 4) and $\phi_f = 0.17 \pm 0.03$ ns (day 6-10; *n*= 6) for 0.2 and 1.0 mM lysozyme, respectively) and for the limiting anisotropies of the samples (r_∞ = 0.34 ± 0.05 (day 6-14; *n*= 4) and r_∞ = 0.31 ± 0.01 (day 6-10; *n*= 6) for 0.2 and 1.0 mM lysozyme, respectively) are in good agreement with the ones recovered in the previous experiments carried out with mature isolated lysozyme fibrils (Table 3.4). In addition, the values recovered for the molar fractions of NR bound to lysozyme fibrils produced in the course of its fibrillation clearly show again that the kinetics is 1-2 days slower for 0.2 mM as compared to 1.0 mM lysozyme at acidic pH and elevated temperature.

In conclusion, the amyloid fibril formation of lysozyme was successfully followed with both standard probes ThT and NR. Again, the steady-state fluorescence anisotropy of NR was confirmed to be a very sensitive parameter that can be used in detecting the presence of lysozyme fibrils in solution. Altogether, the fluorescence results obtained for NR clearly confirm that this dye binds poorly or does not bind at all to native lysozyme at pH 2.2 or to any of the intermediates that are formed during the lag phase of lysozyme fibrillation kinetics. This suggests that these intermediates do not display nonpolar binding pockets that are able to accommodate this hydrophobic dye. Furthermore, a 5-fold decrease in the concentration of lysozyme used in the fibrillation assay carried out under quiescent conditions (from 1.0 to 0.2 mM) was found to increase the lag phase of its sigmoidal kinetics by approximately 2 days.

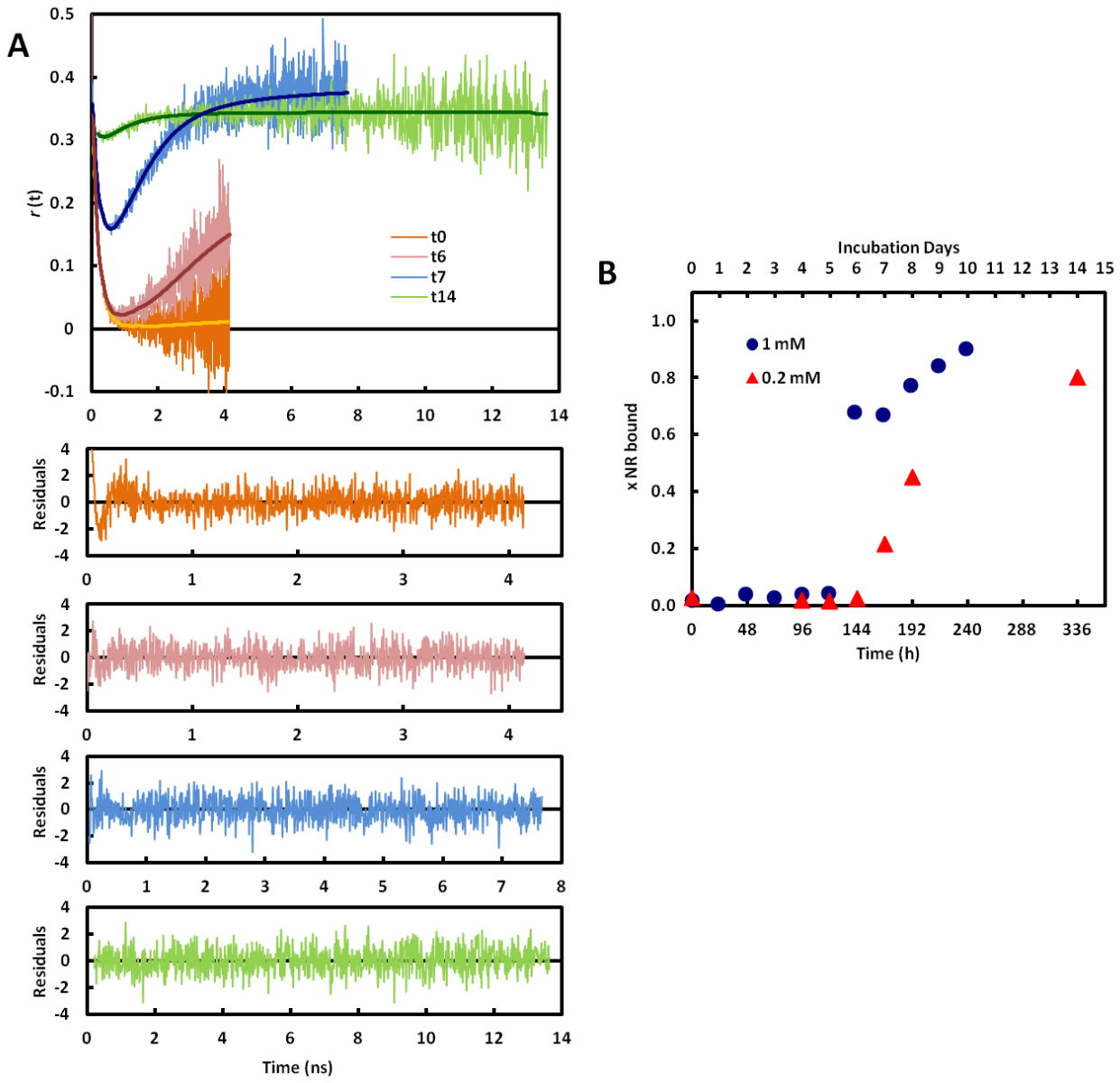

Figure 3.18 - Kinetics of lysozyme amyloid fibril formation monitored by time-resolved fluorescence anisotropy measurements of 2.9 µM of Nile Red.

(**A**) The anisotropy decays of NR were measured using λ_{exc}= 565 nm and λ_{em}= 650 nm at day 0 (t0), day 6 (t6), day 7 (t7) and day 14 (t14) during the fibrillation reaction of 0.2 mM lysozyme at pH 2.2 and 57 ºC. The anisotropy decays were fitted according to an associative model (Eq. 3.9, solid lines) (see the text and the legend of Figure 3.13 for more details). (**B**) Dependence of NR bound molar fraction to amyloid lysozyme fibrils with the incubation time of the protein samples: 0.2 mM (triangles) and 1.0 mM lysozyme (circles), recovered from the previous analysis The fibrillation reactions took course during 14 days, although not all time-points were measured.

3.2.3. Monitoring lysozyme aggregation/fibrillation via A488 fluorescence

After establishing that the fluorophore A488 is a sensitive probe for detecting unfolding transitions of Lz-A488 with temperature, our study proceeded to evaluate (*i*) the ability of this fluorescently-labeled protein to form mixed fibrils with lysozyme, and (*ii*) the influence of the Lz-A488/lysozyme mixing ratio used in the incubation mixture on both the kinetics of lysozyme fibrillation and the structural characteristics presented by the isolated mature lysozyme fibrils.

Several mixing ratios of Lz-A488/lysozyme were investigated in these studies: 1/2 and 1/8 ($[Lz]_t$= 0.2 mM), 1/40, 1/100 and 1/200 ($[Lz]_t$= 1.0 mM). The highest Lz-A488/lysozyme mixing ratios (1/2 and 1/8) were studied using a lower total lysozyme concentration in the incubation mixtures ($[Lz]_t$= 0.2 mM) due to difficulties in concentrating the stock solution of Lz-A488 by ultrafiltration using the Amicon® Ultra-15 filter devices. The flow rate in ultra filtration is affected by numerous factors, namely the sample concentration and its chemical nature, the starting volume, membrane type, temperature, relative centrifugal force and centrifuge rotor angle. Even when using longer centrifugation times than the values suggested in Amicon® Ultra-15 user guide, we were not able to concentrate the stock solution as much as we wanted. A low sample recovery in the concentrate due to adsorptive losses may also have occurred (Amicon® Ultra-15 user guide).

As it was shown in the control assays presented in the previous section, the main consequences of using a lower protein concentration were the extension of lysozyme fibrillation lag phase by 1 – 2 days and the production of a lower amount of lysozyme fibrils at the end of the fibrillation reactions (see section 3.2.3.2).

3.2.3.1. A488 is a versatile probe for detecting lysozyme amyloid fibril formation in vitro

The results obtained for Lz-A488/lysozyme= 1/40 will be presented first in detail as an example. Aliquots from the incubated sample ($[Lz]_t$= 1.0 mM) were withdrawn during 14 days and the fluorescence properties of Lz-A488 were used to monitor lysozyme fibrillation kinetics. Both the steady-state fluorescence emission spectra and anisotropy of Lz-A488 from samples obtained at different time points (Figure 3.2) were measured at room temperature. Figure 3.19 A shows that the integrated area of the fluorescence emission spectra of Lz-A488 decreased sharply during the first 7 days of sample incubation, until reaching a plateau with a signal that was ~10-15 % of its initial value at time 0. Concomitantly, the emission spectra of Lz-A488 did not undergo any spectral shifts (data not shown).

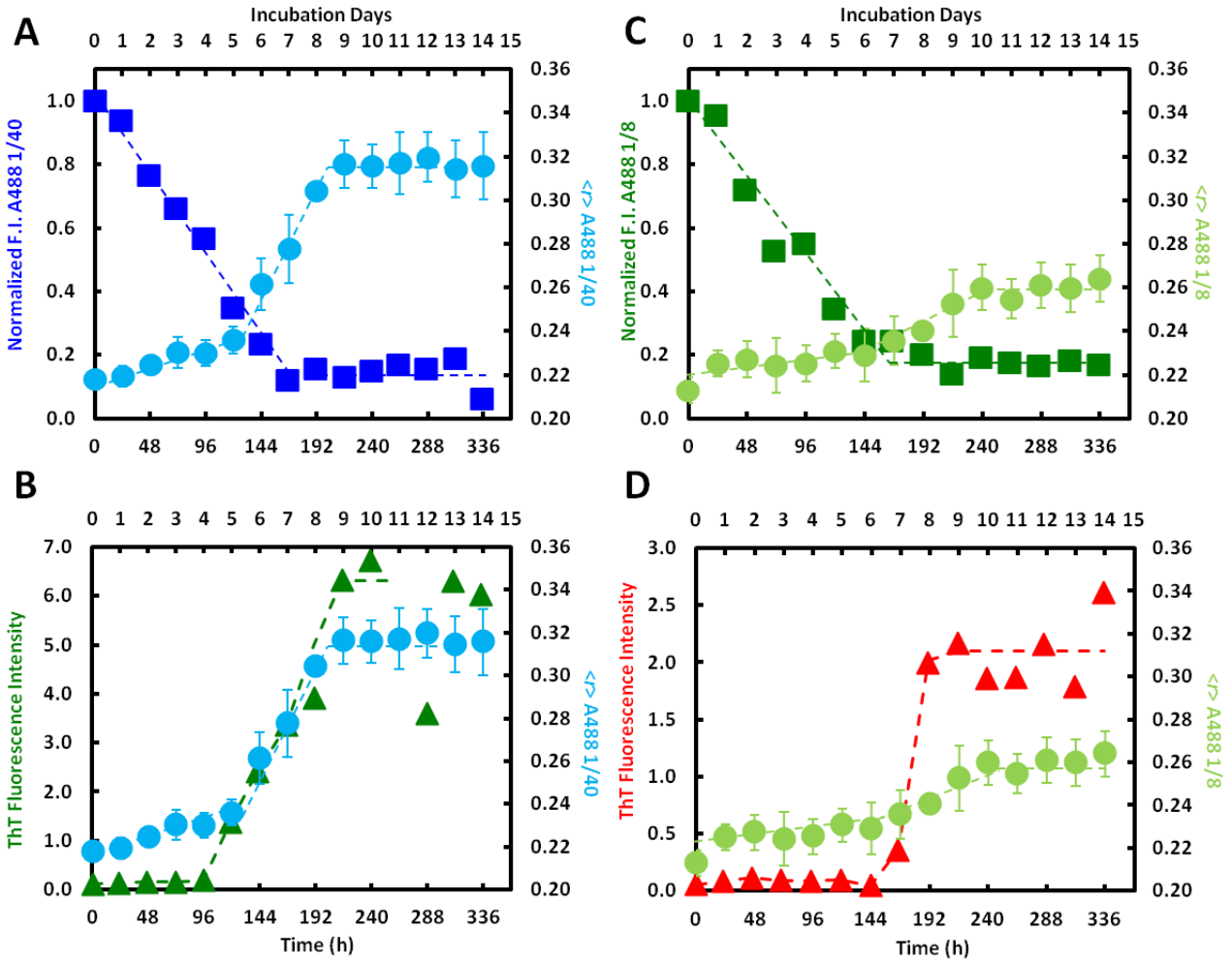

Figure 3.19 - Kinetics of lysozyme amyloid fibril formation at pH 2.2 and 57 ºC monitored by steady-state fluorescence measurements from Lz-A488.

(**A** and **C**) Normalized fluorescence intensities, to their values at 0 hours of incubation (squares) and steady-state fluorescence anisotropies (circles) of Lz-A488 as a function of incubation time during lysozyme fibrillation: (**A** and **B**) $[Lz]_t$= 1.0 mM; Lz-A488/lysozyme molar ratio= 1/40 and (**C** and **D**) $[Lz]_t$= 0.2 mM; Lz-A488/lysozyme molar ratio= 1/8. The fluorescence intensities are the integrated areas of the emission spectra of Lz-A488 using λ_{exc} = 480 nm and λ_{em} = 490-600 nm. In (**B**) and (**D**) the time course of ThT steady-state fluorescence intensity during lysozyme fibrillation kinetics is also plotted for comparison. For more details see the legend of Figure 3.16. The dashed lines are just a guide to the eye.

On the other hand, the variation of the steady-state fluorescence anisotropy of Lz-A488 as a function of its incubation time allowed to clearly identify 3 stages during lysozyme fibrillation kinetics (Figure 3.19 A): (*i*) during the first 5 days, the anisotropy rose gradually from 0.22 to 0.24, (*ii*) after day5, the anisotropy increased sharply from 0.24 up to 0.32 at day9 and finally, (*iii*) after day9 its value remained constant over time (<*r*>= 0.316 ± 0.002). This behavior is again consistent with a nucleation-dependent polymerization mechanism presented by lysozyme during its fibrillation (Butterfield and Lashuel, 2010). Stages 1, 2 and 3 must then correspond to the lag phase,

exponential growth and stationary phases of the kinetics, respectively. Indeed, the overlay of ThT-binding assay intensity and Lz-A488 fluorescence anisotropy showed a close agreement between the midpoints of fiber formation transitions (Figure 3.19 B). These results support the conclusion that Lz-A488 is able to form mixed fibrils with the corresponding unlabeled protein and that fluorescence anisotropy of Lz-A488 is a very good reporter parameter of lysozyme amyloid fibril formation kinetics *in vitro*.

The fluorescence intensity decay kinetics of Lz-A488 from samples obtained at different time points were also measured at room temperature. All the fluorescence decay profiles of Lz-A488 were adequately described by a tri-exponential function (Figure 3.20). The normalized amplitude of the Lz-A488 long lifetime component ($\tau_{3)}$ dropped by half during the exponential phase of this kinetics (Figure 3.20 A); simultaneously, τ_3 presented an increase from $\tau_3 = 3.55 \pm 0.04$ (day0-day7) to $\tau_3 = 3.80 \pm 0.03$ (as of day8). This indicates that Lz-A488 is probably being rigidly locked in a partially-unfolded and quenched conformation in the fibrils formed (Figure 3.20 C).

Finally, the anisotropy decay kinetics of Lz-A488 from samples obtained at each incubation time were also measured at room temperature to complement the steady-state anisotropy data, as it is illustrated in Figure 3.21 A for days 0, 6 and 14. The parameters recovered from the analyses are summarized in Table 3.5. The most striking result was the need to include a non-zero limiting anisotropy, r_∞, in Eq. 3.19 in order to be able to get a good fit of this equation to the experimental data of $r(t)$ for incubation times longer than 4-5 days (Table 3.5). This result clearly shows that Lz-A488 is being progressively incorporated into large lysozyme assemblies (protofibrils and fibrils) that are unable to depolarize the fluorescence emission from Lz-A488 during the time window defined by its excited-state lifetime.

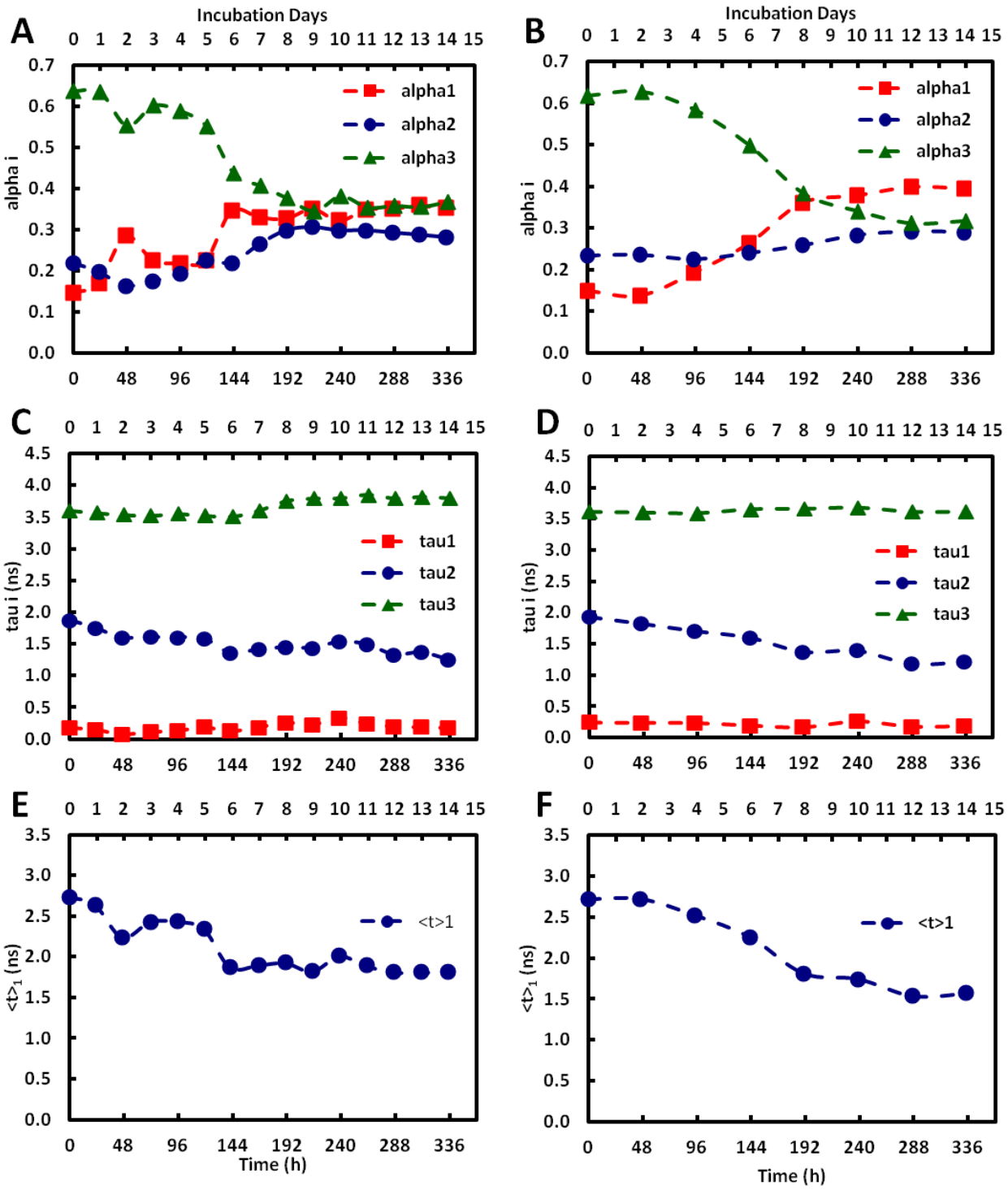

Figure 3.20 – Kinetics of lysozyme amyloid fibril formation at pH 2.2 and 57 ºC monitored by time-resolved fluorescence intensity measurements from Lz-A488.

(**A** and **B**) Fractional amplitudes, (**C** and **D**) lifetime components and (**E** and **F**) amplitude-weighted mean fluorescence lifetimes from Lz-A488 at different time points (measured with λ_{exc}= 460 nm and λ_{em}= 515 nm) during the fibrillation reactions of (**A**, **C** and **E**) $[Lz]_t$= 1.0 mM; Lz-A488/ lysozyme molar ratio= 1/40 and (**B**, **D** and **F**) $[Lz]_t$= 0.2 mM; Lz-A488/lysozyme molar ratio= 1/8. The fibrillation reactions took course during 14 days but not all time points were measured. The dashed lines are just a guide to the eye.

Table 3.5 – Fluorescence anisotropy decay parameters from Lz-A488 at different time points during lysozyme fibrillation kinetics carried out at pH 2.2 and 57 ºC with $[Lz]_t$= 1.0 mM; Lz-A488/lysozyme molar ratio= 1/40.

The steady-state and time-resolved anisotropy decays were measured using λ_{exc}= 495 nm and λ_{exc}= 460 nm, respectively, and λ_{em}= 515 nm. β_i, fractional amplitudes; ϕ_i, rotational correlation times; r_∞, limiting anisotropy; $r(0)= \beta_1 + \beta_2 + r_\infty$. The goodness-of-fit was judge by the χ^2_G value. $<r>_{cal}$ was calculated according to Eq. 3.24. $<r>_{exp}$ are presented as mean ± SD of ten measurements.Values in brackets are the errors of the recovered parameters estimated as the lower and upper bound of the joint confidence interval calculated for a 67% probability level.

Incubation days	β_1	ϕ_1 (ns)	β_2	ϕ_2 (ns)	r_∞	r(0)	χ^2_G	$<r>_{cal}$	$<r>_{exp}$
0	0.06	0.09 [0.05, -]	0.34	5.9 [5.8,6.1]	-	0.40	1.18	0.220	0.218 ± 0.004
1	0.06	0.08 [0.05, -]	0.34	6.0 [5.8,6.1]	-	0.40	1.19	0.224	0.219 ± 0.005
2	0.05	0.14 [0.12,0.21]	0.34	6.1 [6.0,6.4]	-	0.40	1.18	0.228	0.225 ± 0.004
3	0.05	0.18 [0.12,0.21]	0.35	6.3 [6.1,6.4]	-	0.40	1.11	0.231	0.230 ± 0.007
4	0.06	0.08 [0.06,-]	0.34	5.6 [5.4,6.3]	0.01 [0.00,0.02]	0.41	1.16	0.230	0.230 ± 0.006
5	0.04	0.28 [0.07,0.49]	0.34	6.3 [5.7,7.0]	0.02 [0.00,0.03]	0.39	1.07	0.245	0.236 ± 0.006
6	0.05	0.04 [0.02, -]	0.30	5.6 [5.5,6.1]	0.06 [0.04,0.06]	0.41	1.26	0.253	0.261 ± 0.012
7	0.06	0.08 [0.06,0.14]	0.23	5.5 [5.2,5.6]	0.12 [0.12,0.12]	0.41	1.28	0.273	0.278 ± 0.016
8	0.05	0.07 [0.05,0.12]	0.13	4.0 [3.6,4.9]	0.22 [0.21,0.23]	0.40	1.07	0.301	0.304 ± 0.003
9	0.06	0.08 [0.06,0.13]	0.09	3.4 [2.8,4.5]	0.25 [0.24,0.26]	0.41	1.14	0.308	0.316 ± 0.011
10	0.03	0.11 [0.03,0.16]	0.08	3.0 [2.6, 6.0]	0.29 [0.26,0.29]	0.40	1.15	0.328	0.316 ± 0.010
11	0.05	0.09 [0.06, -]	0.09	3.7 [3.1,5.1]	0.26 [0.24,0.27]	0.41	1.12	0.312	0.317 ± 0.014
12	0.05	0.06 [0.04, -]	0.08	2.7 [2.4,3.4]	0.27 [0.26,0.28]	0.41	1.12	0.315	0.320 ± 0.011
13	0.06	0.12 [0.05, -]	0.08	3.0 [2.3,4.7]	0.27 [0.26,0.27]	0.41	1.15	0.310	0.314 ± 0.013
14	0.06	0.03 [0.01, -]	0.09	2.7 [2.4,4.6]	0.26 [0.24,0.26]	0.40	1.14	0.298	0.316 ± 0.016

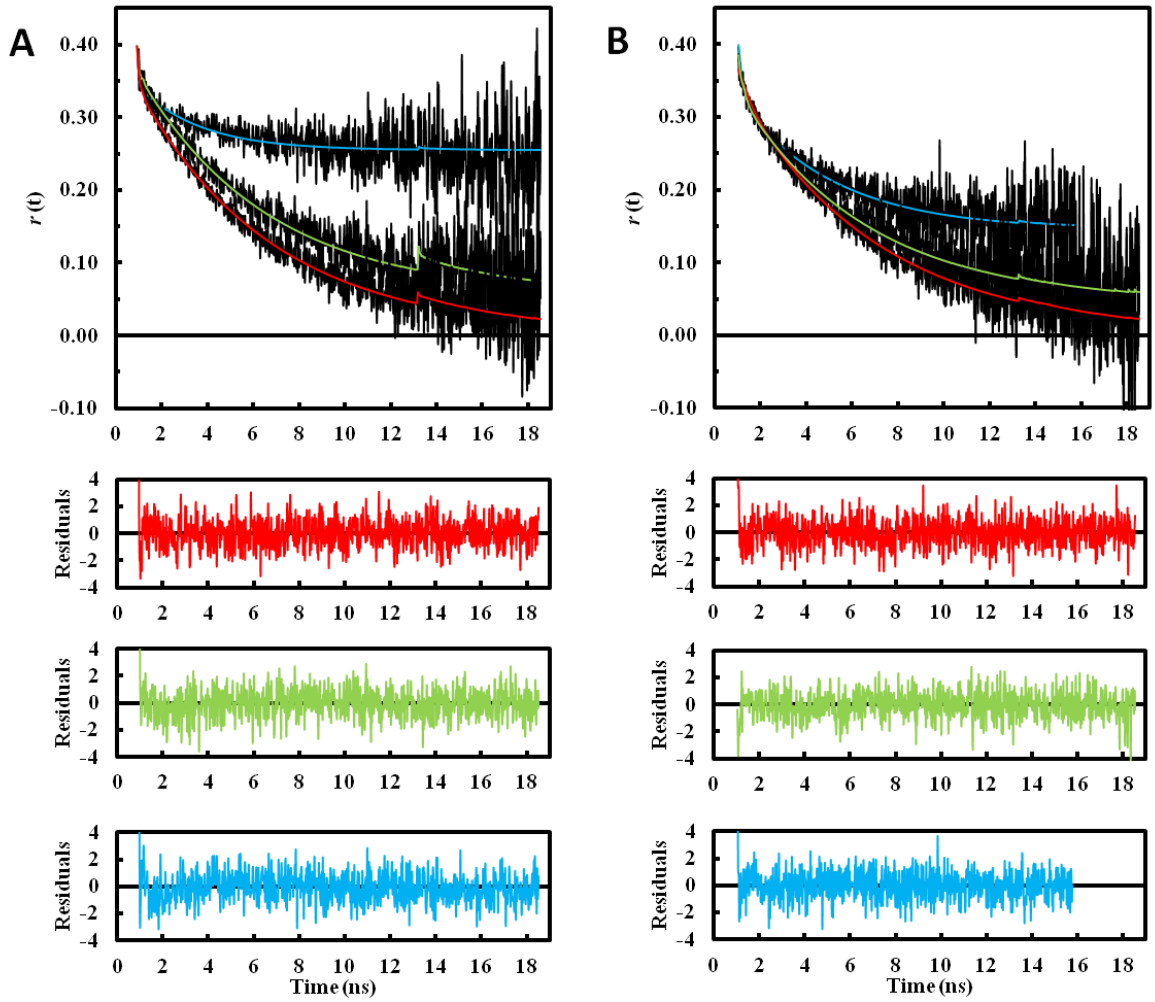

Figure 3.21 - Time-course of fluorescence anisotropy decays for different time-points of lysozyme fibrillation.

(**A**) $[Lz]_t$= 1.0 mM; Lz-A488/lysozyme molar ratio= 1/40 and (**B**) $[Lz]_t$= 0.2 mM; Lz-A488/ lysozyme molar ratio= 1/8. The solid lines are the best fit of Eq. 3.19 to the anisotropy decays of Lz-A488 measured at room temperature from samples obtained at (**A**) 0 (red), 6 (green) and 14 days (blue) and (**B**) 0 (red), 8 (green) and 14 days (blue), respectively. For more details, see Table 3.5. The small "bump" that is seen at approximately 13 ns is due to a secondary pulse of the laser system. This "bump" is more visible when the fluorescence intensity of the sample is lower.

3.2.3.2. Influence of Lz-A488/lysozyme mixing ratio on lysozyme amyloid fibril formation kinetics and on the fluorescence properties of lysozyme mature fibrils

The next question addressed in this study was whether the Lz-A488/lysozyme mixing ratio used in the incubation mixture influenced lysozyme fibril formation kinetics. The steady-state and time-resolved fluorescence data obtained from the samples prepared with 1/100 and 1/200 Lz-A488/lysozyme mixing ratios ($[Lz]_t$= 1.0 mM) were essentially identical to the ones previously described for the 1/40 sample (as can be seen in Figure 3.22 A and B for the steady-state

fluorescence measurements). It was therefore possible to decrease by 5-fold the molar fraction of fluorescently-labeled protein used in the sample mixture and still be able to accurately track the distinct stages of lysozyme fibril formation kinetics.

When the Lz-A488/lysozyme mixing ratio used in the preparation of the samples was increased to 1/8 and 1/2 ($[Lz]_t$= 0.2 mM), the relative drop in Lz-A488 fluorescence intensity at each incubation day was similar to the one previously described in detail for the 1/40 sample (Figure 3.22 A). However, the increase in the steady-state fluorescence anisotropy of Lz-A488 over time was much less pronounced and almost non-existent for the samples 1/8 and 1/2, respectively (Figure 3.22 B). For the sample prepared with a 1/8 ratio, it was still possible to identify the lag phase (from day 0 to day 6), the growth phase (from day 6 to day 10) and the stationary phase (day10 onwards) characteristic of lysozyme fibrillation kinetics (Figure 3.19 C), but the plateau value reached at the final stage of the kinetics ($<r>$= 0.259 ± 0.004) was much lower than the one obtained for the samples 1/40, 1/100 and 1/200 (Figure 3.22 B). Furthermore, although the amplitude of the Lz-A488 long lifetime component also dropped by half during the exponential phases of both these mixtures (exemplified in Figure 3.20 B for the sample 1/8), τ_3 remained essentially constant over time for the samples 1/8 and 1/2 (Figure 3.20 E and data not shown) at variance with the results obtained for the samples 1/40, 1/100 and 1/200 (Figure 3.20 B and data not shown). Again, the overlay of the ThT-binding assay and Lz-A488 fluorescence anisotropy showed a close agreement between the midpoints of fibril formation transition (Figure 3.19 D).

The sharp decrease detected in the fluorescence intensity during the first 7 days of incubation was independent of the initial lysozyme concentration and mixing ratio used, and in the subsequent days its value remained almost invariant at 10 to 20% of the initial value (Figure 3.22 A). Assuming that A488 covalently-labeled to lysozyme undergoes a fluorescence PET-based quenching mechanism, the sharp decrease in fluorescence intensity could be explained by the progressive irreversible unfolding of Lz-A488 over time due to the prolonged exposure of Lz-A488 to pH 2.2 and 57 ºC. As more lysozyme molecules undergo unfolding, less fluorescence emission is measured due to quenching, although only small differences in steady-state fluorescence anisotropy are seen up to day6-7. This suggests that the changes in fluorescence intensity observed in an initial phase are mainly due to conformational alterations rather than a change in the state of aggregation of Lz-A488. In a study performed by Ryan and co-workers, about fibril formation of A488-labeled apolipoprotein C-II, the authors also detected a decrease in fluorescence intensity over time with a parallel increase in anisotropy, but they do not provide any explanation for these results; they just highlighted the sensitivity of A488 fluorescence properties has being convenient for the continuous monitoring of fibril formation (Ryan *et al.*, 2008).

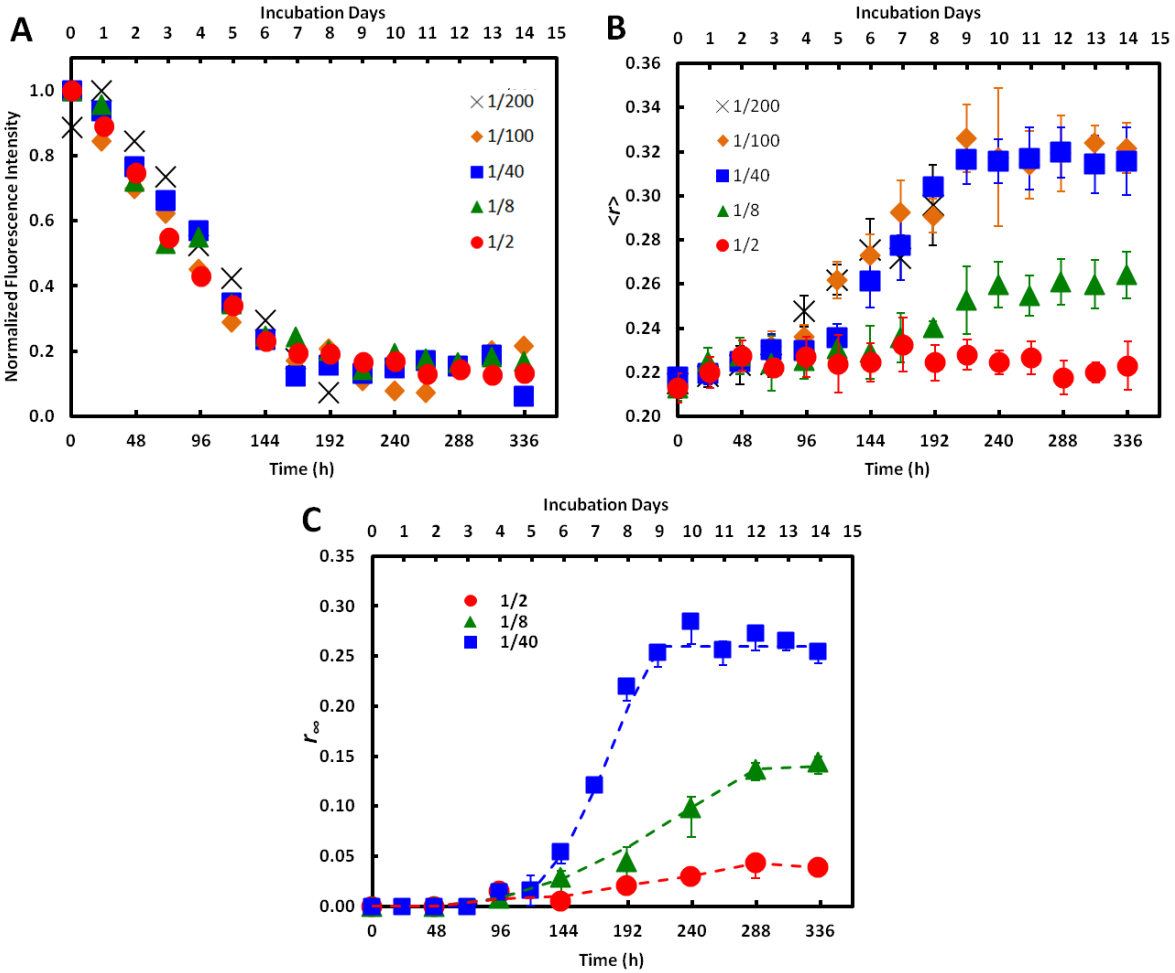

Figure 3.22 – Influence of Lz-A488/lysozyme mixing ratio on lysozyme fibrillation kinetics at pH 2.2 and 57 ºC.

(**A**) Relative fluorescence intensities, (**B**) steady-state fluorescence anisotropies and (**C**) limiting anisotropies from Lz-A488 as a function of incubation time during lysozyme fibrillation. Red circles and green triangles are the results for $[Lz]_t$= 0.2 mM with Lz-A488/lysozyme molar ratio= 1/2 and 1/8, respectively. Blue squares, orange diamonds and black crosses are the results for $[Lz]_t$= 1.0 mM; Lz-A488/lysozyme molar ratio= 1/40, 1/100 and 1/200 respectively. The error bars in (**C**) correspond to the lower and upper bound of the joint confidence intervals calculated for r_∞ at 67% probability level.

The steady-state anisotropy results described above raised the possibility that lysozyme fibril formation could be hampered in samples 1/2 and 1/8 due to the very high labeled/unlabeled mixing ratios used. To clarify if lysozyme fibrils were indeed being formed, NR was added to the aliquots taken from the incubation mixtures 1/8 and 1/2 at day11, and the steady-state fluorescence anisotropy of this dye was measured. The values obtained ($\langle r \rangle$= 0.320 ± 0.017 and $\langle r \rangle$= 0.291 ± 0.022 in each case, respectively) confirmed the presence of lysozyme amyloid fibrils in these samples.

Several alternative hypotheses can be put forward to explain the steady-state fluorescence anisotropy data presented above for the mixtures 1/2 and 1/8, namely:

(*i*) lysozyme fibrils produced in these samples are not fluorescent (*i.e.* lysozyme amyloid fibrils formed in these samples contain exclusively the unlabeled protein). This scenario could occur if the addition of a monomeric fluorescently-labeled lysozyme molecule to the critical "nuclei" prevented its further growth to protofibrils, and ultimately lysozyme fibrils. The increase detected in the steady-state fluorescence anisotropy of these samples would then have to be due to the formation of small oligomeric fluorescent species in solution;

(i*i*) mixed fluorescent lysozyme amyloid fibrils are formed in these samples but in much smaller amounts;

(*iii*) the occurrence of homotransfer (energy migration) between the Lz-A488 molecules incorporated in the mixed fibrils at a high density alters the kinetics of its emission anisotropy (Bader *et al.*, 2011).

It should be noted that the last two hypotheses are not necessarily mutually exclusive.

The first hypothesis was discarded by performing CFM studies of mature lysozyme fibrils isolated from the protein samples 1/2 and 1/8 by centrifugation. As it is shown in Figure 3.23, lysozyme amyloid fibrils could be imaged by CFM using the experimental settings adequate for A488 and NR fluorescence emission detection (Figure 3.23). Furthermore, the analysis of the Lz-A488 anisotropy decays from samples obtained at each incubation time already indicated the progressive formation of large fluorescent entities in solution as the inclusion of a non-zero residual anisotropy in the fitting equation to $r(t)$ was again required for incubation times longer than 4 and 8 days in order to be able to adequately describe the experimental data obtained for the 1/8 (Figure 3.21 B, Figure 3.22 C and Table 3.6) and 1/2 (Figure 3.22 C) incubation mixtures, respectively. In fact, as it is illustrated in Figure 3.22 C, the three stages of lysozyme fibrillation can be clearly identified by plotting r_∞ as a function of sample incubation time for the incubation mixture 1/40 and less pronounced with 1/8. It should be noted, however, that the values recovered for r_∞ from these analysis for the mixtures 1/8 and 1/2 were much lower as compared to the incubation mixture 1/40 as it is shown in Figure 3.22 C.

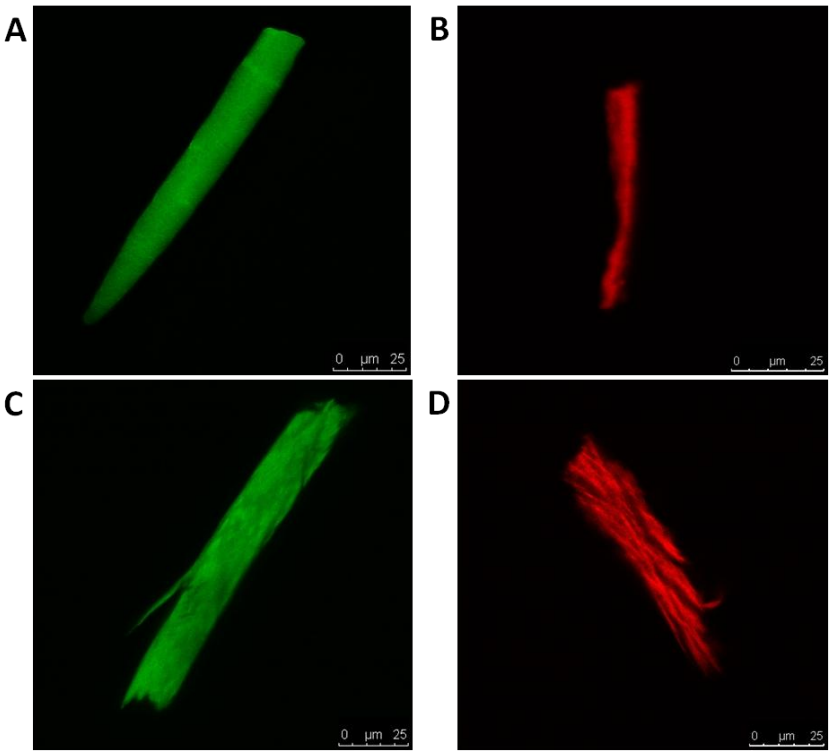

Figure 3.23 - Mature lysozyme fibrils isolated from the protein samples 1/2 and 1/8.

Mature mixed lysozyme fibrils were pelleted by centrifugation at the end of the incubation of mixtures prepared with Lz-A488/lysozyme molar ratios: (**A** and **B**) 1/2 and (**C** and **D**) 1/8. The fibrils were visualized with A488 (**A** and **C**) or stained with NR (**B** and **D**).

The second hypothesis was tested by comparing the final total amount of fibrils produced in mixed *versus* pure lysozyme fibrillation mixtures. After an incubation period of 12 – 14 days at pH 2.2 and 57 ºC under quiescent conditions, mature lysozyme fibrils were isolated by three consecutive centrifugation steps (Figure 3.3) and quantified spectrophotometrically at 280 nm as previously described in section 2.5. The final yields of lysozyme fibril formation are presented on Table 3.7. The yield represents the amount of lysozyme (on a monomer basis) that was included in the fibrils relatively to the initial amount preset in each sample. Several incubations of 1 mM of lysozyme were performed and an average yield of $\eta = (45 \pm 9)$ % ($n = 9$) was calculated. A similar value was obtained for the mixed samples, $\eta = (42 \pm 10)$ % ($n = 4$), excluding the molar ratio 1/2, which had an average yield of 27 %. This value was slightly lower than the rest. For 0.2 mM lysozyme, 4 incubations were performed and a yield of $\eta = (16 \pm 4)$ % ($n = 4$) was calculated, which is clearly lower than the rest. Although the results have a large variability, the control results obtained for 0.2 mM lysozyme show a clear difference from the results obtained with 1.0 mM indicating a lower fibril formation yield for 0.2 mM as compared to 1.0 mM lysozyme. For the mixed samples it is difficult to explain whether the fibrillation is hampered or favored by the

presence of labeled molecules of lysozyme, due to the discrepancies in the results obtained. It is necessary to carry out more experiments to clarify this point.

Table 3.6 - Fluorescence anisotropy decay parameters from Lz-A488 at different time points during lysozyme fibrillation kinetics carried out at pH 2.2 and 57 ºC with $[Lz]_t$= 0.2 mM; Lz-A488/ lysozyme molar ratio= 1/8.

For more details, see the legend of Table 3.5.

Incubation days	β_1	ϕ_1 (ns)	β_2	ϕ_2 (ns)	r_∞	r(0)	χ^2_G	$<r>_{cal}$	$<r>_{exp}$
0	0.04	0.49 [0.19,0.65]	0.33	6.2 [5.9,6.3]	-	0.37	1.16	0.222	0.213 ± 0.006
2	0.05	0.27 [0.23,0.41]	0.34	6.2 [6.1,6.3]	-	0.39	1.10	0.228	0.227 ± 0.008
4	0.05	0.11 [0.09,0.20]	0.34	5.9 [5.7,6.1]	0.01 [0.01,-]	0.40	1.14	0.232	0.225 ± 0.008
6	0.04	0.13 [0.08, -]	0.32	5.2 [5.0,6.0]	0.03 [0.00,0.04]	0.40	1.08	0.233	0.229 ± 0.012
8	0.06	0.15 [0.07,-]	0.28	5.6 [5.0,7.0]	0.04 [0.02,0.06]	0.38	1.25	0.235	0.240 ± 0.003
10	0.07	0.13 [0.09,-]	0.23	4.7 [4.1, 6.6]	0.10 [0.07,0.11]	0.40	1.16	0.247	0.260 ± 0.010
12	0.07	0.09 [0.07,0.13]	0.19	3.7 [3.4,4.0]	0.14 [0.13,0.14]	0.40	1.23	0.251	0.261 ± 0.011
14	0.08	0.19 [0.15,0.31]	0.18	4.2 [3.8,5.1]	0.14 [0.13,0.15]	0.40	1.14	0.260	0.264 ± 0.011

Finally, the fluorescence intensity and anisotropy decays measured for the isolated mature lysozyme amyloid fibrils prepared by centrifugation were also compared to the ones obtained from the aliquots withdrawn from the samples after 14 days of incubation (samples t14) (Table 3.8, Table 3.9 and Figure 3.24). The rationale beyond this approach was to reduce the sample heterogeneity by eliminating the soluble material from the samples by centrifugation (mainly, monomeric unfolded lysozyme molecules as well as small oligomeric intermediates/ protofibrils). If the dominant fluorescent species present at the end of lysozyme incubation were large mature lysozyme fibrils than one would expect to obtain very similar anisotropy decays for both samples (t14 and isolated

fibrils). This was the case found for the sample 1/40 (Figure 3.24 C) as its limiting anisotropies were 0.26 and 0.29 for the t14 samples and isolated mature fibrils, respectively (Table 3.9). The emission decay kinetics was also identical for both samples (Table 3.8).

Table 3.7 - Fibril formation yields in pure *versus* mixed lysozyme fibrillation mixtures after 12 – 14 days of incubation at pH 2.2 and 57 ºC under quiescent conditions.
Lysozyme fibrillation kinetics in the mixed mixtures was carried out using variable Lz-A488/lysozyme molar ratios: 1/2, 1/8, 1/40, 1/100 and 1/200, respectively. The calculations of lysozyme amounts were made on a monomer basis.

$[Lz]_{total}$ (mM)	Sample	*n*	Final yield (%)
0.2	Lz	4	16 ± 4
	1/2	1	27
	1/8	1	38
1.0	Lz	9	45 ± 9
	1/40	1	40
	1/100	1	56
	1/200	1	33

On the other hand, if there was a large amount of fluorescent material at t14 that could not be pelleted by centrifugation, than one would expect the anisotropy decays from the t14 sample to be much faster than the one's obtained for the isolated fibrils. The mixture 1/8 conformed to this scenario as it is shown in Figure 3.24 B. In this case, the residual anisotropies measured for the t14 sample and isolated mature fibrils were 0.14 and 0.28, respectively (Table 3.9). The additional observation that the anisotropy decays obtained for the mature isolated fibrils isolated from samples 1/8 and 1/40 were very similar (Figure 3.24 B and C, and Table 3.9) further indicates that the mixed mature lysozyme fibrils produced in these samples at the end of the incubation time presented very similar sizes, although they were produced in lower amounts in the mixture 1/8.

The anisotropy decays of Lz-A488 measured for the sample 1/2 at t14 and after isolating the mature lysozyme fibrils were totally distinct from the previous ones (Figure 3.24 A). The limiting anisotropy of the sample t14 was very low (r_∞= 0.04 (Table 3.9)). Furthermore, the anisotropy decay of the isolated fibrils was much faster than the ones presented by the samples 1/8 and 1/40 (Figure 3.24), with a limiting anisotropy of only 0.12 (Table 3.9). In addition, the relative contribution of the fast rotational correlation time to the decay was much more important in this

case as compared to the other mixtures studied (29% compared to 17 and 12% for the samples 1/8 and 1/40, respectively). Both these results can be rationalized on the basis of a very efficient energy migration (homotransfer) process between the Lz-A488 molecules incorporated in the mixed fibrils, causing a very efficient depolarization of the fluorescence emission of the sample. In fact, the A488 fluorophore has a very small Stokes shift and therefore when two of these molecules are separated by a short distance, resonance energy transfer may occur between them (Lakowicz, 2006; van Ham *et al*., 2010). It should also be noted that the amplitude-weighted mean fluorescence lifetime of the mature isolated fibrils prepared form the sample 1/2 was much shorter than the values obtained for the samples 1/8 and 1/40 ($<\tau>_1$= 0.6 ns *versus* 1.6 and 1.8 ns, respectively (Table 3.8)). This result further suggests that the final conformation/packing of Lz-A488 in the mature lysozyme fibrils isolated from the sample prepared with a very high labeled/unlabeled protein ratio is different from the other cases.

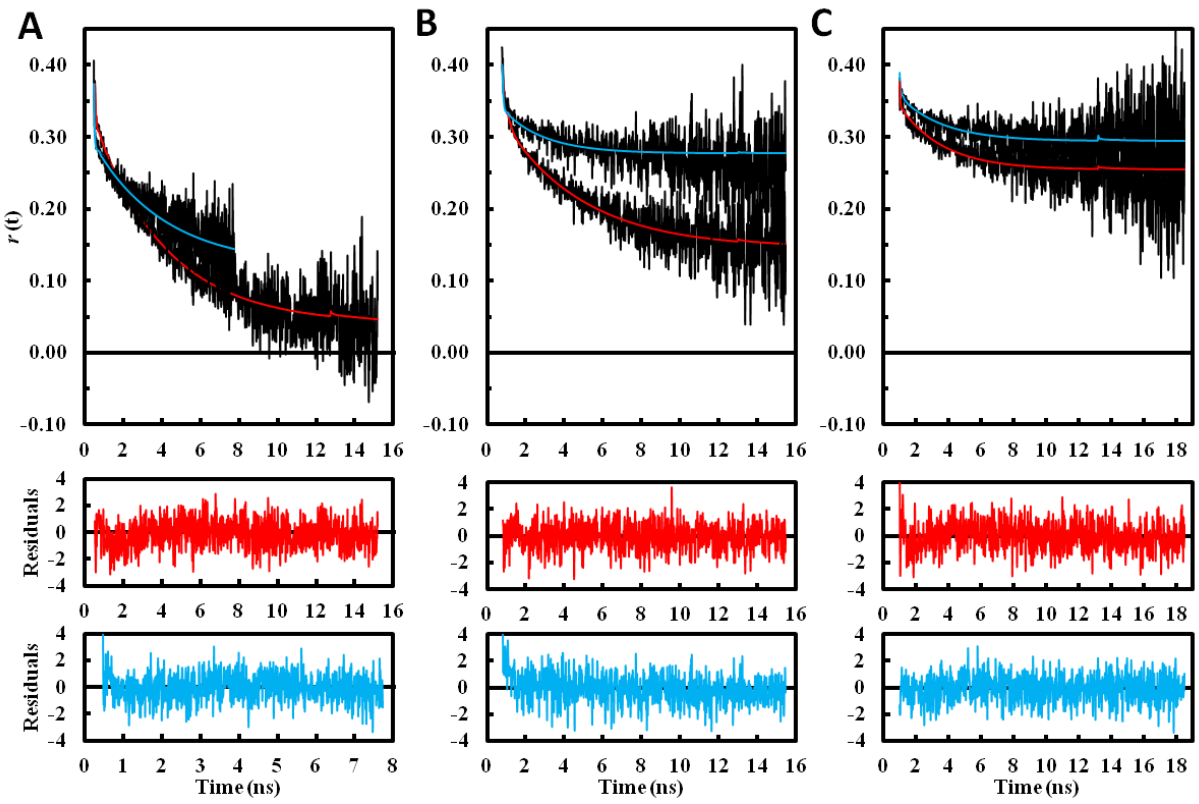

Figure 3.24 – Comparison between the fluorescence anisotropy decays obtained for the sample incubated for 14 days at pH 2.2 and 57 ºC (red) and 5 µM isolated mixed fibrils (blue). The fluorescence anisotropy decays of Lz-A488 were measured at room temperature. The Lz-A488/lysozyme molar ratio used in the incubation mixture was (**A**) 1/2, (**B**) 1/8 and (**C**) 1/40. The total lysozyme concentration in the incubation mixtures were (**A** and **B**) 0.2 mM and (**C**) 1.0 mM. The solid lines are the best fits of Eq. 3.19 to the experimental data. For more details, see Table 3.5.

Table 3.8 – Mean fluorescence lifetimes and intensity decay parameters from Lz-A488 at 14 days of incubation and after isolating the mature lysozyme fibrils by centrifugation.

Lysozyme fibrillation kinetics was carried out at pH 2.2 and 57 ºC using variable Lz-A488/lysozyme molar ratios. Sample 1/2 and 1/8: $[Lz]_t$= 0.2 mM; Lz-A488/lysozyme molar ratio= 1/2 and 1/8, respectively; Sample 1/40: $[Lz]_t$= 1.0 mM; Lz-A488/lysozyme molar ratio= 1/40) (for more details see the legend of Table 3.2).

Sample		α_1	τ_1 (ns)	α_2	τ_2 (ns)	α_3	τ_3 (ns)	$\langle\tau\rangle_1$ (ns)	$\langle\tau\rangle_2$ (ns)	χ^2_G
1/2	14 days	0.46	0.18 [0.16,0.20]	0.27	1.09 [1.02,1.19]	0.27	3.65 [3.60, 3.70]	1.36	2.88	1.23
	5 µM fibrils	0.59	0.11 [0.10,0.12}	0.29	0.67 [0.62,0.69]	0.12	2.66 [2.58,2.72]	0.58	1.70	1.49
1/8	14 days	0.39	0.19 [0.18,0.21]	0.29	1.21 [1.11,1.27]	0.32	3.61 [3.56,3.64]	1.57	2.91	1.16
	5 µM fibrils	0.39	0.28 [0.24,0.31]	0.32	1.34 [1.22,1.45]	0.29	3.57 [3.51,3.65]	1.57	2.73	1.15
1/40	14 days	0.35	0.18 [0.14,0.21]	0.28	1.25 [1.10,1.39]	0.37	3.79 [3.73,3.86]	1.81	3.18	1.30
	5 µM fibrils	0.35	0.20 [0.16,0.23]	0.29	1.36 [1.21,1.48]	0.36	3.81 [3.73,3.87]	1.84	3.14	1.11

In conclusion, we showed that Lz-A488 is able to form mixed fibrils with the corresponding unlabeled protein and the variation of its steady-state fluorescence anisotropy over the incubation period could be used to track the different stages of lysozyme fibrillation kinetics in detail when a low Lz-A488/lysozyme mixing ratio was used in sample preparation (1/40, 1/100 and 1/200).

The labeled/unlabeled protein mixing ratio was found to affect the final structure of the mixed fibrils formed. The population heterogeneity of the samples was evaluated through rotational dynamics by performing time-resolved fluorescence anisotropy measurements. For the Lz-A488/lysozyme mixing ratios 1/40, 1/100 and 1/200, the dominant fluorescent species present in solution at the end of each kinetic were large mature mixed lysozyme fibrils that could be easily pellet by centrifugation. On the other hand, a large amount of fluorescent soluble material that was not easily pelleted by centrifugation was still present in the mixture 1/8 at its 14th day of incubation.

Table 3.9 - Fluorescence anisotropy decay parameters from Lz-A488 at 14 days of incubation and after isolating the mature lysozyme fibrils by centrifugation.

For more details see the legend of Table 3.5 and Table 3.8.

Sample		β_1	ϕ_1 (ns)	β_2	ϕ_2 (ns)	r_∞	r(0)	χ^2_G	$\langle r \rangle_{cal}$	$\langle r \rangle_{exp}$
1/2	14 days	0.09	0.04 [0.03,0.07]	0.28	3.78 [3.62,4.01]	0.04 [0.03,0.04]	0.40	1.22	0.207	0.223 ± 0.011
	5 μM fibrils	0.12	0.01 [0.01,0.02]	0.17	3.71 [2.80,4.21]	0.12 [0.11,0.15]	0.40	1.15	0.241	0.246 ± 0.004
1/8	14 days	0.08	0.19 [0.15,0.31]	0.18	4.21 [3.82,5.13]	0.14 [0.13,0.15]	0.40	1.14	0.260	0.264 ± 0.011
	5 μM fibrils	0.07	0.04 [0.03,-]	0.06	2.17 [1.84,3.29]	0.28 [0.28,-]	0.40	1.15	0.308	0.246 ± 0.004
1/40	14 days	0.06	0.03 [0.02,-]	0.09	2.73 [2.44,4.63]	0.26 [0.24,0.26]	0.38	1.14	0.298	0.316 ± 0.016
	5 μM fibrils	0.05	0.05 [0.03,0.09]	0.06	2.71 [2.29,2.98]	0.29 [0.29,0.30]	0.40	1.24	0.325	0.318 ± 0.010

The fluorescence intensity decays obtained for the mixed mature lysozyme fibrils isolated from the samples 1/40, 1/100 and 1/200 indicate that Lz-A488 must be rigidly locked in a partially-unfolded and quenched conformation in the highly ordered fibrillar structures produced at the end of the incubation time (presenting a characteristic long lifetime component of 3.8 ns (Figure 3.20 C)). The conformation/packing of the fluorescently-labeled protein in the isolated mixed fibrils prepared from the sample 1/2 must be quite different from the previous cases as its amplitude-weighted mean fluorescence lifetime was much shorter in this case (Table 3.8).

Lastly, the time-resolved fluorescence anisotropy data also showed the occurrence of significant energy migration (homotransfer) between Lz-A488 molecules incorporated in the mixed mature fibrils formed only when the highest Lz-A488/lysozyme mixing ratio of 1/2 was used in sample preparation.

3.3. Lysozyme and Thioflavin T binding to anionic lipid membranes

One of the main goals of the undergoing research at the host laboratory is the clarification of the putative role of anionic lipid membranes in triggering amyloid-like fibril formation by several non-amyloidogenic proteins under physiological conditions. In fact, although several studies reported that the presence of negatively charged phospholipids is sufficient to induce rapid formation of fibers by a variety of non-amyloidogenic proteins, including lysozyme (Zhao *et al.*, 2004 and 2005; Alakoskela *et al.*, 2006; Gorbenko *et al.*, 2007), undisputable spectroscopic evidences for this effect are still missing in the literature.

ThT is a cationic probe (Figure 1.8 D) that is widely used to detect the formation of amyloid fibrils in solution (Biancalana and Koide, 2010; Groenning, 2010; Mishra *et al.*, 2011). However, as already mentioned in the Introduction, several studies show fluorescence enhancement of ThT upon binding to anionic macromolecules like DNA or SDS micelles (Kumar *et al.*, 2008; Hawe *et al.*, 2008). These observations immediately raised the question whether this cationic probe is still selective to these amyloid-like assemblies when negatively charged phospholipids are present in solution. It was therefore important to first characterize ThT partition towards POPC LUVs containing variable mol% of POPS. Then, competition binding assays of ThT and lysozyme/mature lysozyme fibrils and POPC LUVs containing 20 mol% of POPS were performed to evaluate the ability of ThT spectroscopic properties to detect amyloid-like fibrils in the presence of anionic lipid membranes. These experiments also allowed to test whether the co-incubation of lysozyme and anionic liposomes in a low ionic strength buffer at pH 7.4.was sufficient to drive amyloid-like fibril formation of lysozyme.

3.3.1. Thioflavin T partition to anionic lipid membranes is electrostatically-driven

ThT partition towards POPC LUVs containing variable mol% of POPS (10, 20 and 30mol%) was studied by fluorescence spectroscopy by monitoring the increase in the fluorescence intensity of 9 μM of ThT upon changing the total lipid concentration in solution from 0 to 6 mM. As it is shown in Figure 3.25 A the relative change in the fluorescence intensity of the dye, ΔI, with the phospholipid concentration in each sample was increasingly more pronounced as the acidic phospholipid content of the lipid vesicles used in the assay was raised. Figure 3.25 A was fitted to the data by linking ΔI_{max} between the three partition curves (ΔI_{max}= 3.99 ± 0.07). *ln* K_p was found to

vary linearly with the mol% of POPS used in the preparation of the liposomes (Figure 3.25 B), confirming that this interaction is predominantly electrostatically-driven.

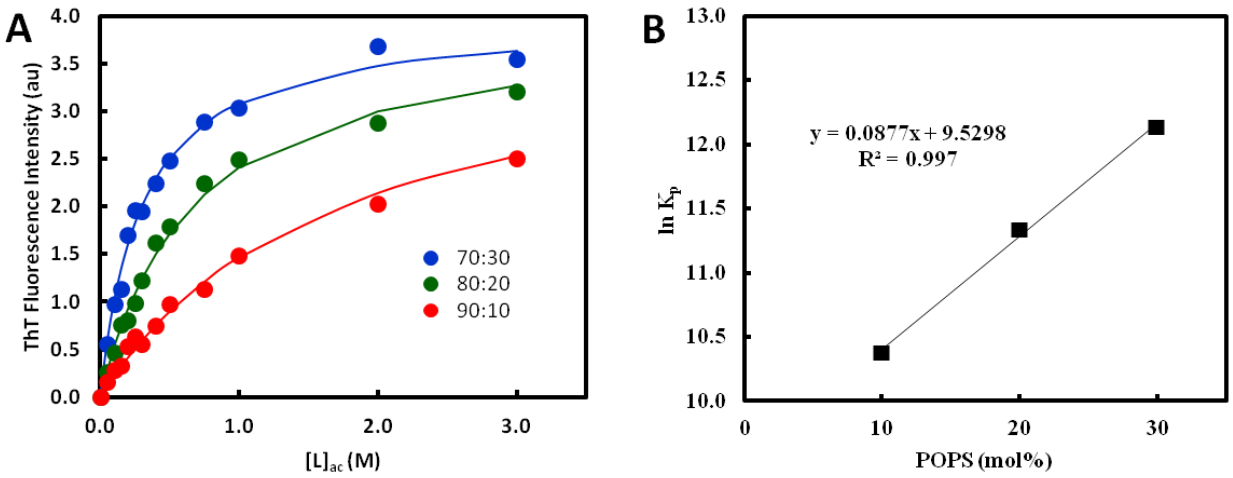

Figure 3.25 - Thioflavin T partition to anionic lipid membranes is electrostatically-driven.

(**A**) A multi-curve fit of the experimental results obtained with different mol% of POPS by Eq. 3.13 was performed by linking ΔI_{max} during the fitting of the three experimental data sets (10 mol% in red (K_p= (3.2 ± 0.2) x 10^4); 20 mol% in green (K_p= (8.4 ± 0.4) x 10^4); 30 mol% in blue (K_p= (1.9 ± 0.1) x 10^5); ΔI_{max}= 3.99 ± 0.07). (**B**) ln(K_p) was linearly dependent on the mol% of POPS used in the preparation of the liposomes.

3.3.2. Lysozyme binding to anionic lipid membranes does not induce amyloid-like fibril formation

To evaluate the ability of ThT to detect amyloid fibrils in the presence of anionic lipid membranes, competition binding assays of ThT and lysozyme/ mature lysozyme amyloid fibrils and POPC LUVs containing 20mol% of POPS to ThT were carried out at room temperature. Lysozyme or pre-formed lysozyme fibrils, ranging from 0 to 6 µM total protein concentration (on a monomer basis) were added to a fixed concentration of 0.86 mM POPC:POPS 80:20 LUVs. After 1 hour incubation of the LUV-protein mixtures at room temperature, 9 µM ThT was added to each sample and the fluorescence emission intensity of ThT in each sample was measured after a further incubation period of 30 minutes.

The ThT fluorescence signal was very low and independent of the native lysozyme concentration in solution (Figure 3.26, open green triangles). Although it has already been reported that ThT binds to some native proteins, like mentioned before, it appears that this does not happen with HEWL. The pre-incubation of 0.86 mM POPC:POPS 80:20 LUVs with native lysozyme only

shifted the ThT fluorescence signal of the samples vertically (Figure 3.26, closed green triangles). This result suggests that the increase detected in the dye´s fluorescence intensity is due to its binding to the anionic lipid vesicles and that these liposomes were not able to induce significant amyloid-like fibril formation of lysozyme under these experimental conditions. The alternative hypothesis that ThT partition towards the lipid vesicles might be preventing its binding to the amyloid-like fibrils was ruled out by repeating the experiments above but this time using mature lysozyme fibrils instead of native lysozyme. In this case, the fluorescence intensity of ThT increased approximately linearly with the concentration of pre-formed lysozyme fibrils added to the solution (Figure 3.26, open red squares); again, the data shifted vertically upon the inclusion of 0.86 mM POC:POPS 80:20 LUVs in the pre-incubation mixtures (Figure 3.26, closed red squares). This result shows that the extra increase in ThT fluorescence intensity is due to the binding of the dye to the LUVs, *i.e.* the partition of the dye to the lipid vesicles is not strong enough to preclude its binding to the lysozyme amyloid fibrils. This simple assay suggests that the presence of anionic lipid membranes does not induce extensive amyloid-like fibril formation of lysozyme, which contradicts other authors (Zhao *et al*., 2004) and reinforces the recommendation to always perform the adequate control assays if ThT is used to follow the fibrillation kinetics of a protein.

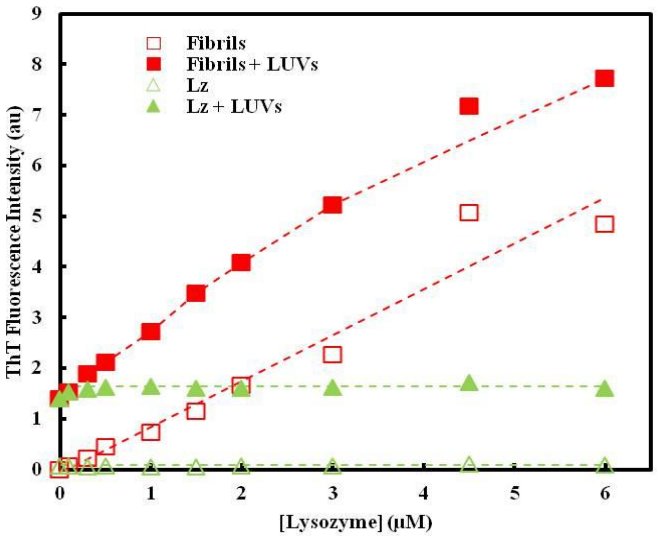

Figure 3.26 - Competition binding assays of Thioflavin T and lysozyme/ mature lysozyme amyloid fibrils and POPC LUVs containing 20 mol% of POPS.

Lysozyme (Lz, green triangles) or pre-formed lysozyme fibrils (Fibrils, red squares), ranging from 0 to 6 μM total protein concentration (on a monomer basis) were added (closed symbols) or not (open symbols) to a fixed concentration of 0.86 mM POPC:POPS 80:20 LUVs. After 1 h of incubation, 9 μM of ThT was added to each sample and its fluorescence emission intensity was measured after a further incubation period of 30 min, with λ_{exc}= 450 nm and λ_{em}= 470-600 nm.

4. Concluding remarks

Despite the many processes that assist protein folding in a cellular environment, misfolding can still arise, if by some reason a specific peptide or protein fails to adopt or maintain its native functional conformational state (Hebda and Miranker, 2009). There is a variety of human diseases associated with alterations in the normal and native structure and function of proteins. In some cases, misfolding can lead to a toxic gain-of-function as a conversion of specific peptides or proteins to highly organized fibrillar aggregates, normally referred to as amyloid fibrils, can occur (Chiti and Dobson, 2006). In the past few years more attention has been focused on the intermediates that precede the formation of amyloid fibrils than on the fibrils themselves, since they have been implicated as the source of toxicity associated with amyloidosis. Moreover, these intermediates appear to interact with biological membranes, promoting the disruption of the membrane integrity, and causing an imbalance in the cell homeostasis, which activates apoptotic signals that lead to cell death (Quist *et al*., 2005; Kinnunen, 2009; Hebda and Miranker, 2009).

In 2004, Kinnunen and his collaborators proposed that negatively-charged liposomes can trigger the formation of amyloid-like assemblies by non-amyloidogenic proteins under essentially physiological conditions (Zhao *et al*., 2004). Later on, further results endorsed this observation (Zhao *et al*., 2005; Alakoskela *et al*., 2006; Gorbenko *et al*., 2007; Mahalka and Kinnunen, 2009; Gorbenko and Trusova, 2011) but no undisputable structural evidence has been presented yet in the literature to support this proposal. An important ongoing research line at the host laboratory is aimed at elucidating the factors that govern the formation of these protein-membrane supramolecular complexes first described by Kinnunen´s group by using HEWL as a model non-amyloidogenic protein. By understanding the fibril formation pathways of model proteins and the intermediates involved upon their interaction with lipid membranes, a major step forward in the comprehension of amyloid fibril formation would be taken and the information would certainly help unravel the pathways of disease-causing proteins.

Lysozyme has been previously covalently conjugated to A488 SE to carry out fluorescence-based measurements at the host laboratory. First, FCS was used to study the partition behavior of Lz-A488 towards POPC LUVs containing variable mol% of POPS, confirming that lysozyme binding to negatively charged liposomes is dominantly driven by electrostatic interactions (Melo *et al*., 2011). Secondly, the variation of Lz-A488 fluorescence properties as a function of total lipid concentration allowed identifying three consecutive stages in lysozyme interaction with acidic lipid vesicles. It was also shown that the critical parameter controlling the emissive properties of Lz-A488 was the surface coverage of the anionic liposomes by the conjugated protein (Melo *et al*., 2012). To clarify the photophysical mechanism underlying these fluorescence changes and to confirm that they were indeed reporting conformational transitions undergone by lysozyme, the

work developed in this thesis started by monitoring the thermal denaturation profiles of Lz-A488 at both pH 2.2 and 7.4 using fluorescence spectroscopy (both steady-state and time-resolved fluorescence measurements were made). The neutral pH 7.4 was investigated since it is the pH most used in protein-lipid interaction studies (Zhao *et al.*, 2004; Gorbenko *et al.*, 2007), which we wanted to further explore; the acidic pH 2.2 was studied because it is often employed in lysozyme fibrillation assays (Mishra *et al*., 2007; Meratan *et al*., 2011). The fluorescence properties of Lz-A488 were first characterized at room temperature at both pH values because A488 is reported to be a pH-insensitive dye from pH 4-10 (Haugland, 2005) but pH 2.2 is out of this range. A 5-nm red-shift was detected in the emission spectra of both the free dye and Lz-A488 at pH 2.2 as compared to 7.4 (Table 3.1), pointing out that the ionization state of the fluorophore must have changed in the more acidic buffer. On the other hand, the time-resolved fluorescence anisotropy decays indicated that the protein is properly folded in both conditions since the global rotational correlation time obtained for Lz-A488 were very similar at both pHs (ϕ_2 = 5.6 ns (Table 3.3)). Furthermore, the covalently-bound dye was found to experience a restricted range of internal angular fluctuations during its excite-sate fluorescence lifetime, with an angle of θ_{seg} = 19.1º and 21.5º in buffer pH 2.2 and 7.4, respectively.

The next step of this work was to evaluate the ability of the covalently-conjugated fluorophore A488 to report conformational changes undergone by Lz-A488 under known destabilizing conditions. The fluorescence emission of Lz-A488 underwent a temperature-dependent quenching process at both pH values that enabled tracking its thermally-induced unfolding. In fact, the melting temperatures, T_{m}, determined for Lz-A488 at pH 2.2 and 7.4 from these studies were 55 ºC and 73.5 ºC, respectively, very close to data from the literature obtained using different biophysical techniques (Figure 4.1) (Arnaudov and Vries, 2005; Lee *et al.*, 2006; Trexler and Nilsson, 2007). These results confirm that the covalent modification of the enzyme with A488 did not perturb its tertiary structure appreciably and suggest that the predominant labeling site of A488 in the enzyme experiences the early unfolding events of its tertiary structure in order to be able to report a T_{m} so close to the published values.

Lz-A488 was proposed to be sensitive to a PET-based quenching mechanism (Figure 3.7), by electron donor(s) present in several possible adjacent amino acid residues close to the dye attached to the protein. Particular good candidates for temperature-dependent quenchers of A488 fluorescence in Lz-A488 are residues W62 and W63 located on the long loop in lysozyme's β domain as temperature-induced lysozyme unfolding is described to begin in this region. Both these residues are close to K97 residue in the native protein (Figure 1.6) which is expected to be the

preferential labeling site of lysozyme (*vide infra*). After being able to maintain its structure almost intact until $T \sim 64$ ºC at neutral pH, lysozyme unfolding progresses by loosing β-sheet structures in the β-domain, along with a small part of the helical structure of α-domain, and then a generally loss of tertiary structure, with increasing temperatures (Meersman *et al.*, 2010). The partial unfolding of lysozyme upon heating the solution must allow the establishment of van der Waals contacts between A488 and residues W62 and W63 (tryptophan residues were found to be strong quenchers of A488 by other authors (Choi *et al.*, 2011)). Due to its disulfide bonds, lysozyme does not unfold completely. There are two disulfide bonds near the long loop (Figure 1.6), one of them links the α-helix C that includes K97 and the cysteine in position 64, which is just close to the tryptophan residues assumed to be responsible for the quenching mechanism. Therefore, even when lysozyme is fairly unfolded, K97 and W62 and W63 residues are expected to remain close enough to each other for the PET-quenching mechanism to persist. This quenching is expected to produce increased populations of Lz-A488 molecules that present a much shorter excited-state lifetime or that even are non-fluorescent, as it was observed (Figure 3.6 D).

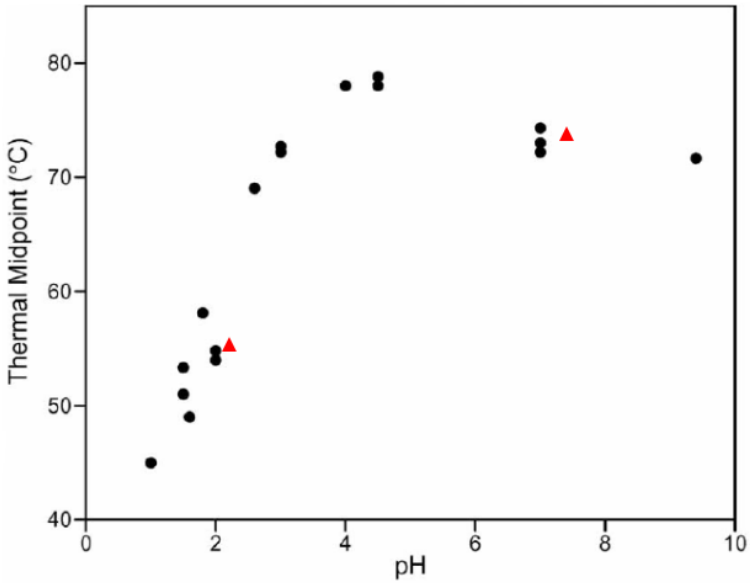

Figure 4.1 – pH dependence of the thermal midpoint for HEWL.

The midpoints represented (black circles) were determined using CD and fluorescence spectroscopy. The experimental midpoints determined in this work are represented as red triangles. Adapted from Trexler and Nilsson, 2007.

The work then proceeded towards monitoring the evolution of Lz-A488 fluorescence properties when subjected to known amyloid fibril formation conditions, namely acidic pH (pH 2.2), elevated temperature (T= 57 ºC) and high protein concentration (0.2 or 1.0 mM total concentration of lysozyme) under quiescent conditions. Several mixing ratios of Lz-A488/ total lysozyme were investigated in this work: for $[Lz]_t$= 0.2 mM, 1/2 and 1/8 ratios were studied, and with $[Lz]_t$= 1.0 mM, 1/40, 1/100 and 1/200 ratios were investigated. Control assays with 0.2 and 1.0 mM unlabeled lysozyme were also carried out under the same fibrillation conditions by employing the amyloid-specific dyes ThT and NR to follow amyloid fibril formation. The main consequences of decreasing by 5-fold the concentration of lysozyme used in these assays was the extension of lysozyme fibrillation lag phase by 1 – 2 days (from 4 to 6 days (Figure 3.16)) and the production of a lower amount of lysozyme fibrils at the end of the fibrillation reactions (Table 3.7).

The fluorescence anisotropy of NR proved to be a very sensitive parameter to detect the presence of lysozyme fibrils in solution, given the fact that time-resolved anisotropy measurements confirmed that this dye does not bind or binds poorly to the intermediates formed during the lag phase of lysozyme fibrillation kinetics (Figure 3.16). These results suggest that these intermediates do not display nonpolar binding pockets that are able to accommodate this hydrophobic dye. A moderate binding affinity of NR to mature lysozyme fibrils at pH 2.2 was also determined by fitting an associative model to the time-resolved anisotropy data obtained for this dye (K_d= (2.0 ± 0.4) μM (Figure 3.15)).

CFM confirmed that Lz-A488 was able to form mixed fibrils with the corresponding unlabeled protein for all Lz-A488/lysozyme mixing ratios tested. The aggregation of lysozyme mixtures 1/40, 1/100 and 1/200 exhibited essentially the same assembly kinetics as unlabeled lysozyme (Figure 3.19 A and B and data not shown). The steady-state fluorescence anisotropy of Lz-A488 proved to be a particularly informative parameter because it could be used to discriminate the different stages of lysozyme fibrillation kinetics for the samples 1/8, 1/40, 1/100 and 1/200: lag, growth and plateau phases, respectively (Figure 3.22 B). The beginning and duration of the different stages correlated well with the ones presented by the unlabeled lysozyme and that were detected using the standard ThT probe (Figure 3.19 B and D).

Altogether these results strongly suggest that lysozyme is indeed preferentially fluorescently-labeled at residue K97 and not K33 as only the first amino acid residue is present on the lysozyme fragments that are incorporated into the mature fibrils. In fact, the fibrillation mechanism of lysozyme under experimental conditions similar to the ones used in this work is extensively characterized in the literature. In 2004, Frare and co-workers showed that HEWL fibrils

obtained from the incubation of a 1.0 mM solution of protein at pH 2.0 and 65 ºC for 10 days were composed of protein fragments encompassing residues 49–100/101 and 53–100/101, derived from the partial acid-mediated cleavage of Asp-containing peptide bonds (Frare *et al*., 2004). To gain further insights into the aggregation properties of HEWL, the authors produced lysozyme fragments by limited proteolysis and found that only fragment 57–107 readily formed amyloid fibrils under the solution conditions used. This is likely to represent a key region responsible for triggering the aggregation process of the entire protein (Frare *et al*., 2004) and correlates well with the previously described fragment 32–108 that was found to be highly amyloidogenic in human lysozyme (Frare *et al*., 2006). Later in 2007, a study of HEWL fibril formation at pH 1.6 and 65 ºC reached similar conclusions, as the intact full-length protein was never found to dominate the composition of the amyloid fibrils. The authors mention that mature amyloid fibrils are composed mainly by the fragments 49/53-101; the non-amyloidogenic parts of the nicked protein (1-48/102-129) are cleaved from the fibrils. By adding mature amyloid fibrils during the amyloid formation process, the rate of formation was accelerated efficiently, while adding the full-length lysozyme at the end of the lag phase slowed the rate of the growth phase (Mishra *et al*., 2007).

The labeled/unlabeled protein mixing ratio was found to affect the structural properties of the mature fibrils (Figure 3.22). The sample heterogeneity at the end of the kinetics was evaluated by performing time-resolved fluorescence anisotropy measurements. For the low Lz-A488/lysozyme mixing ratios studied (mixtures 1/40, 1/100 and 1/200), the dominant fluorescent species present in solution by the end of the incubation time (14 days) were large mature mixed lysozyme fibrils easily pelleted by centrifugation. A large amount of fluorescent soluble material was still present in the mixture 1/8 at its 14^{th} day of incubation, as can be concluded by comparing the different anisotropy decays of day14 and the material pelleted by centrifugation (Figure 3.24 B). This result is probably explained by the lower fibrillation yield obtained when 0.2 mM lysozyme was used. Fluorescence anisotropy decays also showed the occurrence of significant energy migration (homotransfer) between Lz-A488 molecules incorporated in the mixed mature fibrils formed for Lz-A488/lysozyme mixing ratio 1/2.

On the other hand, the fluorescence intensity decays obtained for Lz-A488 incorporated in the mixed mature fibrils indicate that Lz-A488 must be rigidly locked in a partially-unfolded and quenched conformation in the fibril structures produced at the end of the incubation time (presenting a characteristically long lifetime component of τ_3= 3.8 ns (Figure 3.20 C)). Although an extensive characterization of the morphology of the fibrils was not performed in this study, it is clear that the packing of the fluorescently-labeled protein in mature fibrils isolated from the highest Lz-A488/lysozyme mixing ratio (1/2) must be somehow different from the rest of the mixing ratios,

due to its much shorter amplitude-weighted mean fluorescence lifetime (Table 3.8). This result confirms the plasticity of the lysozyme fibrils formed, suggesting that different arrangements in the position and orientation of Lz-A488 within the fibrils are possible, depending on the conditions used in their growth.

The ability of ThT spectroscopic properties to detect amyloid-like fibrils in the presence of anionic lipid membranes was also addressed at the end of this work. The cationic dye ThT was confirmed to partition to POPS-containing LUVs through predominantly electrostatic interactions (Figure 3.25). There was a pronounced increase in the fluorescence intensity of the dye upon increasing the lipid concentration, even in the absence of any protein added to the solution. This result reinforces the recommendation that adequate control assays should always be performed when ThT is used to follow the fibrillation kinetics of a protein in the presence of negatively-charged liposomes. On the other hand, the competition binding assays of ThT and lysozyme/ mature lysozyme amyloid fibrils and POPC LUVs containing 20mol% of POPS (Figure 3.26) showed that the presence of anionic lipid membranes does not induce extensive amyloid-like fibril formation of lysozyme, at variance with was previously proposed by Kinnunen´s group (Zhao *et al.*, 2004). The present study clarifies that the changes undergone by the fluorescence properties of Lz-A488 upon its interaction with POPC LUVs containing variable mol% of POPS (Melo *et al.*, 2012) must be reporting alterations in the conformation/ oligomerization state of the protein upon varying the surface coverage of the lipid vesicles, but without progressing into the formation of amyloid-like assemblies with ThT-binding properties. Additional studies are necessary to evaluate if this conclusion can be generalized to other non-amyloidogenic peptides/proteins in interaction with anionic liposomes.

With a similar characterization for other model proteins, this fluorophore can be one more tool to help clarify the mechanisms associated with amyloid fibril formation, including the intermediates involved, thanks to its photophysical qualities, including the stability at different pHs and the capacity to report modification in its vicinity.

References

Aisenbrey C, Borowik T, Byström R, Bokvist M, Lindström F, Misiak H, Sani M, Gröbner G (2008) How is protein aggregation in amyloidogenic diseases modulated by biological membranes? *Eur. Biophys. J.* **37**: 247-255.

Alakoskela J, Jutila A, Simonsen AC, Pirneskoski J, Pyhäjoki S, Turunen R, Marttila S, Mouritsen OG, Goormaghtigh E, Kinnunen PKJ (2006) Characteristics of fibers formed by cytochrome *c* and induced by anionic phospholipids. *Biochemistry* **45**: 13447-13453.

Anand U, Jash C, Mukherjee S (2011) Protein unfolding and subsequent refolding: a spectroscopic investigation. *Phys. Chem. Chem. Phys.* **13:** 20418-20426.

Arnaudov LN, Vries R (2005) Thermally induced aggregation of hen egg white lysozyme. *Biophys. J.* **88:** 515-526.

Aso Y, Shiraki K, Takagi M (2007) Systematic analysis of aggregates from 38 kinds of non disease-related proteins: identifying the intrinsic propensity of polypeptides to form amyloid fibrils. *Biosci. Biotechnol. Biochem.* **71(5)**: 1313-1321.

Babu KR, Bhakuni V (1997) Ionic-strength-dependent transition of hen egg-white lyszozyme at low pH to a compact state and its aggregation on thermal denaturation. *Eur. J. Biochem.* **245:** 781-789.

Bader AN, Hoetzl S, Hofman EG, Voortman J, van Bergen en Henegouwen PMP, van Meer G, Gerritsen HC (2001) Homo-FRET imaging as a tool to quantify protein and lipid clustering. *ChemPhysChem.* **12**: 475-483.

Banks PR, Paquette DM (1995) Comparison of three common amine reactive fluorescent probes used for conjugation to biomolecules by capillary zone electrophoresis. *Bioconjugate Chem.***6:** 447-458.

Bartlett AI, Radford SE (2009) An expanding arsenal of experimental methods yields an explosion of insights into protein folding mechanisms. *Nat. Struct. Mol. Biol.***16(6):** 582-588.

Biancalana M, Koide S (2010) Molecular mechanism of Thioflavin-T binding to amyloid fibrils. *Biochim. Biophys. Acta* **1804:** 1405-1412.

Bokvist M, Lindstrom F, Watts A, Grobner G (2004) Two types of Alzheimer's β-amyloid (1–40) peptide membrane interactions: aggregation preventing transmembrane anchoring versus accelerated surface fibril formation. *J. Mol. Biol.* **335**: 1039–1049.

Bolognesi B, Kumita JR, Barros TP, Esbjorner EK, Luheshi LM, Crowther DC, Wilson MR, Dobson CM, Favrin G, Yerbury JJ (2010) ANS binding reveals common features of cytotoxic amyloid species. *ACS Chemical Biology* **5(8)**: 735-740.

Booth DR, Sunde M, Belloti V, Robinson CV, Hutchinson WL, Fraser PE, Hawkins PN, Dobson CM, Radford SE, Blake CCF, Pepys MB (1998) Instability, unfolding and aggregation of human lysozyme variants underlying amyloid fibrillogenesis. *Nature* **385**: 787-793.

Brinkley M (1992) A brief survey of methods for preparing protein conjugates with dyes, haptens, and cross-linking reagents. *Bioconjugate Chem.* **3**: 2-13.

Buell AK, Dhulesia A, Mossuto MF, Cremades N, Kumita JR, Dumoulin M, Welland ME, Knowles TPJ, Salvatella X, Dobson CM (2011) Population of nonnative states of lysozyme variants drives amyloid fibril formation. *J. Am. Chem. Soc.* **133**: 7737-7743.

Butterfield SM, Lashuel HA (2010) Amyloidogenic protein-membrane interactions: mechanistic insight from model systems. *Angew. Chem. Int. Ed.* **49**: 5628-5654.

Cao A, Hu D, Lai L (2004) Formation of amyloid fibrils from fully reduced hen egg white lysozyme. *Protein Sci.* **13**: 319-324.

Celej MS, Jares-Erijman EA, Jovin TM (2008) Fluorescent *N*-arylaminonaphthalene sulfonate probes for amyloid aggregation of α-synuclein. *Biophys. J.* **94:** 4867-4879.

Chen H, Ahsan SS, Santiago-Berrios MB, Abrunã HD, Webb WW (2010) Mechanisms of quenching of Alexa fluorophores by natural amino acids. *J. Am. Chem. Soc.* **132:** 7244-7245.

Chen H, Rhoades E, Butler JS, Loh SN, Webb WW (2007) Dynamics of equilibrium structural fluctuations of apomyoglobin measured by fluorescence correlation spectroscopy. *Proc. Natl. Acad. Sci. USA* **104(25)**: 10459–10464.

Chirita CN, Necula M, Kuret J (2003) Anionic micelles and vesicles induce tau fibrillization in vitro. *J. Biol. Chem.* **278**: 25644–25650.

Chiti F, Dobson CM (2006) Protein misfolding, functional amyloid, and human disease. *Annu. Rev. Biochem.* **75**: 333-66.

Choi J, Kim S, Tachikawa T, Fujitsuka M, Majima T (2011) Unfolding dynamics of cytochrome *c* revealed by single-molecule and ensemble-averaged spectroscopy. *Phys. Chem. Chem. Phys.* **13:** 5651-5658.

Czeslik C, Royer C, Hazlett T, Mantulin W (2003) Reorientational dynamics of enzymes adsorbed on quartz: a temperature-dependent time-resolved TIRF anisotropy study. *Biophys. J.* **84:** 2533-2541.

Dobson CM (1999) Protein misfolding, evolution and disease. *Trends Biochem. Sci.* **24**: 329-332.

Doose S, Neuweiler H, Sauer M (2009) Fluorescence quenching by photoinduced electron transfer: a reporter for conformational dynamics of macromolecules. *ChemPhysChem.* **10:** 1389-1398.

Dumoulin M, Canet D, Last AM, Pardon E, Archer DB, Muyldermans S, Wyns L, Matagne A, Robinson CV, Redfield C, Dobson CM (2005) Reduced global cooperativity is a common feature underlying the amyloidogenicity of pathogenic lysozyme mutations. *J. Mol. Biol.* **346**: 773-788.

Dumoulin M, Kumita JR, Dobson CM (2006) Normal and aberrant biological self-assembly: insights from studies of human lysozyme and its amyloidogenic variants. *Acc. Chem. Res.* **39**: 603-610.

Foderá V, Groenning M, Vetri V, Librizzi F, Spagnolo S, Cornett C, Olsen L, van de Weert M, Leone M (2008) Thioflavin T Hydroxylation at basis pH and its effect on amyloid fibril detection. *J. Phys. Chem. B* **112:** 15174-15181.

Frare E, Laureto PP, Zurdo J, Dobson CM, Fontana A (2004) A highly amyloidogenic region of hen lysozyme. *J. Mol. Biol.* **340**: 1153-1165.

Frare E, Mossuto MF, Laureto PP, Dumoulin M, Dobson CM, Fontana A (2006) Identification of the core structure of lysozyme amyloid fibrils by proteolysis. *J. Mol. Biol.* **361**: 551-561.

Gorbenko GP, Ioffe VM, Kinnunen PKJ (2007) Binding of lysozyme to phospholipid bilayers: evidence for protein aggregation upon membrane association. *Biophys. J.* **93:** 140-153.

Gorbenko GP, Kinnunen PKJ (2006) The role of lipid-protein interactions in amyloid-type protein fibril formation. *Chem. Phys. Lipids* **141:** 72-82.

Gorbenko GP, Trusova V (2011) Effects of oligomeric lysozyme on structural state of model membranes. *Biophys. Chem.* **154**: 73-81.

Greenspan P, Fowler SD (1985) Spectrofluorometric studies of the lipid probe, Nile Red. *J. Lipid Res.* **26:** 781-789.

Groenning M (2010) Binding mode of Thioflavin T and other molecular probes in the context of amyloid fibrils – current status. *J. Chem. Biol.* **3:** 1-18.

Groot NS, Pallarés I, Avilés FX, Vendrell J, Ventura S (2005) Prediction of "hot spots" of aggregation in disease-linked polypeptides. *BMC Struct Biol* **5:** 18.

Haber E, Anfinsen CB (1962) Side-chain interactions governing the pairing of half-cystine residues in ribonuclease. *J. Biol. Chem.* **237:** 1839–44.

Hammer ND, Wang X, McGufiie BA, Chapman MR (2008) Amyloids: Friend or Foe? *J. Alzheimers Dis.* **13(4)**: 407-419.

Haugland RP (2005) The Handbook. A Guide to Fluorescent Probes and Labeling Technologies, 10th ed, Eugene, OR.

Hawe A, Sutter M, Jiskoot W (2008) Extrinsic fluorescent dyes as tools for protein characterization. *Pharm. Res.* **25(7):** 1487-1499.

Hebda JA, Miranker AD (2009) The interplay of catalysis and toxicity by amyloid intermediates on lipid bilayers: insights from type II diabetes. *Annu. Rev. Biophys.* **38**: 125-52.

Hill SE, Miti T, Richmond T, Muschol M (2011) Spatial extent of charge repulsion regulates assembly pathways for lysozyme amyloid fibrils. *PLoS ONE* **6(4)**: e18171.

Hill SE, Robinson J, Matthews G, Muschol M (2009) Amyloid protofibrils of lysozyme nucleate and grow via oligomer fusion. *Biophys. J.* **96:** 3781-3790.

Holley M, Eginton C, Schaefer D, Brown LR (2008) Characterization of amyloidogenesis of hen egg lysozyme in concentrated ethanol solution. *Biochem. Biophys. Res. Co.* **373**: 164-168.

Imoto T, Forster LS, Rupley JA, Tanaka F (1972) Fluorescence of lysozyme: emissions from tryptophan residues 62 and 108 and energy migration. *Proc. Natl. Acad. Sci. USA* **69(5)**: 1151-1155.

Kazlauskaite J, Sanghera N, Sylvester I, Venien-Bryan C, Pinheiro TJT (2003) Structural changes of the prion protein in lipid membranes leading to aggregation and fibrillization. *Biochemistry* **42**: 3295–3304.

Kinnunen PKJ (2009) Amyloid Formation on Lipid Membrane Surfaces. *Open Biol.* **2**: 163-175.

Kinosita K, Kawato S, Ikegami A (1977) A theory of fluorescence polarization decay in membranes. *Biophys. J.* **20:** 289-305.

Knight JD, Hebda JA, Miranker AD (2006) Conserved and cooperative assembly of membrane-bound r-helical states of islet amyloid polypeptide. *Biochemistry* **45**: 9496-9508.

Knight JD, Miranker AD (2004) Phospholipid catalysis of diabetic amyloid assembly. *J. Mol. Biol.* **341**: 1175-1187.

Krebs MRH, Wilkins DK, Chung EW, Pitkeathly MC, Chamberlain AK, Zurdo J, Robinson CV, Dobson CM (2000) Formation and seeding of amyloid fibrils from wild-type hen lysozyme and a peptide fragment from the β-domain. *J. Mol. Biol.* **300**: 541-549.

Kumar S, Singh AK, Krishnamoorthy G, Swaminathan R (2008) Thioflavin T displays enhanced fluorescence selectively inside anionic micelles and mammalian cells. *J. Fluoresc.* **18:** 1199–1205.

Kyle RA (2001) Amyloidosis: a convoluted story. *Brit. J. Haematol.* **114**: 529-538.

Lakowicz JR (2006) Principles of Fluorescence Spectroscopy, 3rd ed. Springer, New York.

Lashuel HA, Lansbury PT Jr. (2006) Are amyloid diseases caused by protein aggregates that mimic bacterial pore-forming toxins? *Q. Rev. Biophys.* **39:** 167–201.

Layton CJ, Hellinga HW (2010) Thermodynamic analysis of ligand-induced changes in protein thermal unfolding applied to high-throughput determination of ligand affinities with extrinsic fluorescent dyes. *Biochemistry* **49:** 10831-10841.

Lee RC, Despa F, Guo L, Betala P, Kuo A, Thiyagarajan P (2006) Surfactant copolymers prevent aggregation of heat denatured lysozyme. *Ann. Biomed. Eng.* **34(7):** 1190-1200.

Lindgren M, Hammarström P (2010) Amyloid oligomers: spectroscopic characterization of amyloidogenic protein states. *FEBS J.* **277:** 1380-1388.

Lindgren M, Sörgjerd K, Hammarström P (2005) Detection and Characterization of aggregates, prefibrillar amyloidogenic oligomers, and protofibrils using fluorescence spectroscopy. *Biophys. J.* **88:** 4200-4212.

Lo M, Aulabaugh A, Jin G, Cowling R, Bard J, Malamas M, Ellestad G (2004) Evaluation of fluorescence-based thermal shift assays for hit identification in drug discovery. *Anal. Biochem.* **332:** 153–159.

Luk KC, Hyde EG, Trojanowski JQ, Lee VM.-Y (2007) Sensitive fluorescence polarization technique for rapid screening of α-synuclein oligomerization/fibrillization inhibitors. *Biochemistry* **46**: 12522-12529.

Machuqueiro M, Baptista AM (2008) Acidic range titration of HEWL using a constant-pH molecular dynamics method. *Proteins* **72:** 289-298.

Mahalka AK, Kinnunen PKJ (2009) Binding of amphipathic α-helical antimicrobial peptides to lipid membranes: lessons from temporins B and L. *Biochim. Biophys. Acta* **1788**: 1600-1609.

Matulis D, Kranz JK, Salemme FR, Todd MJ (2005) Thermodynamic stability of carbonic anhydrase; measurements of binding affinity and stoichiometry using ThermoFluor. *Biochemistry* **44:** 5258–5266.

Mayer LD, Hope MJ, Cullis PR (1986) Vesicles of variable sizes produced by a rapid extrusion procedure. *Biochim. Biophys. Acta* **858**: 161-168.

McClare CW (1971) An accurate and convenient organic phosphorus assay. *Anal. Biochem.* **39(2)**: 527-530.

Meersman F, Atilgan C, Miles AJ, Bader R, Shang W, Matagne A, Wallace BA, Koch MHJ (2010) Consistent picture of the reversible thermal unfolding of hen egg-white lysozyme from experiment and molecular dynamics. *Biophys. J.* **99:** 2255-2263.

Melo AM, Prieto M, Coutinho A (2011) The effect of variable liposome brightness on quantifying lipid–protein interactions using fluorescence correlation spectroscopy. *Biochim. Biophys. Acta* **1808:** 2559-2568.

Melo AM, Federov A, Prieto M, Coutinho A (2012) Exploring fluorescence lifetime and homo-FRET measurements to monitor lysozyme oligomerization in anionic lipid membranes: relation to "amyloid-like" fibril formation. *Biophys. J.* **102(3):** 433a-434a.

Meratan AA, Ghasemi A, Nemat-Gorgani M (2011) Membrane integrity and amyloid cytotoxicity: a model study involving mitochondria and lysozyme fibrillation products. *J. Mol. Biol.* **409:** 826-838.

Mishra R, Sjölander D, Hammarström P (2011) Spectroscopic characterization of diverse amyloid fibrils *in vitro* by the fluorescent dye Nile Red. *Mol. BioSyst.***7:** 1232-1240.

Mishra R, Sörgjerd K, Nyström S, Nordigården A, Yu Y, Hammarström P (2007) Lysozyme amyloidogenesis is accelerated by specific nicking and fragmentation but decelerated by intact protein binding and conversion. *J. Mol. Biol.* **366:** 1029-1044.

Morshedi D, Ebrahim-Habibi A, Moosavi-Movahedi AA, Nemat-Gorgani M (2010) Chemical modification of lysine residues in lysozyme may dramatically influence its amyloid fibrillation. *Biochim. Biophys. Acta* **1804:** 714-722.

Mukhopadhyay S, Nayak PK, Udgaonkar JB, Krishnamoorthy G (2006) Characterization of the formation of amyloid protofibrils from barstar by mapping residue-specific fluorescence dynamics. *J. Mol. Biol.* **358:** 935-942.

Munishkina LA, Cooper EM, Uversky VN, Fink AL (2004) The effect of macromolecular crowding on protein aggregation and amyloid fibril formation. *J. Mol. Recognit.* **17:** 456-464.

Munishkina LA, Fink AL (2007) Fluorescence as a method to reveal structures and memebrane-interactions of amyloidogenic proteins. *Biochim. Biophys. Acta* **1768:** 1862-1885.

Nelson DL, Cox MM (2008) Lehninger Principles of Biochemistry 5th Ed. W.H.Freeman & Co Ltd.

Pace CN, Vajdos F, Fee L, Grimsley G, Gray T (1995) How to measure and predict the molar absorption-coefficient of a protein. *Protein Sci*. **4:** 2411–2423.

Pastor I, Ferrer ML, Lillo MP, Gómez J, Mateo CR (2007) Structure and dynamics of lysozyme encapsulated in a silica Sol-Gel matrix. *J. Phys. Chem.* **111:** 11603-11610.

Pepys MB, Hawkins PN, Booth DR, Vigushin DM, Tennent GA, Soutar AK, Totty N, Nguyen O, Blake CC, Terry CJ, Feest TG, Zalin AM, Hsuan JJ (1993) Human lysozyme gene mutations cause hereditary systemic amyloidosis. *Nature **362***: 553-557.

Nilsson KPR (2009) Small organic probes as amyloid specific ligands – Past and recent molecular scaffolds. *FEBS Lett.* **583**: 2593-2599.

Quist A, Doudevski I, Lin H, Azimova R, Ng D, Frangione B, Kagan B, Ghiso J, Lal R (2005) Amyloid ion channels: A common structural link for protein-misfolding disease. *Proc. Natl. Acad. Sci. USA* **102(30)**: 10427–10432.

Rochet J, Lansbury Jr PT (2000) Amyloid fibrillogenesis: themes and variations. *Curr. Opin. Struc. Biol.* **10**: 60-68.

Rusinova E, Tretyachenko-Ladokhina V, Vele OE, Senear DF, Ross JBA (2002) Alexa and Oregon Green dyes as fluorescence anisotropy probes for measuring protein-protein and protein-nucleic acid interactions. *Anal. Biochem.* **308:** 18-25.

Ryan TM, Howlett GJ, Bailey MF (2008) Fluorescence detection of a lipid-induced tetrameric intermediate in amyloid fibril formation by apolipoprotein C-II. *J. Biol. Chem.* **283(20)**: 35118-35128.

Sackett DL, Wolff J. (1987) Nile Red as a polarity-sensitive fluorescent probe of hydrophobic protein surfaces. *Anal. Biochem.* **167(2)**: 228-34.

Santos NC, Prieto M, Castanho MARB (2003) Quantifying molecular partition into model systems of biomembranes: an emphasis on optical spectroscopic methods. *Biochim. Biophys. Acta* **1612**: 123-135.

Schnaible V, Przybylski M (1999) Identification of fluorescein-5'-isothiocyanate-modification sites in proteins by electrospray-ionization mass spectrometry. *Bioconjugate Chem.***10:** 861-866.

Senisterra G, Finerty PJ (2009) High throughput methods of assessing protein stability and aggregation. *Mol. BioSyst*. **5:** 217–223.

Shcharbin D, Szwedzka M, Bryszewska M (2007) Does fluorescence of ANS reflect its binding to PAMAM dendrimer? *Bioorg. Chem.* **35:** 170–174.

Sipe JD, Benson MD, Buxbaum JN, Ikeda S, Merlini G, Saraiva MJM, Westermark P (2010) Amyloid fibril protein nomenclature: 2010 recommendations from the nomenclature committee of the International Society of Amyloidosis. *Amyloid* **17(3–4):** 101–104.

Smith LJ, Mark AE, Dobson CM, van Gunsteren WF (1998) Molecular dynamics simulations of peptide fragments from hen lysozyme: insight into non-native protein conformations. *J. Mol. Biol.* **280**: 703-719.

Sohl JL, Jaswal SS, Agard DA (1998) Unfolded conformations of alpha-lytic protease are more stable than its native state. *Nature* **395:** 817–819.

Sparr E, Engel MFM, Sakharov DV, Sprong M, Jacobs J, Kruijff B, Hoppener JWM, Killian JA (2004) Islet amyloid polypeptide-induced membrane leakage involves uptake of lipids by forming amyloid fibers. *FEBS Lett.* **577:** 117-120.

Steinberg TH, Jones LJ, Haugland RP, Singer VL (1996) SYPRO Orange and SYPRO Red protein gel stains: one-step fluorescent staining of denaturing gels for detection of nanogram levels of protein. *Anal. Biochem.* **239**: 223-237.

Stsiapura VI, Maskevich AA, Kuzmitsky VA, Uversky VN, Kuznetsova IM, Turoverov KK (2008) Thioflavin T as a molecular rotor: fluorescent properties of thioflavin t in solvents with different viscosity. *J. Phys. Chem. B* **112:** 15893-15902.

Suckau D, Mak M, Przybylski M (1992) Protein surface topology-probing by selective chemical modification and mass spectrometric peptide mapping. *Proc. Natl. Acad. Sci. USA* **89**: 5630-5634.

Sun Q, Lu R, Yu A (2011) Structural heterogeneity in the collision complex between organic dyes and tryptophan in aqueous solution. *J. Phys. Chem. B* **116**: 660-666.

Sutter M, Oliveira S, Sanders NN, Lucas B, Hoek A, Hink MA, Visser AJWG, De Smedt SC, Hennink WE, Jiskoot W (2007) Sensitive spectroscopic detection of large and denatured protein aggregates in solution by use of the fluorescent dye Nile Red. *J. Fluoresc.* **17:** 181-192.

Tajalli H, Gilani AG, Zakerhamidi MS, Tajalli P (2008) The photophysical properties of Nile Red and Nile Blue in ordered anisotropic media. *Dyes Pigments* **78**: 15-24.

Teske CA, Simon R, Niebisch A, Hubbuch J (2007) Changes in retention behavior of fluorescently labeled proteins during ion-exchange chromatography caused by different protein surface labeling positions. *Biotechnol. Bioeng.* **98**: 193-200.

Thirunavukkuarasu S, Jares-Erijman EA, Jovin TM (2008) Multiparametric fluorescence detection of early stages in the amyloid protein aggregation of pyrene-labeled α-synuclein. *J. Mol. Biol.* **378**: 1064-1073.

Trexler AJ, Nilsson MR (2007) The formation of amyloid fibrils from proteins in the lysozyme family. *Curr. Protein Pept. Sci.* **8:** 537-557.

Uversky VN, Fink AL (2004) Conformational constrains for amyloid fibrillation: the importance of being unfolded. *Biochim. Biophys. Acta* **1698**: 131-153.

van Ham TJ, Esposito A, Kumita JR, Hsu SD, Schierle GSK, Kaminski CF, Dobson CM, Nollen EAA, Bertoncini CW (2010) Towards multiparametric fluorescent imaging of amyloid formation: studies of a YFP model of α-synuclein aggregation. *J. Mol. Biol.* **395:** 627-642.

Wang SS, Liu K, Lu Y (2009) Amyloid fibrillation of hen egg-white lysozyme is inhibited by TCEP. *Biochem. Biophys. Res. Co.* **381**: 639-642.

Westermark P, Benson MD, Buxbaum JN, Cohen AS, Frangione B, Ikeda S, Masters CL, Merlini G, Saraiva MJM, Sipe JD (2007) A primer of amyloid nomenclature. *Amyloid* **14(3):** 179–183.

Winklhofer KF, Tatzelt J, Haass C (2008) The two faces of protein misfolding: gain- and loss-of-function in neurodegenerative diseases. *EMBO J.* **27**: 336-349.

Yip CM, Elton EA, Darabie AA, Morrison MR, McLaurin J (2001) Cholesterol, a modulator of membrane-associated Aβ-fibrillogenesis and neurotoxicity. *J. Mol. Biol.* **311**: 723–734.

Yonezawa Y, Tanaka S, Kubota T, Wakabayashi K, Yutani K, Fujiwara S (2002) An Insight into the pathway of the amyloid fibril formation of hen egg white lysozyme obtained from a small-angle X-ray and neutron scattering study. *J. Mol. Biol.* **323**: 237-251.

Zhao H, Jutila A, Nurminen T, Wickstrom SA, Keski-Oja J, Kinnunen PKJ (2005) Binding of endostatin to phosphatidylserine-containing membranes and formation of amyloid-like fibers. *Biochemistry* **44**: 2857–2863.

Zhao H, Tuominen EKJ, Kinnunen PKJ (2004) Formation of amyloid fibers triggered by phosphatidylserine-containing membranes. *Biochemistry* **43**: 10302-10307.

Zhu M, Li J, Fink AL (2003) The association of α-synuclein with membranes affects bilayer structure, stability and fibril formation. *J. Biol. Chem.* **278**: 40186–44097.